A COMPUTATIONAL STUDY ON THERMO-SOLUTAL CONVECTION IN MAGNETOHYDRODYNAMICS (MHD) FLOW WITH DUFOUR EFEECT

BY

TIMOTHY CHIBUNDO DURU

DEPARTMENT OF MATHEMATICS,

FACULTY OF PHYSICAL SCIENCE,

AHMADU BELLO UNIVERSITY,

ZARIA, NIGERIA

MAY, 2018

A COMPUTATIONAL STUDY ON THERMO-SOLUTAL CONVECTION IN MAGNETOHYDRODYNAMICS (MHD) FLOW WITH DUFOUR EFFECT

BY

Timothy Chibundo, DURU

B.Sc MATHEMATICS (ABU)

P16PSMT8079

(M.Sc/SCI/23683/12-13)

A DISSERTATION SUBMITTED TO THE SCHOOL OF POSTGRADUATE STUDIES, AHMADU BELLO UNIVERSITY, ZARIA, IN PARTIAL FULFILLMENT OF THE REQUIREMENTS FOR THE AWARD OF MASTER OF SCIENCE DEGREE IN MATHEMATICS,

DEPARTMENT OF MATHEMATICS,

FACULTY OF PHYSICAL SCIENCE,

AHMADU BELLO UNIVERSITY,

ZARIA, NIGERIA

MAY, 2018

DECLARATION

I declare that the work in this dissertation titled "A COMPUTATIONAL STUDY ON THERMO-SOLUTAL CONVECTION IN MAGNETOHYDRODYNAMICS (MHD) FLOW WITH DUFOUR EFFECT" has been carried out by me in the Department of Mathematics under the supervision of Prof. Abiodun O. Ajibade and Prof. Basant K. Jha. The information derived from the literature has been duly acknowledged in the text and a list of references provided. No part of this dissertation was previously presented for another degree or diploma at this or any institution.

_____ _____

DURU, Timothy Chibundo Date

CERTIFICATION

This dissertation titled "A COMPUTATIONAL STUDY ON THERMO-SOLUTAL CONVECTION IN MAGNETOHYDRODYNAMICS (MHD) FLOW WITH DUFOUR EFFECT" by DURU, Timothy Chibundo, P16PSMT8079 (M.Sc/SCI/23683), meets the regulation governing the award of the degree of Masters of Science of Ahmadu Bello University, Zaria and is approved for its contribution to knowledge and literary presentation.

Prof. A. O. Ajibade

_____	_____	_____
Chairman, Supervisory Committee	Signature	Date

Prof. B. K. Jha

_____	_____	_____
Member, Supervisory Committee	Signature	Date

_____	_____	_____
External Examiner	Signature	Date

Prof .A .A .Tijjani

_____	_____	_____
Head of Department	Signature	Date

Prof. S.Z. Abubakar

_____	_____	_____
Dean, School of Postgraduate Studies	Signature	Date

DEDICATION

I dedicate this work first and foremost to the Supreme Creator for His extravagant grace, faithfulness, love and protection upon me. I also dedicate this work to all my true friends and that includes you!

ACKNOWLEDGEMENT

I would like to start by expressing my immeasurable gratitude to the Almighty God, for the gift of life, extravagant grace, uncommon inspiration and wisdom upon me in the course of researching and compiling this dissertation.

I acknowledge that this research work could not have recorded a huge success as it were without the outstanding contributions of my major supervisor, Prof. A. O. Ajibade, a scholar whom I hold so much in high esteem. Thank you so very kindly for your highly immeasurable suggestions and support.

I would like to acknowledge also my minor supervisor, Prof. B. K. Jha, a man I fondly refer to as an "oracle of Computational Fluid Dynamics", for imparting so much in me academically in the classroom right from my undergraduate days to this present time. Thank you most sincerely for taking out time to peruse through the manuscripts meticulously and also proffering useful suggestions where necessary in order to make this research work very rich. You are such a fantastic human being.

My profound gratitude goes to the HOD, Prof. A. A. Tijjani, Departmental Secretary, MrsAgbo, Dr. A. Yahaya, Mr. Taiwo Yusuf, Mr. Michael Oni and Mr Peter Malgwi for all their support.

Finally, to everyone who contributed morally and financially towards making this project a dream come true especially my Dad, Mazi C. N Duruh, my brothers, Mr. Joseph C. Duru, Dr. Benjamin C. Duruh, Dr. Raymond E. Duru, Mr. Henry C. Duruh, Mr. Luke C. Duruhson and my big sister, Mrs. Georgina N. Onyewotu, I say, thank you most sincerely and may the Almighty God repay you all bountifully.

Thanks, a whole lot to all of you once more and God bless you.

ABSTRACT

A computational study on thermo-solutal convection in Magnetohydrodynamics (MHD) flow with Dufour effect is the subject of this research work. A fully developed unsteady natural convection flow of viscous, incompressible and electrically conducting fluid in a microchannel formed by two vertical plates under the influence of transverse magnetic field of uniform strength B_0 which is applied in the direction perpendicular to that of the flow is considered. In this flow formation, temperature is influenced by concentration of the introduced chemical species, leading to diffusion-thermo effect on the heat and mass transfer. In an extended study, the flow is subjected to suction of the fluid from one porous plate and at the same rate fluid is being injected through the other porous plate. Fluid motion is induced by asymmetric heating of the channel plates taking into consideration velocity slip and temperature as well as concentration jumps on the boundaries. Heat source parameter as well as Dufour effects are also taken into cognizance. Partial differential equations that describe the energy and concentration within the system follow the dual-phase-lag model for heat conduction. Laplace transform approach is used to solve the resulting governing equations in Laplace domain while the inversion into time domain is made possible through the Riemann-sum approximation technique. The response of mean chemical concentration, bulk fluid temperature and mass flux within the channel to different flow parameters are investigated. It is worth noting that regardless of temperature gradient or heat flux influence on the fluid flow, the resultant mass flux decreases by increasing the Hartmann number (m) and also, it increases with an increase in Biot number (Bi) as well as Dufour number (D). In addition, the mean temperature rises following an increase in Dufour (D) number but decreases with growing thermal retardation time (τ_T). Furthermore, it is observed that heat generation (δ) increases temperature profile, velocity profile and also skin friction.

TABLE OF CONTENT

Cover Page i

Fly Leaf i

Title Page ii

DECLARATION iii

CERTIFICATION iv

DEDICATION v

ACKNOWLEDGEMENT vi

ABSTRACT vii

TABLE OF CONTENT viii

LIST OF TABLES x

LIST OF FIGURES xi

LIST OF APPENDICES xiii

NOMENCLATURE AND GREEK LETTERS xiv

CHAPTER ONE 1

INTRODUCTION 1

1.1 Background of the study 1

1.2 Statement of the problem 3

1.3 Significance of the study 4

1.4 Aim and objectives 4

1.6 Basic Definitions 5

CHAPTER TWO 8

LITERATURE REVIEW 8

2.1 Natural Convection 8

2.2 Magnetohydrodynamics 9

2.3 Convective Boundary Condition 10

2.4 Heat Generation 11

2.5 Dual-Phase-Lag 11

2.6 Suction/Injection 13

2.7 Dufour effect 13

CHAPTER THREE 15

MATHEMATICAL MODELS 15

3.1 Flow formation and Geometry 15

3.2 Dual-Phase-Lag Heat Conduction with Convective Boundary 17
3.2.1 Dimensionless Analysis 18
3.3 Dual-Phase-Lag Heat Conduction in a Vertical Porous Channel 20
3.3.1 Governing Equations in dimensionless form 22
CHAPTER FOUR 23
SOLUTIONS TO THE PROBLEMS 23
4.1 Solution to the Problem on Convective Boundary Condition 23
4.1.1 Riemann Sum Approximation 24
4.1.2 Sherwood Number 26
4.1.3 Nusselt Number 26
4.1.4 Skin Friction 27
4.1.5 Mass Flux 27
4.1.6 Mean Concentration 28
4.1.7 Mean Temperature 28
4.2 Solution to the Problem on Heat Generating Fluid in Porous Microchannel 29
4.2.1 Sherwood Number 30
4.2.2 Nusselt Number 30
4.2.3 Skin Friction 31
4.2.4 Mass Flux 31
4.2.5 Mean Concentration 31
4.2.6 Mean Temperature 32
CHAPTER FIVE 33
RESULTS AND DISCUSSION 33
5.1 Convective Boundary Condition 33
5.2 Heat Generating Fluid in Porous Microchannel 55
CHAPTER SIX 78
SUMMARY, CONCLUSION AND RECOMMENDATION 78
6.1 Summary 78
6.2 Conclusion 78
6.3 Recommendations 79
REFERENCES 80

LIST OF TABLES

Table 1: Effect of different flow parameters on mass flux through the channel 51
Table 2: Effect of different flow parameters on mean concentration of chemical species. 53
Table 3: Effect of different flow parameters on mean temperature of fluid 54
Table 4: Comparison of the velocity in the present work with Ajibade (2014) 55
Table 5: Effect of different flow parameters on mass flux through the channel 74
Table 6: Effect of different flow parameters on mean concentration of chemical species. 75
Table 7: Effect of different flow parameters on mean temperature of fluid 76
Table 8: Comparison of the present work with Ajibade (2014) 77

LIST OF FIGURES

Figure 3.1. Schematic diagram of the problem (Case 1) 16
Figure 3.2. Schematic diagram of the problem (Case 2) 20
Figure 5.1.1a: Concentration profile for different *Sc* 34
Figure 5.1.1b: Velocity profile for different *Sc* 34
Figure 5.1.2a: Concentration profile for different *t* 35
Figure 5.1.2b: Temperature profile for different *t* 36
Figure 5.1.2c: Velocity profile for different *t* 36
Figure 5.1.3a: Concentration profile for different *Kn* 37
Figure 5.1.3b: Temperature profile for different *Kn* 38
Figure 5.1.3c: Velocity profile for different *Kn* 38
Figure 5.1.4: Cross-sectional concentration for different λ_q 39
Figure 5.1.5: Cross-sectional temperature for different τ_q 40
Figure 5.1.6: Cross-sectional velocity for different τ_q 41
Figure 5.1.7a: Temperature profile for different *Pr* 42
Figure 5.1.7b: Velocity profile for different *Pr* 42
Figure 5.1.8a: Temperature profile for different *D* 43
Figure 5.1.8b: Velocity profile for different *D* 43
Figure 5.1.9a: Temperature profile for different *Bi* 44
Figure 5.1.9b: Velocity profile for different *Bi* 45
Figure 5.1.10: Velocity profile for different *m* 45
Figure 5.1.11: Velocity profile for different *N* 46
Figure 5.1.12: Sherwood number for different λ_C 47
Figure 5.1.13: Nusselt number for different *Kn* 48
Figure 5.1.14: Nusselt number vs τ_T for different τ_q 49
Figure 5.1.15: Skin-friction for different *Kn* 50
Figure 5.1.16: Skin-friction for different *Bi* 50
Figure 5.2.1a: Concentration profile for different *Sc* 56
Figure 5.2.1b: Velocity profile for different *Sc* 57
Figure 5.2.2a: Concentration profile for different *t* 58
Figure 5.2.2b: Temperature profile for different *t* 58
Figure 5.2.2c: Velocity profile for different *t* 59
Figure 5.2.3a: Concentration profile for different *Kn* 60
Figure 5.2.3b: Temperature profile for different *Kn* 60
Figure 5.2.3c: Velocity profile for different *Kn* 61
Figure 5.2.4: Cross-sectional concentration for different λ_f 62
Figure 5.2.5: Cross-sectional temperature for different τ_f 62
Figure 5.2.6: Cross-sectional Velocity for different τ_f 63
Figure 5.2.7a: Concentration profile for different *S* 64
Figure 5.2.7b: Temperature profile for different *S* 64
Figure 5.2.7c: Velocity profile for different *S* 65

Figure 5.2.8a: Temperature profile for different *Pr* 66
Figure 5.2.8b: Velocity profile for different *Pr* 66
Figure 5.2.9a: Temperature profile for different *D* 67
Figure 5.2.9b: Velocity profile for different *D* 67
Figure 5.2.10a: Temperature profile for different δ 68
Figure 5.2.10b: Velocity profile for different δ 68
Figure 5.2.11: Velocity profile for different *m* 69
Figure 5.2.12: Velocity profile for different *N* 70
Figure 5.2.13: Sherwood number vs λ_f for different λ_C 70
Figure 5.2.14: Nusselt number vs τ_f for different *D* 71
Figure 5.2.15: Nusselt number vs τ_T for different *Kn* 72
Figure 5.2.16: Skin-friction vs *Kn* for different *D* 73
Figure 5.2.17: Skin-friction vs *m* for different 73

LIST OF APPENDICES

APPENDIX A 84
List of constants used to define the solutions of the problem in the dissertation 84
DUAL-PHASE-LAG HEAT CONDUCTION WITH CONVECTIVE BOUNDARY 84
DUAL-PHASE-LAG HEAT CONDUCTION IN VERTICAL POROUS CHANNEL 85
MATLAB PROGRAMS 86
MATLAB PROGRAM (CASE 1) 86
MATLAB PROGRAM (CASE 2) 93

NOMENCLATURE AND GREEK LETTERS

Notation

Bi Biot number

B_o Magnetic parameter

Cdimensionless chemical concentration

C_0 initial concentration

C' dimensional chemical concentration

C_m dimensionless mean concentration

C'_m dimensional mean concentration

C_p specific heat at constant pressure

DDufour number

D_m mass diffusivity $[m^2 s^{-1}]$

D_1 diffusion-thermo effect

g acceleration due to gravity $[ms^{-2}]$

$h$channel width $[m]$

k thermal conductivity $[Wm^{-1}K^{-1}]$

KnKnudsen number

m Hartmann number

Nsustentation parameter

NuNusselt number

PrPrandtl number

$\underset{\sim}{q}$ mass flux vector

$\vec{q}$ heat flux vector

Q dimensionless mass flux

Q' dimensional mass flux

$\vec{r}$ three-dimensional position vector

s Laplace parameter

S suction/injection parameter

Sc Schmidt number

t dimensionless time

t' dimensional time [s]

T dimensionless temperature of the fluid

T_0 initial temperature [K]

T' dimensional temperature of the fluid [K]

T_m dimensionless mean temperature

T_m' dimensional mean temperature [K]

u dimensionless velocity of fluid

u' dimensional velocity of fluid [ms^{-1}]

V transformed velocity (in Laplace domain)

x' vertical co-ordinate, direction of flow [m]

y dimensionless horizontal coordinate

y' dimensional horizontal coordinate [m]

Greek Letters

α thermal diffusivity $[m^2 s^{-1}]$

β coefficient of thermal expansion $[K^{-1}]$

$\tilde{\beta}$ coefficient of chemical expansion

δ heat generation parameter

θ transformed temperature (in Laplace domain)

$\lambda_{\underline{q}} = \lambda_f$ dimensionless phase lag in the mass flux

$\lambda^*_{\underline{q}} = \lambda^*_f$ dimensional phase lag in the mass flux $[s]$

λ_C dimensionless phase lag in concentration gradient

λ^*_C dimensional phase lag in concentration gradient $[s]$

μ coefficient of viscosity $[Kgm^{-1}s^{-1}]$

ν kinematic viscosity $[m^2 s^{-1}]$

ρ density of fluid $[Kgm^{-3}]$

σ electrical conductivity $[Sm^{-1}]$

τ skin-friction

$\tau_q = \tau_f$ dimensionless thermal relaxation time

$\tau^*_q = \tau^*_f$ dimensional thermal relaxation time

τ_T dimensionless thermal retardation time

τ^*_T dimensional thermal retardation time

Φ transformed concentration (in Laplace domain)

CHAPTER ONE

INTRODUCTION

1.1 Background of the study

Fluid mechanics can be described as the study of fluids either in motion (fluid *dynamics*) or at rest (fluid *statics*) and the subsequent effects of the fluid upon the boundaries, which may be either solid surfaces or interfaces with other fluids. It is worth mentioning that both gases and liquids are classified as fluids, and the number of fluids engineering applications are enormous. These include: breathing, blood flow, swimming, pumps, fans, turbines, airplanes, ships, rivers, windmills, pipes, missiles, icebergs, engines, filters, jets, and sprinklers, just to name a few. In fact, there is no gain saying that almost everything on this planet either is a fluid or moves within or near a fluid.

A very key component of fluid mechanics is natural convection. Natural convection flows have in contemporary times attracted a great deal of attention due to its diverse applications in the field of engineering, industrial and heat transfer processes. Gebhart and Pera (1971), in their work explained that the phenomenon of natural convective flow is caused by density differences induced by temperature gradients, chemical composition gradients, and material composition. Convection is also seen to play a very vital role in defining our weather patterns, oceanic currents, and sea-wind formation. In engineering applications, convection is commonly visualized in the formation of micro-structures during the cooling of molten metals, and fluid flows around shrouded heat dissipation fins, and solar ponds. A very common industrial application of natural convection is free air cooling without the aid of fans: this can happen on small scales (computer chips) to large scale process equipment. Wubshet and Makinde (2013), asserted that there are many physical problems as well as engineering applications where heat

transfer by natural convection can be found to happen more frequently. They include: heat exchangers, geothermal systems, petroleum reservoirs and nuclear waste repositories, chemical catalytic reactors, packed beds, fiber and granular insulation.

On the other hand, the study of magnetohydrodynamics (MHD) flows have inspired great curiosity owing to its relevance in meteorology, cosmic fluid dynamics, solar physics and in the motion of Earth's core. On a wider perspective, applications of MHD can be appreciated in areas such as; engineering, astrophysics and geophysics. MHD therefore, is concerned with the mutual interaction of fluid flow and magnetic fields. The fluids in question must be electrically conducting and non-magnetic, which limits us to liquid metals, hot ionised gases (plasmas) and strong electrolytes.

In the course of modelling fluid flow through a microchannel, one parameter which proves very instrumental is the Knudsen number. It is defined as the ratio of the fluid's mean free path λ to the characteristic length *b* of the physical system (i.e. $Kn = \lambda / b$). It can also be seen as channels whose dimensions are less than 1 millimeter and greater than 1 micron. Above 1 millimeter the flow exhibits behavior that is the same as most macroscopic flows. Currently, microchannels have characteristic dimensions anywhere from the submicron scale to hundreds of microns. Microchannels can be fabricated in many materials-glass, polymers, silicon, metals-using various processes including surface micromachining, bulk micromachining, molding, embossing, and conventional machining with microcutters. Microchannels are used to transport biological materials such as (in order of size) proteins,DNA, cells, and embryos or to transport chemical samples and analytes. For a given microchannel, when Kn<0.001, the flow domain is considered as a continuum and as such modelled by the Navier–Stokes equation with the no-slip wall boundary condition. However, in the interval 0.001<Kn<0.1, the no-slip boundary condition

becomes invalid thereby giving way to the slip flow regime. Fluid flow through microchannel has in recent years become a hunting ground for researchers.Chen and Weng (2005)analytically studied the fully developed natural convection in open-ended vertical parallel plate micro-channel with asymmetric wall temperature distribution in which the effect of rarefaction and fluid wall interaction was shown to increase the volume flow rate and decrease the heat transfer.In another study by Khadrawi et al (2005) on the transient hydrodynamics and thermal behaviours of fluid flow in a vertical parallel-plate microchannel, under the effect of the hyperbolic-heat-conduction model,it was observed that increasing Kn results in an increase in the slip hydrodynamics and thermal boundary condition.

Therefore, in the light of the background above, this research work shall be investigating the Dual-phase-lag and diffusion-thermo effects on thermosolutal convection in MHD flow both in a microchannel and micro-porous channel.

1.2 Statement of the problem

Jha and Ajibade (2010, 2011) investigated the effect of diffusion-thermo on natural convection heat and mass transfer under symmetric boundary conditions as well as asymmetric boundary conditions. These works were further extended by Ajibade (2014) when he investigated the combined effects of diffusion-thermo (Dufour) and dual-phase-lags (DPL) on unsteady double diffusive convection flow in a vertical microchannel filled with porous material. None of these studies mentioned above has been able to examine what effects magnetohydrodynamics (MHD), convective heat exchange as well as heat generation parameters could have on the fluid flow. Therefore, this work will attempt to fill the vacuum in Ajibade (2014) by considering the impacts of the parameters earlier mentioned on an electrically conducting fluid. In addition, this dissertation will also take into account the role of suction/injection on the hydrodynamic behaviour of the micro-fluidic flow.

1.3 Significance of the study

This research work derived and presented a computational study on thermo-solutal convection inMHD flow with Dufour effect which is subject to asymmetric wall heating conditions. Its physical applications can be found in microelectronic devices, MHD marine propulsion, MHD stirring of molten metal, electronic packages, thermal insulation, petroleum reservoirs, magnetic-levitation casting and exothermic reaction in packaged reactors, transportation cooling and drying of materials. More importantly, it is hoped that the results obtained in this research work will not only serve as an improvement on the previous studies related to such flows but also provide useful information for the advancement of industrial or engineering applications.

1.4 Aim and objectives

The aim of this research is to carry out a computational study on thermo-solutal convection in MHD flow with Dufour effect.

The objectives to attain the set aim are to:

i. Examine thermal and hydrodynamic responses of the fluid to convective heat exchange parameter and also diffusion-thermo effects;
ii. Examine the effect of externally applied transverse magnetic field on natural convection flow in both microchannel and micro-porous channel;
iii. Observe the impact of heat generation parameter (δ) on temperature, velocity profile and skin-friction of the fluid;
iv. Investigate the impact of suction/injection on fluid velocity and skin-friction on micro-porous channel flow formation.

1.5 Research Methodology

To successfully attain the above set goals, a well-known Laplace transform technique is employed to solve the time dependent governing concentration, momentum and energy equations and then the method of Riemann-sum approximation is applied to invert the Laplace domain analytical solutions into time domain in order to obtain the velocity, temperature, skin-friction and rate of heat transfer. Using a computer package, MATLAB (R2012b), the results obtained are presented graphically to investigate the influence of each governing parameter. Numerical comparison of the result obtained and previously published results is presented to establish the accuracy of the current solution.

1.6 Basic Definitions

1. **Compressible and incompressible fluid**: A compressible flow is a flow which the fluid density varies significantly within the flow field while in an incompressible flow the density does not vary within the flow field.
2. **Free or Natural Convection**: Free or Natural convection is a mechanism in which fluid motion is generated only by density differences in fluid caused by temperature gradients, concentration gradients or both. It is a type of heat transport in which the fluid motion is not generated by an external source (pump,fan, suction devices).
3. **Conducting and non-conducting fluid**: Materials that conducts electricity have free ions (charged particle) thus there is flow of current while Materials that do not have free ions (charged particle) to help in the flow of current are known as Non-conducting fluid.
4. **Boussinessq approximation**: Boussinessq approximation is the assumption that the fluid flow is considered under little variations of temperature and density.
5. **Skin friction**: Is a component of drag, the force resisting the motion of a solid body through a fluid. It arises from the friction of the fluid against the skin of the object that is

moving through it. Skin friction follows the drag equation and rises with the square of the velocity. Skin friction can be reduced by shaping the moving body so that smooth flow is possible.

6. **Injection**: Is a force that causes a fluid to be drawn out of an interior space or to adhere to a surface because of the difference between the external and internal pressures.
7. **Suction**: is a force that causes a fluid to be drawn into an interior space or to adhere to a surface because of the difference between the external and internal pressures
8. **Symmetric/asymmetric heating**: This is a type of heating of the boundary layers in which equal/unequal amount of constant heating is applied on boundary surfaces of the system.
9. **Dimensionless quantity**: is a quantity without an associated physical dimension.
10. **Magnetic field**: is the magnetic effect of electric currents and magnetic material.
11. **Microchannel**: is a channel with hydraulic diameter less than 1*mm*.
12. **Hartmann Number:** is the ratio of electromagnetic force to the viscous force.
13. **Magnetic Field:** is the magnetic effect of electric currents and magnetic materials.
14. **Biot Number:** is the ratio of conductive heat resistance within the object to the convective heat transfer resistance across the object's boundary.
15. **Schmidt number:** is a dimensionless number defined as the ratio of momentum diffusivity (viscocity) and mass diffusivity, and is used to characterize fluid flow in which there are simultaneous momentum and mass diffusion convection process.
16. **Sherwood number:** this is a dimensionless number which represents the ratio of convective mass transfer to the rate of diffusive mass transport.
17. **Thermo-solutal:** is a phenomenon which describes convection in a liquid caused by a combination of heat and varying concentration of solute.

18. **Dufour effect:** refers to the energy flux due to a mass concentration gradient occurring as a coupled effect of irreversible process.
19. **MHD:** implies Magnetohydrodynamics which is the study of the magnetic properties of electrically conducting fluids. Since the magnetohydrodynamic equations combine the full complexity of Maxwell's equations with the fluid dynamics equations, it is clear that they will be extremely difficult to solve in their general form. However, by adopting some approximations, the general equations are simplified as follows:

Maxwell's equations:

$$\nabla \times E = \frac{\partial B}{\partial t}$$

$$\nabla \times B = \mu_0 j$$

$$\nabla \bullet B = 0$$

$$K_0 \nabla \bullet E = \rho_e$$

Conservation of Mass:

$$\frac{\partial \rho}{\partial t} + \nabla \bullet (\rho \upsilon) = 0$$

Equation of motion:

$$\rho \frac{D\upsilon}{Dt} = -\nabla p + \psi + j \times B$$

Conservation of energy:

$$\rho\left(\frac{De}{Dt} + \frac{1}{2}\frac{D\upsilon^2}{Dt}\right) = E \bullet j + \nabla \bullet (K \nabla T) - \sum_s \nabla \bullet (V_s \rho_s h_s) - \nabla \bullet (p\upsilon) + \phi$$

CHAPTER TWO

LITERATURE REVIEW

2.1 Natural Convection

Natural convection flows have in contemporary times attracted a great deal of attention due to its diverse applications in the field of engineering, industrial and heat transfer processes. In the work of Gebhart and Pera (1971), the phenomenon of natural convective flow is caused by density differences induced by temperature gradients, chemical composition gradients, and material composition. Wubshet and Makinde (2013), explained that convection cells produced from air arising above sunlight-warmed land or water are naturally a major feature of all weather systems. They explained further that convection is also seen in the rising plume of hot air from fire, oceanic currents, and sea-wind formation (where upward convection is also modified by Coriolis forces). In engineering applications, convection is commonly visualized in the formation of micro-structures during the cooling of molten metals, and fluid flows around shrouded heat dissipation fins, and solar ponds. A very common industrial application of natural convection is free air cooling without the aid of fans: this can happen on small scales (computer chips) to large scale process equipment. There are many physical problems as well as engineering applications where heat transfer by natural convection can be found to happen more frequently. They include: heat exchangers, geothermal systems, petroleum reservoirs and nuclear waste repositories, chemical catalytic reactors, packed beds, fiber and granular insulation. There have been a lot of research works on natural convection flow especially in a vertical channel under different boundary conditions studied by many authors. Gebhart and Pera (1971) studied the nature of vertical natural convection flows resulting from the combined buoyancy effects of thermal and mass diffusion. Soundalgekar and Wavre (1977) investigated heat and mass transfer effects on unsteady free convective flow along vertical porous plate with constant suction. Soundalgekar

(1979) also examined the effect of mass transfer and free convection currents on flow past an impulsively started vertical plate. He observed that injecting foreign gases into the fluid flow resulted in a reduction in shear stress and mass transfer conductance. Jha*et al* (2012), investigated the Natural Convection Flow of Heat Generating/Absorbing Fluid near a Vertical Plate with Ramped Temperature. They concluded that the presence of the heat sink parameter, reduces temperature and velocity profile as well as the skin friction for both ramped and isothermal cases.

2.2 Magnetohydrodynamics

The study of magnetohydrodynamics (MHD) flows have inspired great curiosity owing to its relevance in meteorology, cosmic fluid dynamics, solar physics and in the motion of Earth's core. On a wider perspective, applications of MHD can be appreciated in areas such as; engineering, astrophysics and geophysics particularly in geothermal energy recovery, oil extraction and thermal insulations.In the light of these, several studies on MHD natural convection flow of different fluids under different geometries have been done by many researchers. They include: Cramer and Pai (1973), Chawla (1967), Soundalgekar and Takhar (1977), and so on. Raptis and Singh (1983)studied MHD free convection flow past an accelerated verticalplate. Gupta (1961) studied the steady and transient free convection of an electrically conducting fluid from a vertical plate in the presence of magnetic field.Makinde (2009) obtained a similarity solution for the MHD boundary-layer flow and mass transfer past a vertical plate in a porous medium with constant heat flux. He found out that for positive values of the buoyancy parameters, the skin friction increased with increasing values of both the Eckert number (*Ec*) and the magnetic field intensity parameter (*m*) and decreased with increasing values of both the Schmidt number (*Sc*) and the permeability parameter (*K*). Quite recently, Jha*et al* (2014) studied MHD natural convection flow in a vertical parallel plate microchannel. They

found that increase in the effects of rarefaction and fluid wall interaction led to an increase in volume flow rate while the volume flow rate decreases with increase in Hartmann number.

2.3 Convective Boundary Condition

Convective heat transfer has attracted huge interest due to its relevance in industrial and environmental technologies including energy storage, gas turbines, nuclear plants, rocket propulsion, geothermal reservoirs, photovoltaic panels just to mention a few. The convective boundary condition has also attracted some interest and this usually is simulated through a Biot number in the wall thermal boundary condition. Ishak (2010) discussed the similarity solutions for flow and heat transfer over a permeable surface with convective boundary condition while Aziz (2009) provided a similarity solution for laminar thermal boundary layer over a flat surface with a convective surface boundary condition. Aziz (2010) further studied hydrodynamic and thermal slip flowboundary layers with an iso-flux thermal boundary condition. The buoyancy effects on thermal boundary layer over a vertical plate with a convective surface boundary condition was studied by Makinde and Olanrewaju (2010). They conluded that the effects of a combined increase in Prandtl and Grashof numbers tends to decrease the thickness of the thermal boundary layer along the plate. Furthermore, Makinde and Aziz (2010) submitted that as the convective heat transfer parameter increases, both the fluid velocity and temperature increase as well. Bég*et al*. (2014) analyzed Biot number and buoyancy effects on magnetohydrodynamic thermal slip flows. They observed that rising thermal radiation flux increases thermal boundary layer thickness as does increasing the magnetic field effect. In addition, they noticed that growing the hydrodynamic slip parameter reduces skin friction but enhances both local Nusselt and Sherwood numbers.

2.4 Heat Generation

Heat source impact on heat transfer has been shown to be of great relevance to a whole lot of physical problems. In many applications of free convection flow problems industrially, there exists a heat source or a sink which can either be constant, temperature gradient or temperature dependent heat source. This heat source can be found in the form of a battery or a coil. Again, it plays a significant role in the field of nuclear energy and fire combustion modelling, Foraboschi and Federico (1964). Crepeau and Clerksean (1997) have used a space-dependent exponentially decaying heat generation or absorption in their study on flow and heat transfer from a vertical plate. Sharma and Singh (2008) studied unsteady MHD Free Convective flow and heat transfer along a vertical porous plate with variable suction and internal heat generation. Singh (1984) investigated Stokes problem for a porous vertical plate with heat sinks by finite difference method. Mohammed (2014) analyzed the unsteady MHD free convective flow along a vertical porous plate embedded in a porous medium with heat generation, variable suction and chemical reaction effects. He observed that the velocity and temperature increased as the heat generation parameter increases. However, the exact opposite behavior was predicted as the magnetic field strength was increased.

2.5 Dual-Phase-Lag

Fourier equation of heat conduction results in a parabolic equation for the temperature field when combined with the conservation of energy law. The parabolic temperature equation implies an infinite speed of heat propagation, which is in good agreement with experimental data in many situations. However, there are some cases in which the Fourier model is not adequate to describe the heat conduction process. More precisely, Fourier equation of heat conduction is diffusive and cannot predict the finite temperature propagation speed in transient situations. Interestingly, there are other models of heat conduction which have been developed apart from the Fourier model.

Since these heat conduction models are non-Fourier, they constitute a non-zero or finite speed of heat propagation. Joseph and Preziosi (1989) and Tzou (1997) asserted that they play a key role in the analysis of those phenomena which appear in responses considered to be transient at microscale level such as heat waves and delayed responses to thermal disturbances. The relevance of these models cannot be overemphasized. This is due to its crucial role in the modelling of heat transfer in nano-fluids-Wang and Wei (2009), laser irradiation of biological tissues, Zhou *et al*. (2009), bio-heat transfer during thermal therapy, Xu*et al*. (2008) and in ultra-fast laser processing of thin-film engineering structures, Qiu and Tien (1992) and Qiu and Tien (1993).

Meanwhile, Tzou (1995a, 1995b), proposed a very vital non-Fourier heat conduction model called the dual-phase-lag (DPL). The DPL heat conduction model as proposed by Tzou was captured mathematically as:

$$\vec{q}(t'+\tau_q^*,\vec{r}) = -k\vec{\nabla}T(t'+\tau_T^*,\vec{r})$$

(2.1.1)

Where τ_T^* and τ_q^* are the phase lags in the temperature gradient and flux vector, respectively. If $\tau_T^* > \tau_q^*$, the temperature gradient in the material is the resultant effect of the heat flow, which makes the heat flux vector the cause and temperature gradient the effect. On the other hand, if $\tau_q^* > \tau_T^*$, then heat flow is induced by temperature gradient, thereby making the heat flux vector the effect while temperature gradient is the cause. If the temperature gradient phase lag τ_T^* is absent (τ_T^*=0), equation (2.1.1) reduces to the well-known Cattaneo–Vernotte model of hyperbolic heat

conduction, Cattaneo (1958), while the absence of both phase lags ($\tau_q^* = \tau_T^* = 0$) reduces equation (2.1.1) to the classical parabolic heat equation employing Fourier's law.

2.6 Suction/Injection

Nowadays, the unsteady MHD free-convection flow dominated by the effect of suction or injection has become a feasting ground for many researchers. For example, the suction or blowing process has its relevance in many engineering activities such as thermal oil recovery and in the design of thrust bearing and radial diffusers. Suction is applied to chemical processes to remove reactants and injection is used to add reactants, cool the surface, prevent corrosion or scaling and reduce the drag, Labroopulu*et al*. (1996). Attia(2010), illustrated the effect of suction and injection on Couette flow with variable properties. Ahmed and Khatun(2013), carried out a theoretical analysis on Magnetohydrodynamic oscillatory flow in a planer porous channel with suction and injection. Mutuku-Njane and Makinde(2013) examined the effect of magnetic field on boundary layer flow with slip boundary condition in the presence of suction. Makinde*et al*. (2011) studied the unsteady flow of reactive variable viscosity third-grade fluid between two parallel plates filled with a porous medium. Very recently, Jha*et al* (2016), analyzed the combined effect of suction/injection on MHD free-convection flow in a vertical channel with thermal radiation. They submitted that as radiation, temperature difference, suction/injection and non-dimensional time parameters increase both the velocity and temperature increase while velocity decreases with magnetic parameter.

2.7 Dufour effect

When heat and mass transfer are occurring simultaneously the relationship between the energy and mass fluxes and the driving potentials become more intricate in nature. In this case, rigorous studies have revealed that, the generation of energy flux is not dependent on only the temperature

gradient but also the concentration gradient. This is same for the generation of the mass flux as well. In an enlightened form, when heat transfer occurring in a fluid is as a result of the concentration gradient, the effect is called diffusion-thermo. This is also called the Dufour effect. Equivalently, when mass transfer occurring in a fluid is as a result of the temperature gradient, the effect is called thermal-diffusion. This is also called Soret effect. Many of the research works on heat and mass transfer have neglected the effects of Dufour and Soret on the heat and mass transfer under the assumption that they are negligible in magnitude than that prescribed by the Fourier's and Fick's laws. Recent advancement in heat and mass transfer shows that Dufour effect is important in transport problems while Soret effect is influential in mass transfer phenomenon. Soret and Dufour effects are also critical in various porous flow regimes occurring in chemical and geophysical systems. There are few studies about the Soret and Dufour effects in a Darcian or non-Darcian porous medium. Kafoussias and Williams (1995) presented thermal-diffusion and diffusion-thermo effects on mixed freeconvective and mass transfer boundary layer flow with temperature dependent viscosity. Postelnicu (2004) studied the influence of a magnetic field on heat and mass transfer by natural convection from vertical surfaces in porous media considering Soret and Dufour effects. Jha and Ajibade(2010) examined Dufour effects on free convection heat and mass transfer flow in a vertical channel while in another research work, Jha and Ajibade (2011) observed that diffusion-thermo effect exerts a very significant influence on the temperature and velocity distribution which transitivelyaffects Nusselt number, skin-friction and volume flow rate.Quite recently, Ajibade(2014) studied the effects of diffusion-thermo and dual-phase-lags on unsteady double-diffusive convection flow in a vertical microchannel filled with porous material. He concluded that as porosity increases within the channel, so does the

mass flux increase. Also, he added that mean temperature of the fluid could be increased by simultaneously growing the Dufour number and thermal retardation time, τ_T.

CHAPTER THREE

MATHEMATICAL MODELS

3.1 Flow formation and Geometry

Consider a fully developed unsteady natural convection flow of viscous, incompressible, electrically conducting fluid in a microchannel formed by two vertical plates under the influence of transverse magnetic field of uniform strength B_0 which is assumed to be applied in the direction perpendicular to that of the flow. The flow is assumed to be in the direction of x', which is taken vertically upward along the channel plates, and the y' axis is taken to be normal to the plates that are *h* distance apart.At the time $t' \le 0$, the fluid is to be at rest with the initial temperature T_0 and concentration C_0. At time $t' > 0$, the temperature as well as concentration on the wall $y' = 0$ are increased or decreased to T_{P_1} and C_{P_1} respectively where T_{P_1} is the isothermal heating with temperature jump and C_{P_1} also has concentration jump added to the constant application of concentration on the boundary. The temperature T_{P_2} and concentration C_{P_2} on the other plate $y' = h$ are maintained at T_0 and C_0 respectively with jumps. The geometry of the system under consideration in this present study is shown schematically in figure3.1.

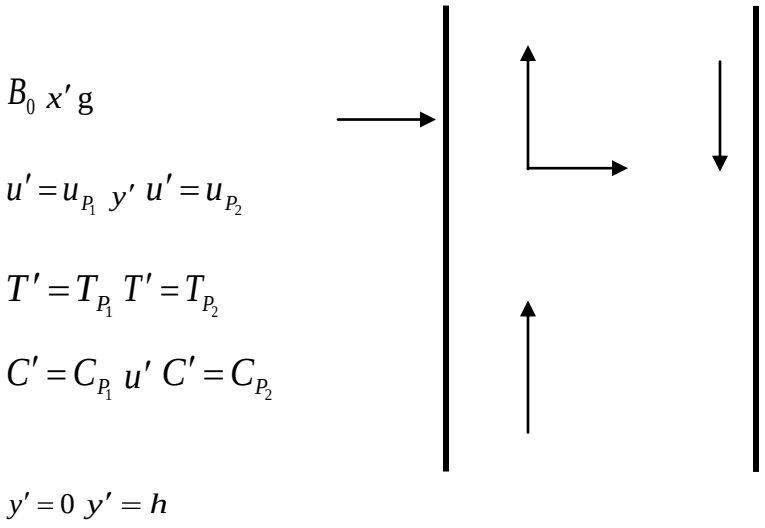


Figure 3.1. Schematic diagram of the problem (Case 1)

In the governing equations, the temperature is influenced by concentration of the introduced chemical species, leading to diffusion-thermo (Dufour) effect on the heat and mass transfer. Furthermore, just as in Ajibade (2014), the following assumptions were made in the present problem:

i. The flow is assumed to be fully developed in terms of concentration, thermally and hydrodynamically.
ii. The energy as well as concentration follows the DPL heat conduction model.
iii. Concentration jump, temperature jump and velocity slip are considered on the channel plates.

iv. Fluid temperature is governed by concentration of the chemical species introduced (i.e. Dufour effect)

3.2 Dual-Phase-Lag Heat Conduction with Convective Boundary

In addition to the flow situations as described in section 3.1, the boundary plates are assumed to allow thermal convection with the ambience so that fluid flow and thermodynamics within the channel is dependent on the isothermal heat input on the boundary as well as flux through the boundary plates. So, taking into consideration the above assumptions and using Boussinessq's approximation, the governing momentum equation, neglecting the induced magnetic field is given in dimensional form as:

$$\frac{\partial u'}{\partial t'} = \upsilon \frac{\partial^2 u'}{\partial y'^2} - \frac{\sigma B_0^2}{\rho} u' + g\beta(T' - T_0) + g\tilde{\beta}(C' - C_0) \qquad (3.2.1)$$

Using Taylor's series expansion of equation (2.1.1) with respect to time leads to the following equation

$$\vec{q} + \tau_q^* \frac{\partial \vec{q}}{\partial t'} = -k\left(\frac{\partial T'}{\partial y'} + \tau_T^* \frac{\partial^2 T'}{\partial t' \partial y'} \right) (3.2.2)$$

Equation (3.2.2) is combined with energy equation

$$-\frac{\partial \vec{q}}{\partial y'} = \rho C_P \frac{\partial T'}{\partial t'} \qquad (3.2.3)$$

where C_P is the specific heat of the material at constant pressure, ρ is its density and $\vec{q}$ is the heat flux.

Eliminating the heat flux from equations (3.2.2) and (3.2.3) and introducing the Dufour effect lead to the heat conduction equation under the DPL.

$$\tau_q^* \frac{\partial^2 T'}{\partial t'^2} + \frac{\partial T'}{\partial t'} = \frac{k}{\rho C_P}\left(\frac{\partial^2 T'}{\partial y'^2} + \tau_T^* \frac{\partial^3 T'}{\partial t' \partial y'^2} \right) + D_1 \frac{\partial^2 C'}{\partial y'^2} \qquad (3.2.4)$$

Applying the same procedure, having it in mind that the speed of propagation of the diffusing species is finite. The appropriate model for concentration equation is the DPL model which is given as:

$$\lambda_q^* \frac{\partial^2 C'}{\partial t'^2} + \frac{\partial C'}{\partial t'} = D_m \left(\frac{\partial^2 C'}{\partial y'^2} + \lambda_C^* \frac{\partial^3 C'}{\partial t' \partial y'^2} \right) \qquad (3.2.5)$$

Now, for boundary conditions on temperature, the same flux conditions in (3.2.2) is expected to be used where; $\vec{q} = H(T_w - T)$ on the plate $y = 0$ and $\vec{q} = H(T - T_0)$ on the plate $y = h$

With the initial conditions

$t' \le 0 : u' = 0,\ T' = T_0,\ C' = C_0$

For $t' > 0$, boundary conditions are:

$$\left.\begin{aligned} u' = u_{P_1} &= \frac{2-F}{F} \lambda \frac{\partial u'}{\partial y'} \\ T' = T_{P_1} &= T_w + \tau_q^* \frac{\partial T'}{\partial t'} + \left(\frac{k}{H} + \frac{2-F_T}{F_T} \frac{\lambda k}{\mu C_P} \right) \frac{\partial T'}{\partial y'} + \frac{\tau_T^* k}{H} \frac{\partial^2 T'}{\partial t' \partial y'} \text{ at } y' = 0 \\ C' = C_{P_1} &= C_w + \frac{2-F_C}{F_C} \frac{\lambda D_m \rho}{\mu} \frac{\partial C'}{\partial y'} \end{aligned}\right\}$$

$$\left.\begin{aligned} u' = u_{P_2} &= -\frac{2-F}{F} \lambda \frac{\partial u'}{\partial y'} \\ T' = T_{P_2} &= T_0 - \left[\tau_q^* \frac{\partial T'}{\partial t'} + \left(\frac{k}{H} + \frac{2-F_T}{F_T} \frac{\lambda k}{\mu C_P} \right) \frac{\partial T'}{\partial y'} + \frac{\tau_T^* k}{H} \frac{\partial^2 T'}{\partial t' \partial y'} \right] \text{ at } y' = h \\ C' = C_{P_2} &= C_0 - \frac{2-F_C}{F_C} \frac{\lambda D_m \rho}{\mu} \frac{\partial C'}{\partial y'} \end{aligned}\right\}$$

3.2.1 Dimensionless Analysis

Using the following dimensionless parameters;

$$y=\frac{y'}{h},\qquad t=\frac{t'\nu}{h^2},\qquad T=\frac{T'-T_0}{T_w-T_0},\qquad u=\frac{u'\nu}{g\beta h^2(T_w-T_0)},\qquad C=\frac{C'-C_0}{C_w-C_0},$$

$$Kn=\frac{\lambda}{h},\quad m^2=\frac{\sigma B_0^2 h^2}{\nu\rho},\quad N=\frac{\tilde{\beta}(C_w-C_0)}{\beta(T_w-T_0)},\quad D=\frac{D_1(C_w-C_0)}{\alpha(T_w-T_0)},\quad \Pr=\frac{\mu C_P}{k},\qquad (3.2.6)$$

$$Sc=\frac{\nu}{D_m},\qquad \tau_T=\frac{\tau_T^*\nu}{h^2},\qquad \lambda_C=\frac{\lambda_C^*\nu}{h^2},\qquad \tau_q=\frac{\tau_q^*\nu}{h^2},\qquad \lambda_q=\frac{\lambda_q^*\nu}{h^2},\qquad Bi=\frac{hH}{k}$$

Equations (3.2.1), (3.2.4) and (3.2.5) are then transformed into dimensionless forms as:

$$\frac{\partial u}{\partial t}=\frac{\partial^2 u}{\partial y^2}-m^2u+T+NC \qquad (3.2.7)$$

$$\tau_q\frac{\partial^2 T}{\partial t^2}+\frac{\partial T}{\partial t}=\frac{1}{\Pr}\left(\frac{\partial^2 T}{\partial y^2}+\tau_T\frac{\partial^3 T}{\partial t\partial y^2}\right)+\frac{D}{\Pr}\frac{\partial^2 C}{\partial y^2} \qquad (3.2.8)$$

$$\lambda_q\frac{\partial^2 C}{\partial t^2}+\frac{\partial C}{\partial t}=\frac{1}{Sc}\left(\frac{\partial^2 C}{\partial y^2}+\lambda_C\frac{\partial^3 C}{\partial t\partial y^2}\right) \qquad (3.2.9)$$

Subject to the initial conditions

$$t\le 0:\quad u=0,\ T=0,\ C=0 \qquad (3.2.10)$$

And boundary conditions:

$t>0$:

$$u=Kn\frac{\partial u}{\partial y},\quad T=1+\tau_q\frac{\partial T}{\partial t}+\left(\frac{1}{Bi}+\frac{Kn}{\Pr}\right)\frac{\partial T}{\partial y}+\frac{\tau_T}{Bi}\frac{\partial^2 T}{\partial t\partial y},\quad C=1+\frac{Kn}{Sc}\frac{\partial C}{\partial y}\ \text{at}\ y=0$$

(3.2.11)

$$u=-Kn\frac{\partial u}{\partial y},\quad T=-\left[\tau_q\frac{\partial T}{\partial t}+\left(\frac{1}{Bi}+\frac{Kn}{\Pr}\right)\frac{\partial T}{\partial y}+\frac{\tau_T}{Bi}\frac{\partial^2 T}{\partial t\partial y}\right],\quad C=-\frac{Kn}{Sc}\frac{\partial C}{\partial y}\ \text{at}\ y=1$$

Where *Bi* is the ratio of internal resistance of a body to heat conduction, to external resistance to heat convection, *m* is the ratio of electromagnetic force to the viscous force, *Pr* is the Prandtl number, *Kn* refers to the Knudsen number and *Sc* is the Schmidt number. A full list of all the physical quantities used in equation (3.1.6) are given in the nomenclature.

Setting $Bi \to \infty$, and $m = 0$, the results in the present problem coincide withthat investigated by Ajibade (2014) with $\gamma = 1$.

3.3 Dual-Phase-Lag Heat Conduction in a Vertical Porous Channel

By extension, using the same model above, we introduce suction/injection on the microchannel surfaces. Figure 3.2 below illustrates a geometrical representation of the system under consideration for this present study.

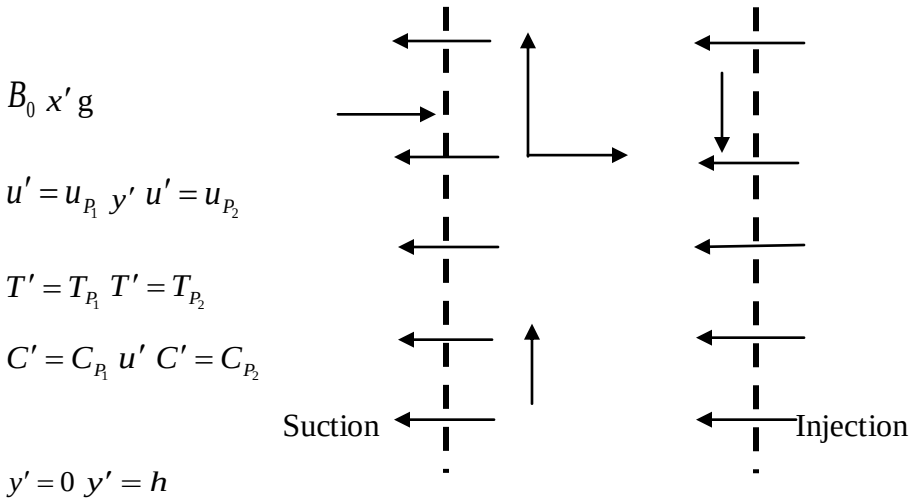


Figure 3.2. Schematic diagram of the problem (Case 2)

Now, taking into account the aforementioned assumptions and the usual Boussinessq's approximation, the governing momentum equation, neglecting the induced magnetic field between two vertical porous plates is given in dimensional form as:

$$\frac{\partial u'}{\partial t'} - \nu_0 \frac{\partial u'}{\partial y'} = \upsilon \frac{\partial^2 u'}{\partial y'^2} - \frac{\sigma B_0^2}{\rho} u' + g\beta(T' - T_0) + g\tilde{\beta}(C' - C_0) \quad (3.3.1)$$

Applying Taylor's series expansion of equation (2.1) with respect to time results to the following equation

$$\vec{q} + \tau_q^* \frac{\partial \vec{q}}{\partial t'} - \nu_0 \rho C_P \frac{\partial T'}{\partial y'} = -k\left(\frac{\partial T'}{\partial y'} + \tau_T^* \frac{\partial^2 T'}{\partial t' \partial y'}\right) \qquad (3.3.2)$$

Equation (3) is combined with energy equation

$$-\frac{\partial \vec{q}}{\partial y'} = \rho C_P \frac{\partial T'}{\partial t'} \qquad (3.3.3)$$

where C_P is the specific heat of the material at constant pressure and ρ is its density.

Eliminating the heat flux from equations (3.3.2) and (3.3.3) and introducing the Dufour effect and heat generation lead to the heat conduction equation under the DPL.

$$\tau_f^* \frac{\partial^2 T'}{\partial t'^2} + \frac{\partial T'}{\partial t'} - \nu_0 \frac{\partial T'}{\partial y'} = \frac{k}{\rho C_P}\left(\frac{\partial^2 T'}{\partial y'^2} + \tau_T^* \frac{\partial^3 T'}{\partial t' \partial y'^2} + \frac{H_0}{k}(T' - T_0)\right) + D_1 \frac{\partial^2 C'}{\partial y'^2} \qquad (3.3.4)$$

Using the same technique and bearing in mind the fact that speed of propagation of the diffusing species is finite. The appropriate model for concentration equation is the DPL model which is given as:

$$\lambda_f^* \frac{\partial^2 C'}{\partial t'^2} + \frac{\partial C'}{\partial t'} - \nu_0 \frac{\partial C'}{\partial y'} = D_m\left(\frac{\partial^2 C'}{\partial y'^2} + \lambda_C^* \frac{\partial^3 C'}{\partial t' \partial y'^2}\right) \qquad (3.3.5)$$

With the initial conditions

$t' \le 0 : u' = 0,\ \ T' = T_0,\ \ C' = C_0$

For $t' > 0$, boundary conditions are:

$$u' = u_{P_1} = \frac{2-F}{F}\lambda \frac{du'}{dy'}, \qquad T' = T_{P_1} = T_w + \frac{2-F_T}{F_T}\frac{\lambda k}{\mu C_P}\frac{dT'}{dy'}, C' = C_{P_1} = C_w + \frac{2-F_C}{F_C}\frac{\lambda D_m \rho}{\mu}\frac{dC'}{dy'} \text{ at}$$

$y' = 0$

$$u' = u_{P_2} = -\frac{2-F}{F}\lambda\frac{du'}{dy'}, \quad T' = T_{P_2} = T_0 - \frac{2-F_T}{F_T}\frac{\lambda k}{\mu C_P}\frac{dT'}{dy'}, \quad C' = C_{P_2} = C_0 - \frac{2-F_C}{F_C}\frac{\lambda D_m \rho}{\mu}\frac{dC'}{dy'}$$

at $y' = h$

3.3.1 Governing Equations in dimensionless form

Using the dimensionless parameters as defined in (3.2.6), equations (3.3.1), (3.3.4) and (3.3.5) are then transformed into dimensionless forms as:

$$\frac{\partial u}{\partial t} - S\frac{\partial u}{\partial y} = \frac{\partial^2 u}{\partial y^2} - m^2 u + T + NC \qquad (3.3.6)$$

$$\tau_f \frac{\partial^2 T}{\partial t^2} + \frac{\partial T}{\partial t} - S\frac{\partial T}{\partial y} = \frac{1}{\Pr}\left(\frac{\partial^2 T}{\partial y^2} + \tau_T \frac{\partial^3 T}{\partial t \partial y^2} + \delta T\right) + \frac{D}{\Pr}\frac{\partial^2 C}{\partial y^2} \qquad (3.3.7)$$

$$\lambda_f \frac{\partial^2 C}{\partial t^2} + \frac{\partial C}{\partial t} - S\frac{\partial C}{\partial y} = \frac{1}{Sc}\left(\frac{\partial^2 C}{\partial y^2} + \lambda_C \frac{\partial^3 C}{\partial t \partial y^2}\right) \qquad (3.3.8)$$

Subject to the initial conditions

$$t \le 0: \quad u = 0, \ T = 0, \ C = 0 \qquad (3.3.9)$$

And boundary conditions:

$$\left.\begin{aligned} t > 0: \ u = Kn\frac{\partial u}{\partial y}, \ T = 1 + \frac{Kn}{\Pr}\frac{\partial T}{\partial y}, \ C = 1 + \frac{Kn}{Sc}\frac{\partial C}{\partial y} \quad &\text{at } y = 0 \\ u = -Kn\frac{\partial u}{\partial y}, \ T = -\frac{Kn}{\Pr}\frac{\partial T}{\partial y}, \ C = -\frac{Kn}{Sc}\frac{\partial C}{\partial y} \quad &\text{at } y = 1 \end{aligned}\right\} \qquad (3.3.10)$$

Where $\delta = \frac{H_0 h^2}{k}$ is the heat source parameter and $S = \frac{v_0 h}{\nu}$ is the suction/injection parameter. A full list of all the physical quantities used in equation (3.2.6) are given in the nomenclature.

Setting $S = 0$, $\delta = 0$ and $m = 0$, the results in the present problem agree with those in Ajibade (2014) with $\gamma = 1$.

CHAPTER FOUR

SOLUTIONS TO THE PROBLEMS

4.1 Solution to the Problem on Convective Boundary Condition

By introducing the Laplace transform of the dimensionless velocity, temperature and concentration equations, John (1985),

$V(y,s)=\int_0^\infty u(y,t)e^{-st}dt$, $\Theta(y,s)=\int_0^\infty T(y,t)e^{-st}dt$ and $\Phi(y,s)=\int_0^\infty C(y,t)e^{-st}dt$, (where s is the Laplace parameter) and by applying the properties of Laplace transforms, equations (3.2.7)–(3.2.9) subject to the initial condition (3.2.10) give

$$\frac{d^2V}{dy^2}-E_1V=-(\Theta+N\Phi)$$

(4.1.1)

$$\frac{d^2\Theta}{dy^2}-B_{10}\Theta=B_{11}e^{y\sqrt{B_3}}+B_{12}e^{-y\sqrt{B_3}}$$

(4.1.2)

$$\frac{d^2\Phi}{dy^2} - B_3\Phi = 0$$

(4.1.3)

while the boundary conditions (3.2.11) are transformed as:

$t > 0$:

$$\left.\begin{aligned} V = Kn\frac{dV}{dy},\ \ \Theta = \frac{1}{s} + \tau_q s\Theta + \left(\frac{1}{Bi} + \frac{Kn}{\Pr}\right)\frac{d\Theta}{dy} + \frac{s\tau_T}{Bi}\frac{d\Theta}{dy},\ \ \Phi = \frac{1}{s} + \frac{Kn}{Sc}\frac{d\Phi}{dy} \text{ at } y = 0 \\ V = -Kn\frac{dV}{dy},\ \ \Theta = -\tau_q s\Theta - \left(\frac{1}{Bi} + \frac{Kn}{\Pr} + \frac{s\tau_T}{Bi}\right)\frac{d\Theta}{dy}, \Phi = -\frac{Kn}{Sc}\frac{d\Phi}{dy} \text{ at } y = 1 \end{aligned}\right\} \quad (4.1.4)$$

Now, using the boundary conditions (4.1.4), the solutions of (4.1.1)-(4.1.3) in Laplace domain are obtained as:

$$V = C_5 e^{y\sqrt{E_1}} + C_6 e^{-y\sqrt{E_1}} + E_2 e^{y\sqrt{B_3}} + E_3 e^{-y\sqrt{B_3}} + E_4 e^{y\sqrt{B_{10}}} + E_5 e^{-y\sqrt{B_{10}}} + E_6 e^{y\sqrt{B_3}} + E_7 e^{-y\sqrt{B_3}}$$

(4.1.5)

$$\Theta = C_3 e^{y\sqrt{B_{10}}} + C_4 e^{-y\sqrt{B_{10}}} + B_{13} e^{y\sqrt{B_3}} + B_{14} e^{-y\sqrt{B_3}}$$

(4.1.6)

$$\Phi = C_1 e^{y\sqrt{B_3}} + C_2 e^{-y\sqrt{B_3}}$$

(4.1.7)

Where B_i: i=1, 2, 3,…, 26, C_i: i=1, 2, 3,…,6 and E_i: i=1, 2, 3,…, 25 are defined in the Appendix A.

4.1.1 Riemann Sum Approximation

In a bid to determine the concentration, temperature and velocity of fluid in the time domain, equations (4.1.5)–(4.1.7) are to be inverted. However, since the inversion of these equations in

closed form are a bit cumbersome, a numerical inversion based on the Riemann-sum approximation as used in Khadrawi and Al-Nimr (2007) is employed. In this method, functions in the Laplace domain *s* can be inverted to the time domain *t* as follows:

$$u(y,t) = \frac{e^{\varepsilon t}}{t}\left(\frac{1}{2}V(y,\varepsilon) + \mathrm{Re}\sum_{k=1}^{N}(-1)^k V\left(y, \varepsilon + \frac{ik\pi}{t}\right)\right)$$

(4.1.8)

$$T(y,t) = \frac{e^{\varepsilon t}}{t}\left(\frac{1}{2}\Theta(y,\varepsilon) + \mathrm{Re}\sum_{k=1}^{N}(-1)^k \Theta\left(y, \varepsilon + \frac{ik\pi}{t}\right)\right)$$

(4.1.9)

$$C(y,t) = \frac{e^{\varepsilon t}}{t}\left(\frac{1}{2}\Phi(y,\varepsilon) + \mathrm{Re}\sum_{k=1}^{N}(-1)^k \Phi\left(y, \varepsilon + \frac{ik\pi}{t}\right)\right)$$

(4.1.10)

where Re refers to the ‘‘real part of’’ and $\sqrt{-1}$ is the imaginary number, *N* is the number of terms used in the Riemann-sum approximation and ε is the real part of the Bromwich contour that is used in inverting Laplace transforms. The Riemann-sum approximation for the Laplace inversion involves a single summation for the numerical process. Its accuracy depends on the value of ε and the truncation error dictated by *N*. The value of ε must be selected so that the Bromwich contour encloses all the branch points as in Kafoussias and Williams (1995). For faster convergence, however, numerous numerical experiments have shown that a value satisfying the relation $\varepsilon t \cong 4.7$ gives the most satisfactory results as seen in Khadrawi and Al-Nimr (2007). Hence, the appropriate value of ε for faster convergence depends on the instant of time (*t*) at which the lagging phenomenon is studied. The criterion shown by $\varepsilon t \cong 4.7$ is

independent of the value of *t*. The number *N* of terms used in the Riemann-sum is determined. Thus, a prescribed threshold for the accumulated partial sum is satisfied at given values of ε, y and *t*.

4.1.2 Sherwood Number

This represents the rate of mass transfer of chemical species on the boundary. In order to capture this phenomenon, equation (4.1.7) is differentiated with respect to space on the surface of both boundaries to obtain:

$$\widetilde{Sh} = \frac{d\Phi}{dy} = \sqrt{B_3}\left(C_1 e^{y\sqrt{B_3}} - C_2 e^{-y\sqrt{B_3}}\right) \tag{4.1.11}$$

Setting $y = 0$ and $y = 1$ in equation (4.1.11), Sherwood number on the boundary surfaces are defined as:

$$\widetilde{Sh}_0 = \left.\frac{dC}{dy}\right|_{y=0} \quad \text{and} \quad \widetilde{Sh}_1 = \left.\frac{dC}{dy}\right|_{y=1} \tag{4.1.12a}$$

So, in time domain, $$Sh(y,t) = \frac{e^{\varepsilon t}}{t}\left(\frac{1}{2}\widetilde{Sh}(y,\varepsilon) + \mathrm{Re}\sum_{k=1}^{N}(-1)^k \widetilde{Sh}\left(y, \varepsilon + \frac{ik\pi}{t}\right)\right) \tag{4.1.12b}$$

4.1.3 Nusselt Number

This defines the rate of heat transfer on the boundaries and it is obtained by differentiating equation (4.1.6) with respect to *y* as shown below:

$$\widetilde{Nu} = \frac{d\Theta}{dy} = \sqrt{B_{10}}\left(C_3 e^{y\sqrt{B_{10}}} - C_4 e^{-y\sqrt{B_{10}}}\right) + \sqrt{B_3}\left(B_{13} e^{y\sqrt{B_3}} - B_{14} e^{-y\sqrt{B_3}}\right) \tag{4.1.13}$$

Setting $y = 0$ and $y = 1$ in equation (4.1.13), the Nusselt number on both channel plates is obtained as:

$$\tilde{Nu}_0 = \left.\frac{d\Theta}{dy}\right|_{y=0} \quad \text{and} \quad \tilde{Nu}_1 = \left.\frac{d\Theta}{dy}\right|_{y=1}$$

(4.1.14a)

So, in time domain $Nu(y,t) = \frac{e^{\varepsilon t}}{t}\left(\frac{1}{2}\tilde{Nu}(y,\varepsilon) + \mathrm{Re}\sum_{k=1}^{N}(-1)^k \tilde{Nu}\left(y, \varepsilon + \frac{ik\pi}{t}\right)\right)$ (4.1.14b)

4.1.4 Skin Friction

Taking the derivative of the fluid velocity at the surfaces of the channel plates, the skin friction on the surface of the boundary plates is obtained as:

$$\tilde{\tau} = \frac{dV}{dy} = \sqrt{E_1}C_5 e^{y\sqrt{E_1}} - \sqrt{E_1}C_6 e^{-y\sqrt{E_1}} + \sqrt{B_3}E_2 e^{y\sqrt{B_3}} - \sqrt{B_3}E_3 e^{-y\sqrt{B_3}}$$
$$+ \sqrt{B_{10}}E_4 e^{y\sqrt{B_{10}}} - \sqrt{B_{10}}E_5 e^{-y\sqrt{B_{10}}} + \sqrt{B_3}E_6 e^{y\sqrt{B_3}} - \sqrt{B_3}E_7 e^{-y\sqrt{B_3}}$$

(4.1.15)

Setting $y = 0$ and $y = 1$ in equation (4.1.15), skin friction is obtained as:

$$\tilde{\tau}_0 = \left.\frac{dV}{dy}\right|_{y=0} \quad \text{and} \quad \tilde{\tau}_1 = \left.\frac{dV}{dy}\right|_{y=1}$$

(4.1.16a)

So, in time domain, $\tau(y,t) = \frac{e^{\varepsilon t}}{t}\left(\frac{1}{2}\tilde{\tau}(y,\varepsilon) + \mathrm{Re}\sum_{k=1}^{N}(-1)^k \tilde{\tau}\left(y, \varepsilon + \frac{ik\pi}{t}\right)\right)$ (4.1.16b)

4.1.5 Mass Flux

To obtain the mass flux within the channel, the following definite integral is evaluated

$$Q' = \frac{1}{Uh}\int_0^h u'dy' \qquad (4.1.17)$$

And presented in dimensionless form as

$$Q = \int_0^1 u dy \tag{4.1.18}$$

4.1.6 Mean Concentration

Mean concentration within the channel is obtained by evaluating the definite integral below:

$$C'_m = \frac{1}{(C_w - C_0)} \frac{\int_0^h u'(C' - C_0)dy'}{\int_0^h u'dy'}$$

(4.1.19)

It is presented in dimensionless form as:

$$C_m = \frac{\int_0^1 uCdy}{\int_0^1 udy}$$

(4.1.20)

4.1.7 Mean Temperature

Mean temperature of fluid within the channel is obtained by evaluating the following integral

$$T'_m = \frac{1}{(T_w - T_0)} \frac{\int_0^h u'(T' - T_0)dy'}{\int_0^h u'dy'}$$

(4.1.21)

Equation (4.1.21) is presented in dimensionless form as:

$$T_m = \frac{\int_0^1 uTdy}{\int_0^1 udy} \tag{4.1.22}$$

4.2 Solution to the Problem on Heat Generating Fluid in Porous Microchannel

Applying the properties of Laplace transforms, equations (3.3.6)–(3.3.8) subject to the initial conditions (3.3.9) give

$$\frac{d^2V}{dy^2} + S\frac{dV}{dy} - K_1 V = -(\Theta + N\Phi) \qquad (4.2.1)$$

$$\frac{d^2\Theta}{dy^2} + A_{16}\frac{d\Theta}{dy} - A_{17}\Theta = A_{18}e^{A_7 y} + A_{19}e^{A_8 y} \qquad (4.2.2)$$

$$\frac{d^2\Phi}{dy^2} + A_3\frac{d\Phi}{dy} - A_4\Phi = 0 \qquad (4.2.3)$$

while the boundary conditions (3.3.10) are transformed as:

$$\left.\begin{aligned} &t>0:\ V = Kn\frac{dV}{dy},\ \Theta = \frac{1}{s} + \frac{Kn}{\Pr}\frac{d\Theta}{dy},\ \Phi = \frac{1}{s} + \frac{Kn}{Sc}\frac{d\Phi}{dy} && \text{at } y=0 \\ &V = -Kn\frac{dV}{dy},\ \Theta = -\frac{Kn}{\Pr}\frac{d\Theta}{dy},\quad \Phi = -\frac{Kn}{Sc}\frac{d\Phi}{dy} && \text{at } y=1 \end{aligned}\right\} \qquad (4.2.4)$$

Employing the boundary conditions given in (4.2.4), the solutions of equations (4.2.1)-(4.2.3) in Laplace domain are found as:

$$V = C_5 e^{K_4 y} + C_6 e^{K_5 y} + K_6 e^{A_{26} y} + K_7 e^{A_{27} y} + K_8 e^{A_7 y} + K_9 e^{A_8 y} + K_{10} e^{A_7 y} + K_{11} e^{A_8 y} \qquad (4.2.5)$$

$$\Theta = C_3 e^{A_{26} y} + C_4 e^{A_{27} y} + A_{22} e^{A_7 y} + A_{24} e^{A_8 y} \qquad (4.2.6)$$

$$\Phi = C_1 e^{A_7 y} + C_2 e^{A_8 y} \qquad (4.2.7)$$

Where A_i: i=1, 2, 3,…, 38, C_i: i=1, 2, 3,…,6 and K_i: i=1, 2, 3,…, 21 are defined in Appendix A.

In a bid to determine the concentration, temperature and velocity of fluid in the time domain, equations (4.2.5)–(4.2.7) are to be inverted using the Riemann-sum approximation as presented in section 4.1.1.

4.2.1 Sherwood Number

In order to examine the rate of mass transfer of chemical species on the boundary, equation (4.2.7) is differentiated with respect to space on the surface of both boundaries to obtain:

$$\widetilde{Sh} = \frac{d\Phi}{dy} = A_7 C_1 e^{A_7 y} + A_8 C_2 e^{A_8 y}$$

(4.2.8)

Setting $y = 0$ and $y = 1$ in equation (4.2.8), Sherwood number on the boundary surfaces are defined as:

$$\widetilde{Sh}_0 = \left.\frac{dC}{dy}\right|_{y=0} \qquad \text{and} \qquad \widetilde{Sh}_1 = \left.\frac{dC}{dy}\right|_{y=1}$$

(4.2.9)

4.2.2 Nusselt Number

This defines the rate of heat transfer on the boundaries and it is obtained by differentiating equation (4.2.6) with respect to *y* as shown below:

$$\widetilde{Nu} = \frac{d\Theta}{dy} = C_3 A_{26} e^{A_{26} y} + C_4 A_{27} e^{A_{27} y} + A_7 A_{22} e^{A_7 y} + A_8 A_{24} e^{A_8 y} \qquad (4.2.10)$$

Setting $y = 0$ and $y = 1$ in equation (4.2.10), the Nusselt number on both channel plates is obtained as:

$$\widetilde{Nu}_0 = \left.\frac{d\Theta}{dy}\right|_{y=0} \qquad \text{and} \qquad \widetilde{Nu}_1 = \left.\frac{d\Theta}{dy}\right|_{y=1}$$

(4.2.11)

4.2.3 Skin Friction

Taking the derivative of the fluid velocity at the surfaces of the channel plates, the skin friction on the surface of the boundary plates is obtained as:

$$\tilde{\tau} = \frac{dV}{dy} = C_5 e^{K_4 y} + C_6 e^{K_5 y} + K_6 e^{A_{26} y} + K_7 e^{A_{27} y} + K_8 e^{A_7 y} + K_9 e^{A_8 y} + K_{10} e^{A_7 y} + K_{11} e^{A_8 y}$$

(4.2.12)

Setting $y = 0$ and $y = 1$ in equation (4.2.12), skin friction is obtained as:

$$\tilde{\tau}_0 = \left.\frac{dV}{dy}\right|_{y=0} \quad \text{and} \quad \tilde{\tau}_1 = \left.\frac{dV}{dy}\right|_{y=1}$$

(4.2.13)

It should be noted that the inversion of Sherwood number, Nusselt number and skin friction are also done in a similar way as in equations (4.1.12b), (4.1.14b) and (4.1.16b) respectively.

4.2.4 Mass Flux

To obtain the mass flux within the channel, the following definite integral is evaluated

$$Q' = \int_0^h u' dy' \qquad (4.2.14)$$

And presented in dimensionless form as

$$Q = \int_0^1 u dy \qquad (4.2.15)$$

4.2.5 Mean Concentration

Mean concentration within the channel is obtained by evaluating the definite integral below:

$$C'_m = \frac{1}{(C_w - C_0)} \frac{\int_0^h u'(C' - C_0)dy'}{\int_0^h u'dy'}$$

(4.2.16)

It is presented in dimensionless form as:

$$C_m = \frac{\int_0^1 uCdy}{\int_0^1 udy}$$

(4.2.17)

4.2.6 Mean Temperature

Mean temperature of fluid within the channel is obtained by evaluating the following integral

$$T'_m = \frac{1}{(T_w - T_0)} \frac{\int_0^h u'(T' - T_0)dy'}{\int_0^h u'dy'}$$

(4.2.18)

Equation (4.2.18) is presented in dimensionless form as:

$$T_m = \frac{\int_0^1 uTdy}{\int_0^1 udy} \text{(4.2.19)}$$

CHAPTER FIVE

RESULTS AND DISCUSSION

5.1 Convective Boundary Condition

The effect of dual-phase-lag on transient MHD natural convection heat and mass transfer flow in a vertical microchannel with convective boundary conditions was examined. Having solved the governing equations analytically in Laplace domain, the method of Riemann-sum approach is used to revert the transformed expressions to the time domain. The values obtained from the numerical inversion were presented graphically in figures 5.1.1–5.1.16 so that the influence of the different flow parameters such as Schmidt, Knudsen, Prandtl, Biotand Dufour numbers can easily be discussed. It should be noted that for the purpose of this discussion,the values of some dimensionless parameters have been defined within the ranges of $0.001 \le Kn \le 0.01$, $1 \le D \le 10$, $1 \le m \le 10$ and $1 \le Bi \le 10$. Meanwhile, the values of Prandtl numbers are chosen conveniently between 0.001 and 7.0 to accommodate some important fluids such as mercury, water vapour, airand water(Lienhard and Lienhard, 2006). Likewise, important diffusing species (for air) used

in this analysis are ammonia (*Sc*=0.78), hydrogen (*Sc*=0.22), water (*Sc*=0.60) and methanol (*Sc*=0.97) as seen in Gebhart and Pera (1971) and Jha and Ajibade (2011).

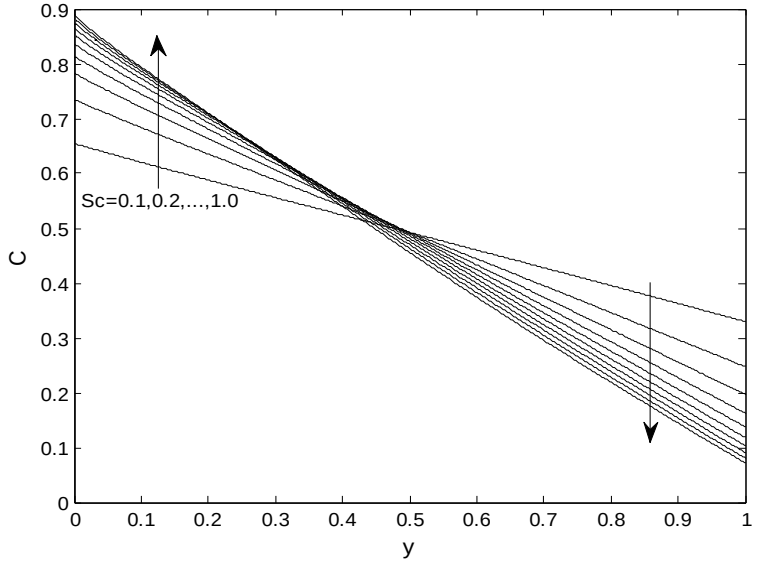


Figure 5.1.1a: Concentration profile for different *Sc*
(*Kn*=0.1, *t*=0.4, λ_q =0.001, λ_C =0.01)

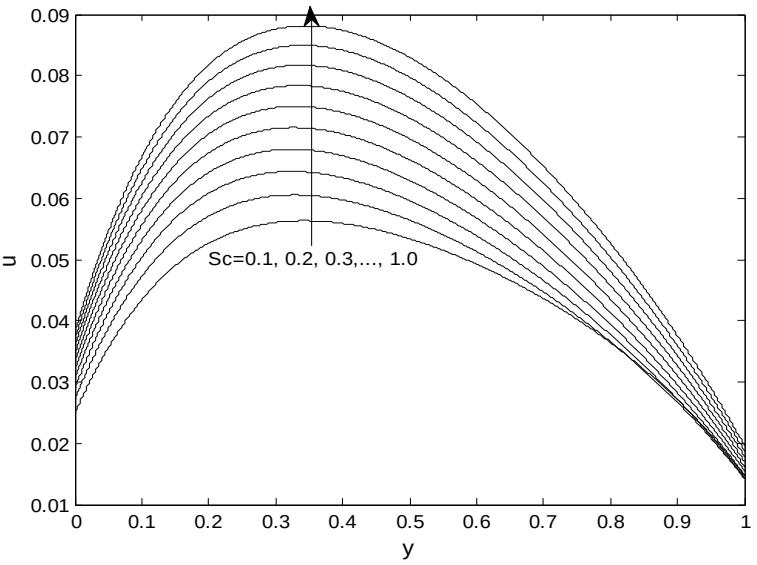


Figure 5.1.1b: Velocity profile for different *Sc*
(*Bi*=5, *t*=0.4, *D*=5, *N*=2, *Kn*=0.1, *Pr*=0.71, *m*=5)

Figure 5.1.1a shows the effect of Schmidt number on the concentration of chemical species. It isobserved from this figure thatfluid concentration jump decreases as *Sc* increases on both channel plates. This is evident because the jump conditions due to rarefaction imposed on the channel plates decreases with growing *Sc*. However, towards the centre of the channel, the effect of concentration to change in Schmidt number is almost negligible. A vivid picture of fluid velocity response to different Schmidt numbers is presented in figure 5.1.1b. It is observed that as Sc increases, fluid velocity rises as well within the channel. This is very obvious because increase in Schmidt number means a decrease in chemical concentration which causes an increase in fluid temperature owing to Dufour effect. This consequently builds up convection currents within the channel and velocity increase is the result.

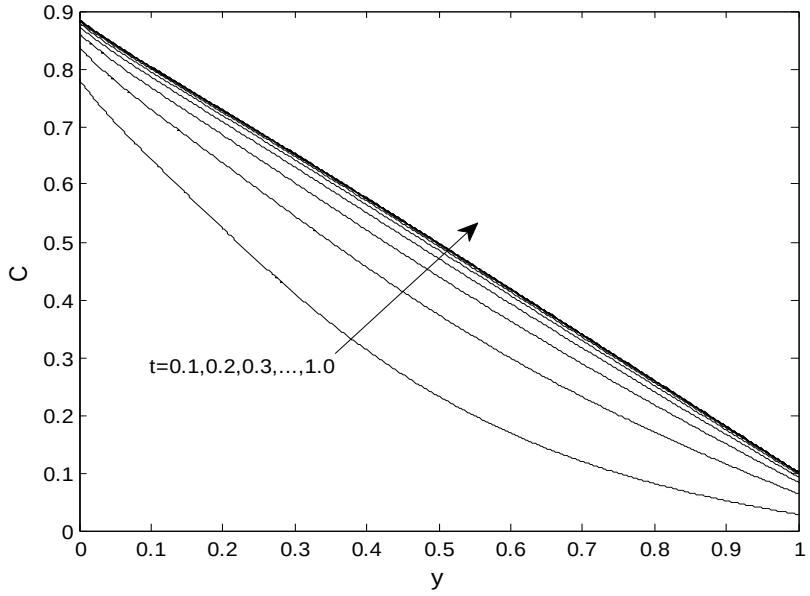


Figure 5.1.2a: Concentration profile for different *t*
(*Kn*=0.1, *Sc*=0.78, λ_C =0.01, λ_q =0.001)

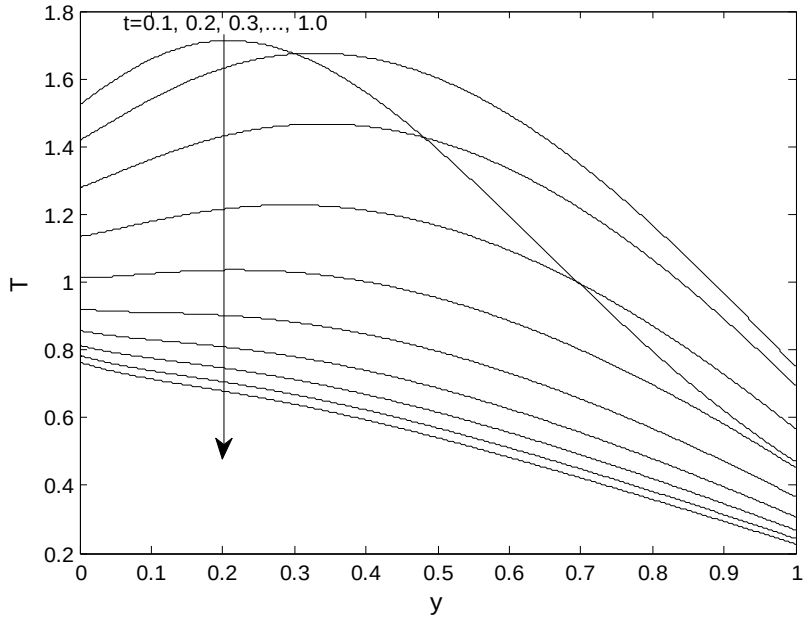


Figure 5.1.2b: Temperature profile for different *t*
(*Kn*=0.1, *Sc*=0.78, *Pr*=0.71, τ_T =0.01, τ_q =0.001, *D*=5, *Bi*=5)

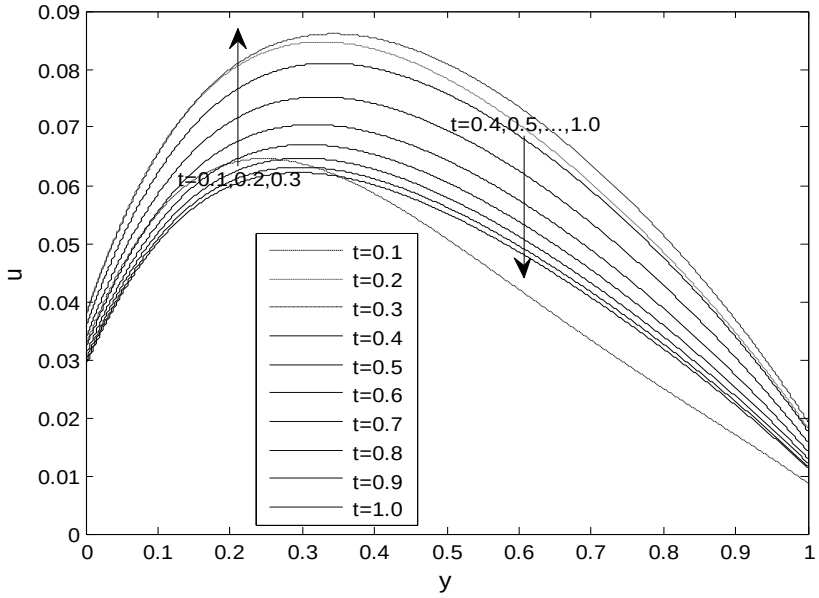


Figure 5.1.2c: Velocity profile for different *t*
(*Sc*=0.78, *D*=5, *N*=2, *Kn*=0.1, *Pr*=0.71, *Bi*=5, *m*=5)

In figure 5.1.2a, concentration profile for different time values is shown. Here, it can be seen that fluid concentration rises correspondingly to time. Moreso, the concentration level of the fluid

attains a steady state as time values grow bigger. Furthermore, thermal diffusivity of the fluid is observed to be decreasing as concentration grows with time due to Dufour effect consideration. This is evident in figure 5.1.2b in which temperature is observed to decrease as time increases. Meanwhile, two interesting scenarios play out in Figure 5.1.2c. Firstly, fluid velocity rises for smaller values of *t* and reaches a maximum. However, in the second case, we can see that as the values of *t* grows bigger, fluid velocity drops with further increase in time until it attains a steady state within the channel. This irregular behaviour is brought about by Dufour effects in which high temperature is obtained for small values of time while the temperature decreases and by extension, convection currents is weakened as time is increased further until the steady state is reached.

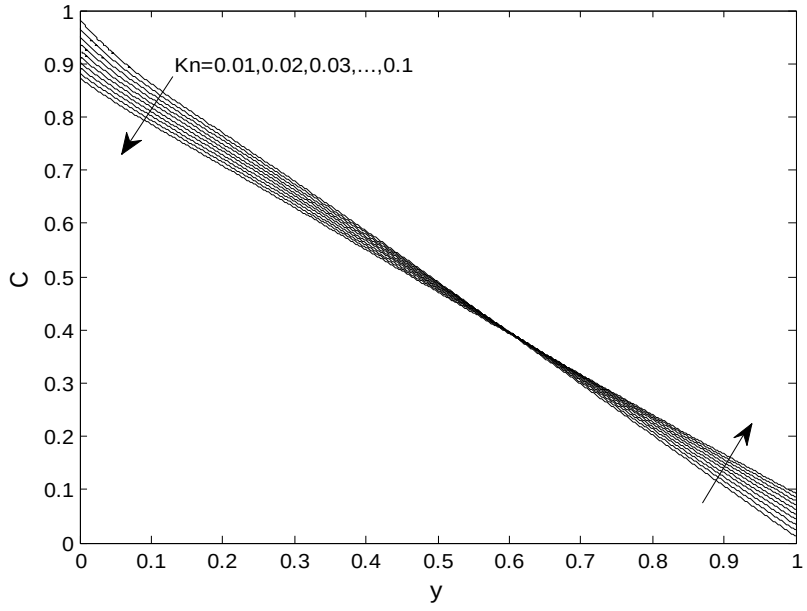


Figure 5.1.3a: Concentration profile for different *Kn*
(*Sc*=0.78, *t*=0.4, λ_C =0.01, λ_q =0.001)

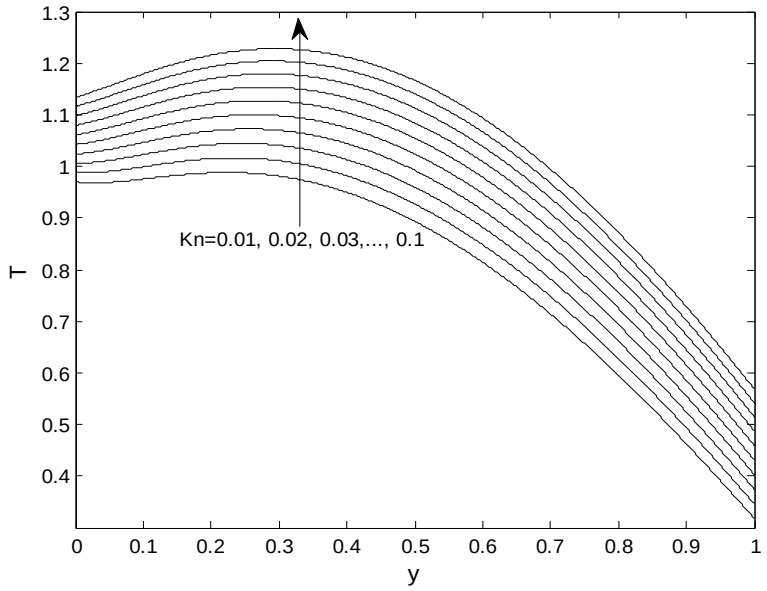


Figure 5.1.3b: Temperature profile for different *Kn*
(*Sc*=0.78, *t*=0.4, τ_T =0.01, τ_q =0.001, *Bi*=5, *D*=5)

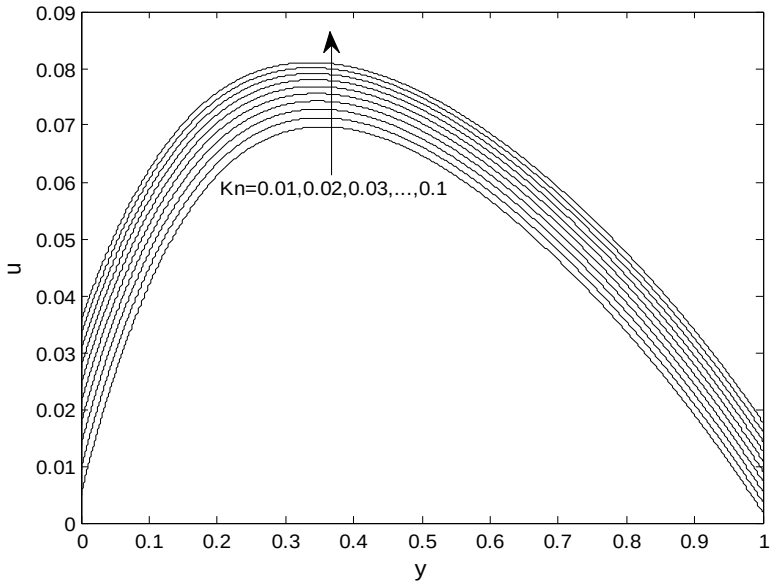


Figure 5.1.3c: Velocity profile for different *Kn*
(*Sc*=0.78, *Pr*=0.71,*N*=2, *m*=5, *Bi*=5, *D*=5)

The effect of rarefaction on fluid concentration is illustrated in figure 5.1.3a. It can be seen that as the boundary jump increases there is a decline in concentration of the fluid near the heated

plate whereas it increases near the cold plate. The physical interpretation of this phenomenon is that increase in Kn decreases the fluid-plate interaction on the boundary plates. Meanwhile, close to the centreline of the channel, the effect of concentration to varying Kn is not at all felt. Temperature is noticed to increase with rising fluid rarefaction within the channel as shown in figure 5.1.3b. This is due to a decrease in concentration (Figure 5.1.2a) which enhances thermal diffusivity (due to the Dufour effect) so that temperature increase is the result. In figure 5.1.3c, it can be observed that slip conditions on the plates has brought about an increase in hydrodynamic slip flow near both plates.

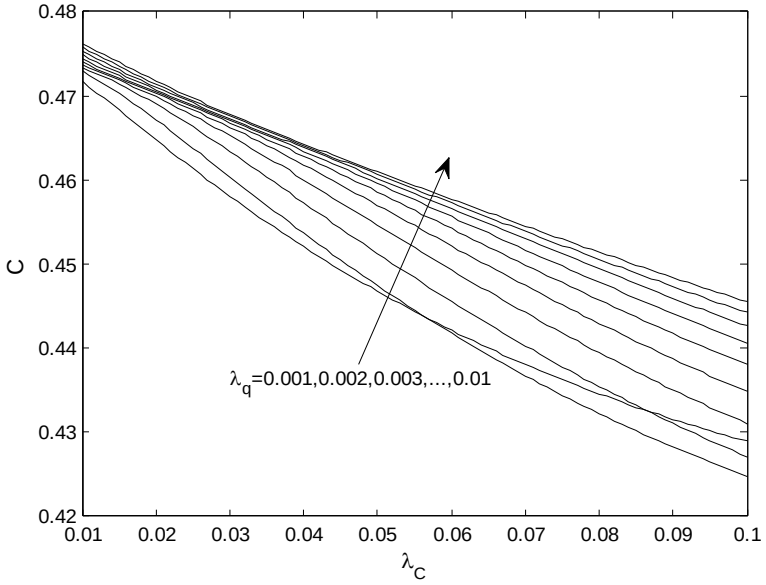


Figure 5.1.4: Cross-sectional concentration for different λ_q
(*Kn*=0.1, *Sc*=0.78, *t*=0.4, *y*=0.5, *m*=5)

Figures 5.1.4 – 5.1.6 show the effects of phase lags on chemical concentration, temperature and velocity. Figure 5.1.4 indicates that chemical concentration increases with increase in λ_q while it decreases within the channel as λ_C increases. This is very correct from a physical perspective because increasing the relaxation time (λ_q)for the flux of chemical speciedelays the diffusion of

the chemical specie and by implication builds up concentration. Moreso, increasing the mass retardation time implies that the speed of mass gradient change decreases and consequently lead to a decrease in chemical concentration.

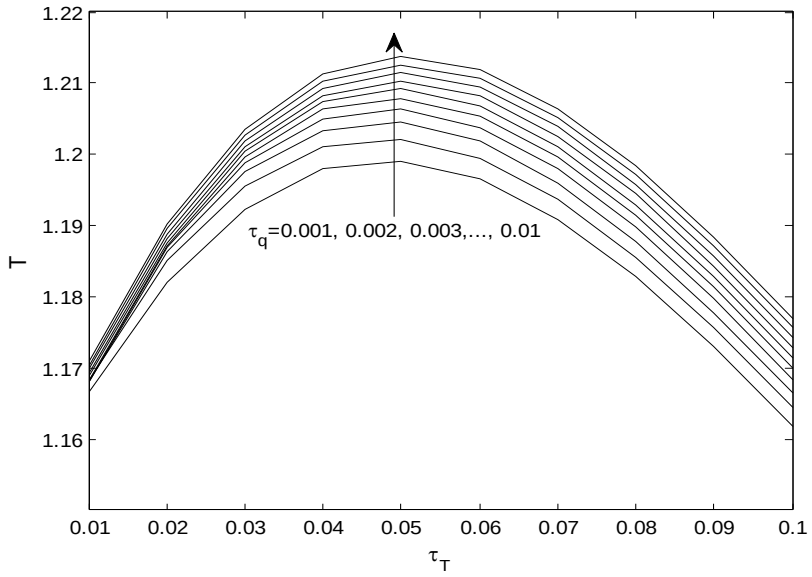


Figure 5.1.5: Cross-sectional temperature for different τ_q
(*Kn*=0.1, *Pr*=0.71, *t*=0.4, *y*=0.5, *Bi*=5, *m*=5, *D*=5)

Figure 5.1.5 describes a cross-sectional temperature variation with thermal relaxation time (τ_q). Here, it can be seen that as τ_T increases, temperature rises to a peak and then drops with further increase in τ_T. Also, it increases as τ_q grows in value. This however precipitates an accumulation of heat within the channel. Again, when τ_T assume small values, effect of τ_q is quite minimal but it becomes very prominent at higher values of τ_T. Meanwhile within the channel, as can be observed in figure 5.1.6, fluid velocity increases with an increase in τ_q whereas it falls as thevalues of τ_T becomes large. This is physically true since an increase in the

thermal relaxation contributes to an increase in fluid temperature which strengthens convection current and consequent increase in the velocity.

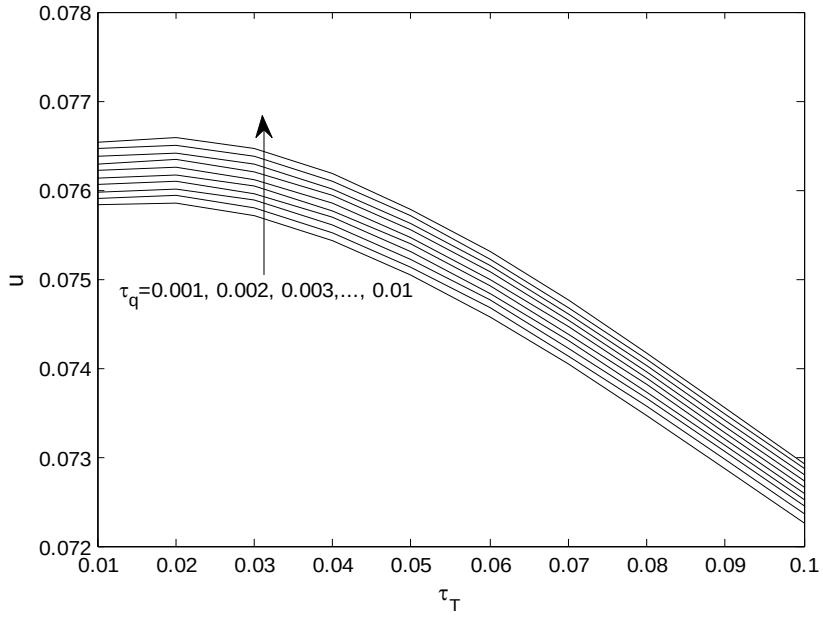


Figure 5.1.6: Cross-sectional velocity for different τ_q

(*Kn*=0.1, *Pr*=0.71, *t*=0.4, *y*=0.5, *Bi*=5, *m*=5, *D*=5)

The behaviour of thermal diffusivity on fluid temperature is illustrated in figure 5.1.7a. It is evident that the effect of temperature jump on the boundary plates is more pronounced on fluid with low *Pr* as well as towards the cold plate. Moreso, near the heated plate, temperature generally appears to rise significantly and the drops towards the cold plate. In figure 5.1.7b, the effect of Prandtl number on fluid velocity can be seen. It indicates that a decrease in fluid velocity is caused by increasing *Pr*. This is physically true since an increase in *Pr* decreases thermal diffusivity of the fluid which weakens the convection current due to heat transfer and hence decreases fluid velocity.

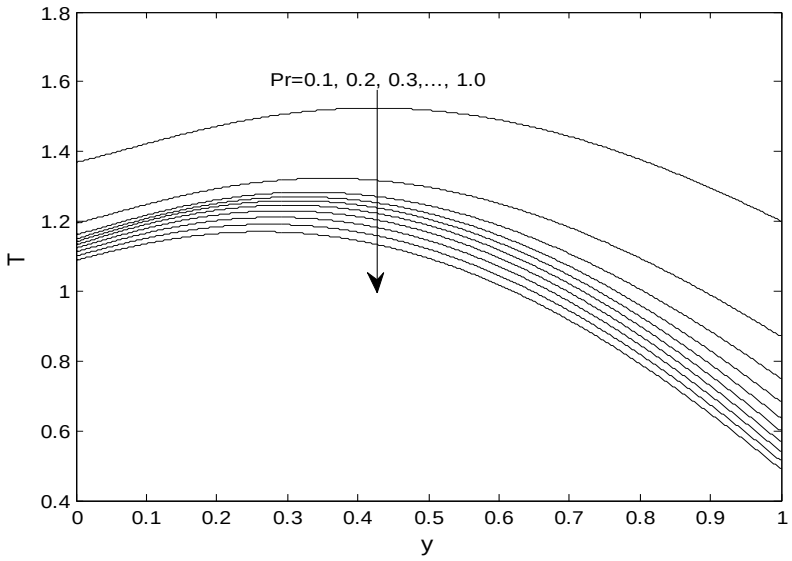


Figure 5.1.7a: Temperature profile for different *Pr*
(*Kn*=0.1, *t*=0.4, *Bi*=5, *D*=5)

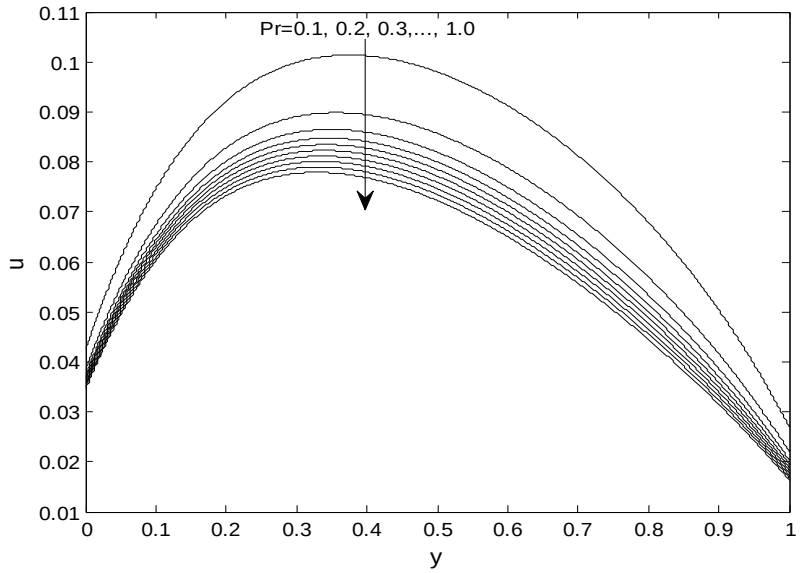


Figure 5.1.7b: Velocity profile for different *Pr*
(*Sc*=0.78, *t*=0.4, *D*=5, *N*=2, *Kn*=0.1, *Bi*=5, *m*=5)

The response of temperature and fluid velocity to diffusion-thermo effect is shown in figures 5.1.8a and 5.1.8b respectively. It is noticed that increasing Dufour number causes an increase in

temperature within the channel. This is very obvious because an increase in the Dufour effect acts

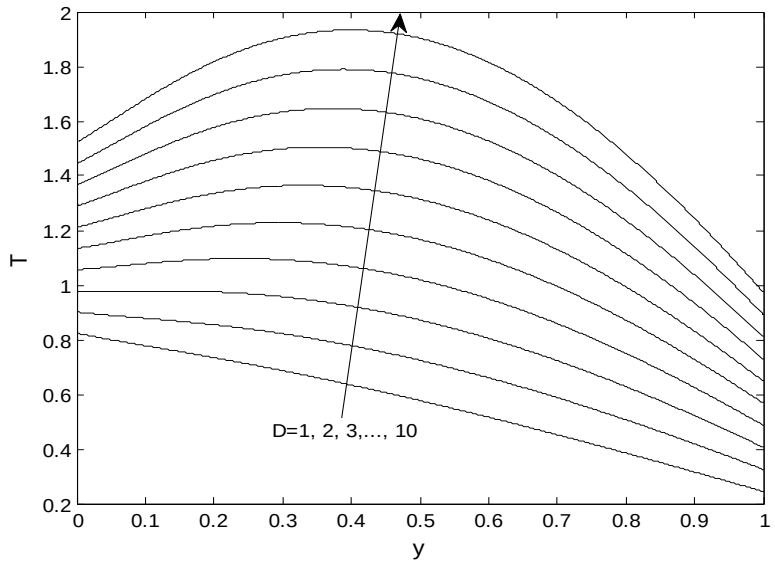


Figure 5.1.8a: Temperature profile for different *D*
(*Kn*=0.1, *Sc*=0.78, *t*=0.4, *Pr*=0.71, *Bi*=5)

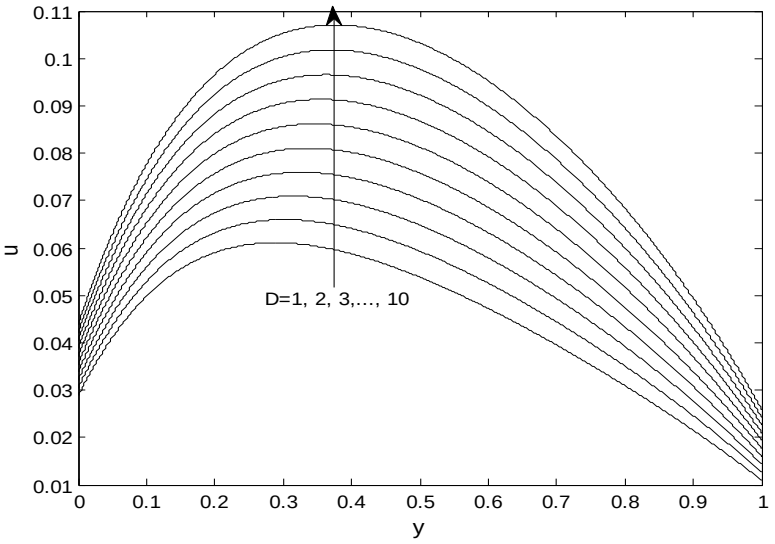


Figure 5.1.8b: Velocity profile for different *D*
(*Kn*=0.1, *Sc*=0.78, *Pr*=0.71, *t*=0.4, *Bi*=5, *N*=2)

to amplify the influence of chemical concentration on the temperature so that thermal diffusivity is enhanced leading to an increase in the fluid temperature. It is consequent upon the temperature increase that convection current become strenghtened so that velocity increases with an increase in the diffusion-thermo effect as shown in figure 5.1.8b.

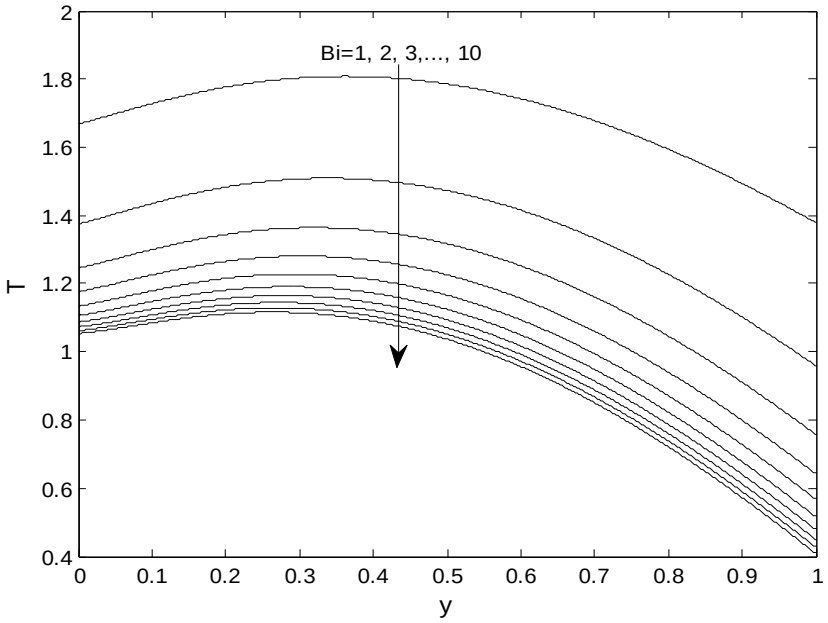


Figure 5.1.9a: Temperature profile for different *Bi*
(*Kn*=0.1, *Sc*=0.78, *t*=0.4, *Pr*=0.71, *D*=5)

Fluid temperature behaviour for different Biot numbers is shown in figure 5.1.9a. It is observed that fluid temperature declines as Biot number rises. This can be attributed to convective heat transfer at the plate surface. Again, temperature jump is noticed near the hot plate for low values of *Bi* while for higher values, fluid temperature decreases steadily. This is due to the reduction in the effect of boundary convection on fluid temperature as the Biot number increases. Hydrodynamic behaviour on varying convective heat exchange parameter is illustrated in figure 5.1.9b. Here, it is seen that fluid velocity decreases consistently by growing the values of *Bi*. The

figure further reveals a considerable reduction in the effect of *Bi* on velocity as the value of $Bi \to \infty$. This phenomenon is same as presented in Table 4.

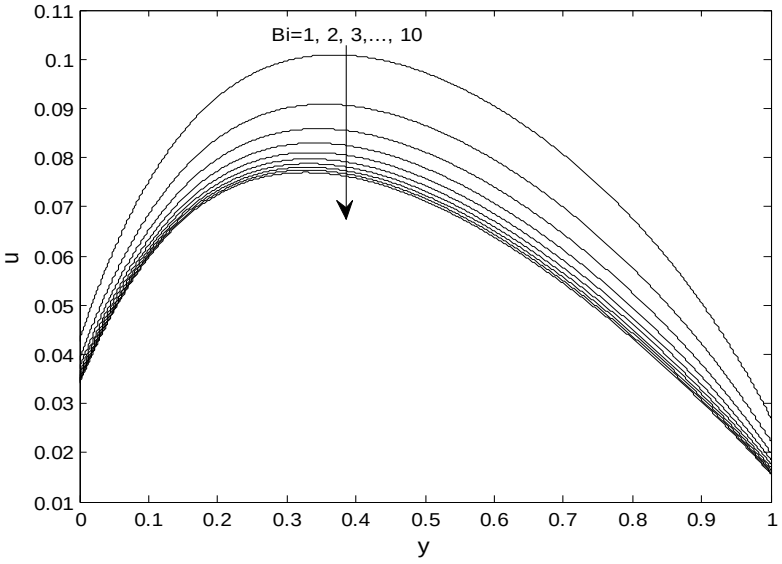


Figure 5.1.9b: Velocity profile for different *Bi*
(*Sc*=0.78, *t*=0.4, *D*=5, *N*=2, *Kn*=0.1, *Pr*=0.71, *m*=5)

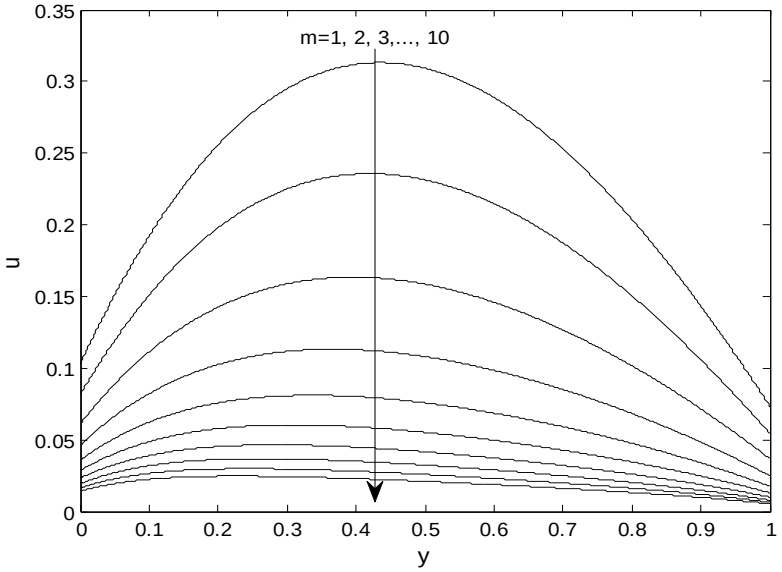


Figure 5.1.10: Velocity profile for different *m*
(*Kn*=0.1, *Sc*=0.78, *Pr*=0.71, *N*=2, *Bi*=5, *D*=5)

Figure 5.1.10 describes hydrodynamic response within the channel owing to variations in Hartmann number (*m*). Fluid velocity is observed to be decreasing and this is triggered by the rise in *m*. This is physically true due to the presence of transverse magnetic field which creates a resistive force known as Lorentz force. In other words, the Lorentz force set up by this magnetic field in the flow domain opposes the induced bouyancy force in the upward direction and as such the net force acting on the fluid reduces. Therefore fluid velocity is retarded. Meanwhile, as sustensation parameter ($N>0$) increases, fluid bouyancy due to mass transfer becomes strenghtened and this also imply an increase in its velocity as convection owing to mass transfer acts in favour of heat transfer. Such is the case in figure 5.1.11. On the other hand, when ($N<0$), convection due to mass transfer acts against that of heat transfer, hence, there is a decrease in bouyancy of the fluid as well as velocity.

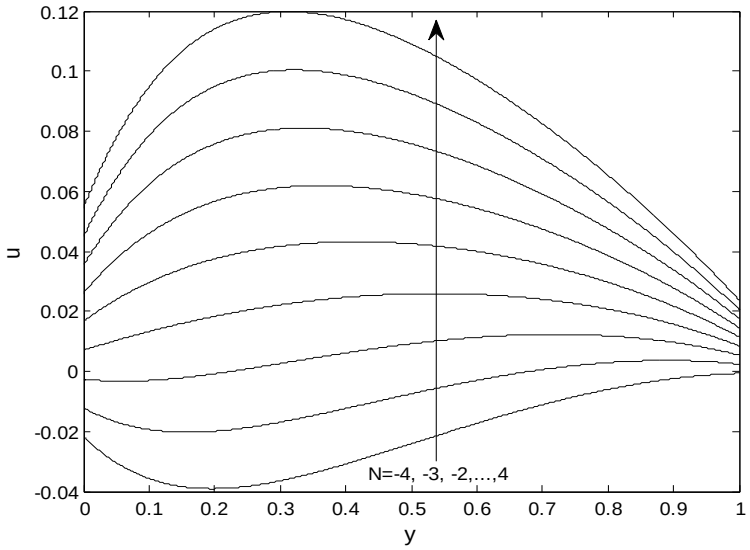


Figure 5.1.11: Velocity profile for different *N*
(*Kn*=0.1, *Sc*=0.78, *t*=0.4, *Pr*=0.71, *m*=5, *D*=5)

Figure 5.1.12 illustrates phase-lags effect on the transfer of chemical specie on the boundaries. On the heated plate ($y=0$), it can be observed that as both λ_C and flux relaxation time (λ_q)

increase, mass transfer increases. However the increament become more pronounced only when λ_q grows bigger. This is evident because increase in mass-flux relaxation time delays the flux of chemical species from plate to fluid so that concentration gradient between plates and fluid increases. On the cold plate (y=1), however, fluid chemical concentration and mass transfer are observed to be reducing as λ_C increases within the channel. Also, sherwood number was observed to decrease for small values of λ_q, reach a minimum value and then increase for further increase in λ_q. This local minimum which is observed when λ_C becomes very large is absent at small values of λ_C.

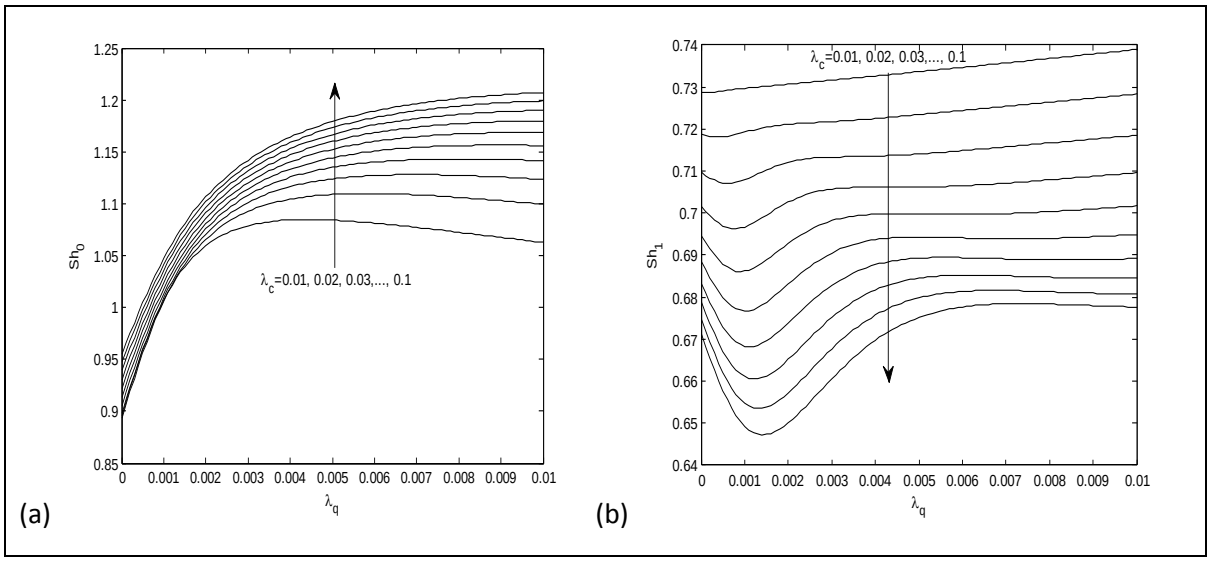


Figure 5.1.12: Sherwood number for different λ_C (Kn=0.1, Sc=0.78, t=0.4):

(a) heated plate and (b) cold plate

The effects of temperature jump and diffusion-thermo on heat transfer between the boundaries and the fluid are revealed in figure 5.1.13. Earlier, it was shown in figures 5.1.3b and 5.1.8a that fluid temperature rises due to an increase in Knudsen number as well as Dufour effects. This by

implication means that rising fluid temperature causes a decrease in temperature gradient towards the heated plate while it rises near the cold plate.

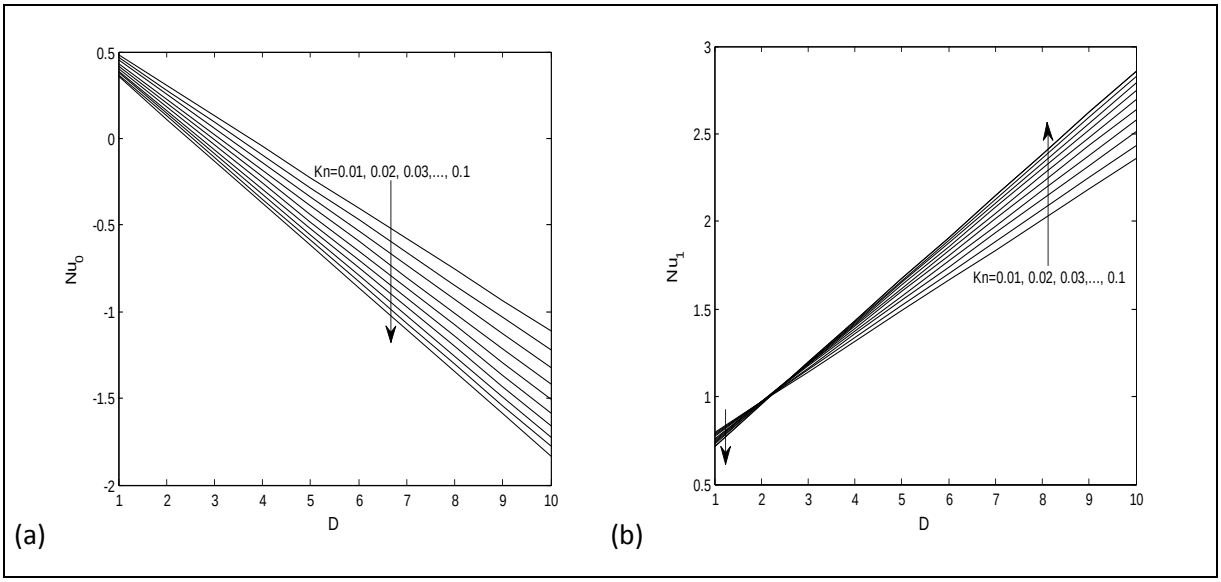


Figure 5.1.13: Nusselt number for different *Kn*(*Pr*=0.71, *Bi*=5, *t*=0.4, τ_q =0.001, τ_T =0.01):

(a) heated plate and (b) cold plate

From figure 5.1.14, it is observed that the rate of heat transfer decreases with growing thermal relaxation time (τ_q) at the heated plate. However, in the case of thermal retardation time (τ_T),there is an initial decrease in the rate of heat transfer while an increase is observed for larger values of τ_T. Meanwhile, a reversed trend is observed on the cold plate in which growing τ_q contributes an increase to the rate of heat transfer. Also, an initial increase in Nusselt number is seen for small values of τ_T while it decreases as τ_T grows further. The physical fact behind this is that growing τ_q causes a delay in the heat flux so that the rate of heat transfer decreases on the heated plate while it increases on the cold plate. However, the increase observed in the rate of

heat transfer on the cold plate could be attributed to thermal accumulation near the cold plate which increases with growing τ_q.

The behaviour of skin-friction with respect to variations in *Kn* is shown in figures 5.1.15(a) and (b). It is clear from figure 5.1.15(a) that the effect of increasing *Kn* is to decrease skin-friction on the surface of the heated plate. Furthermore, in figure 5.1.15(b), the impact of *Kn* is initially weak at *D*=2. Beyond that, skin-friction increases as *Kn* grows bigger in value. On the overall, the effect of higher Dufour number appear to be dominant at both plates since it increases skin-friction.

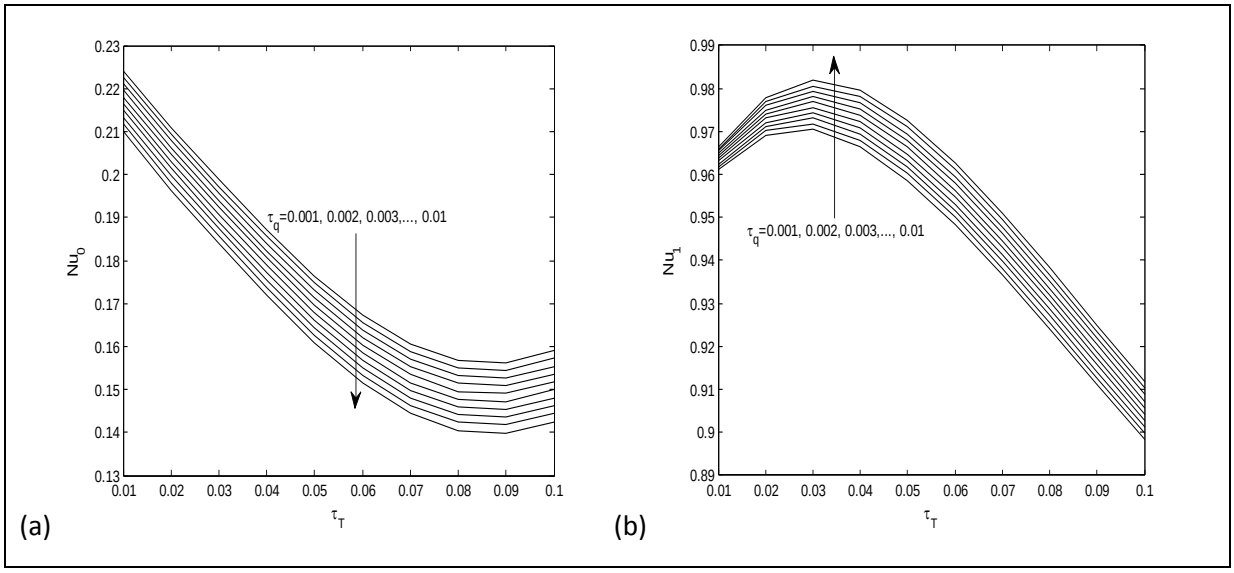


Figure 5.1.14: Nusselt numbervs τ_T for different τ_q (*Pr*=0.71, *Bi*=5, *t*=0.2, *D*=2):

(a) heated plate and (b) cold plate

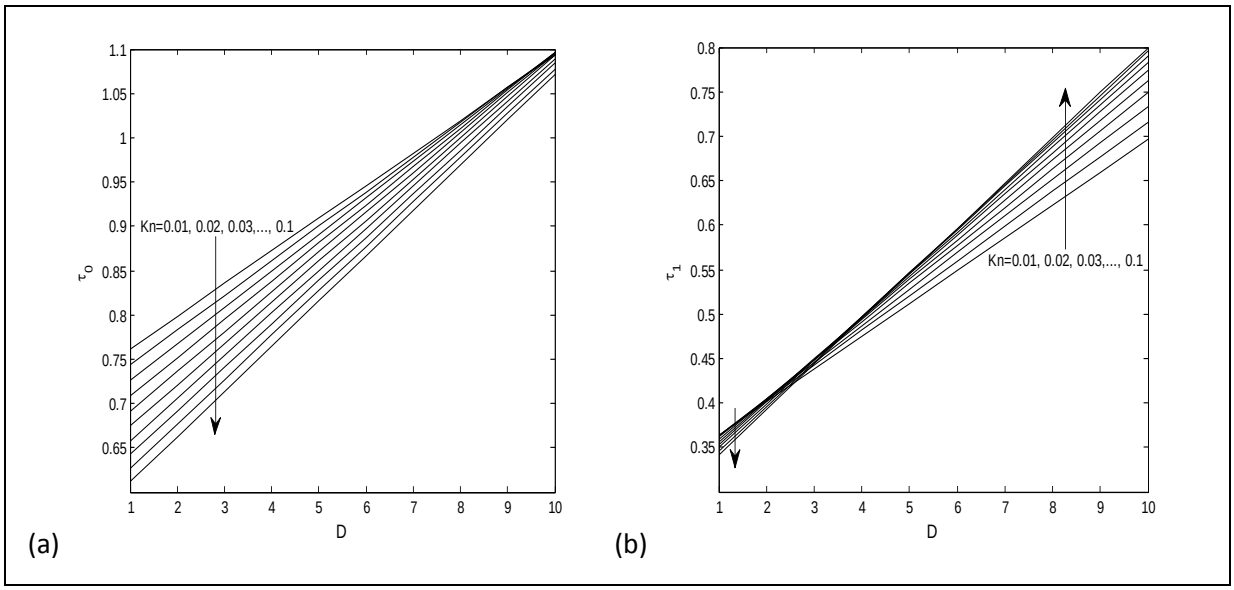


Figure 5.1.15: Skin-friction for different *Kn*(*Pr*=0.71, *N*=2, *t*=0.4, *D*=5, *m*=2):

(a) heated plate and (b) cold plate

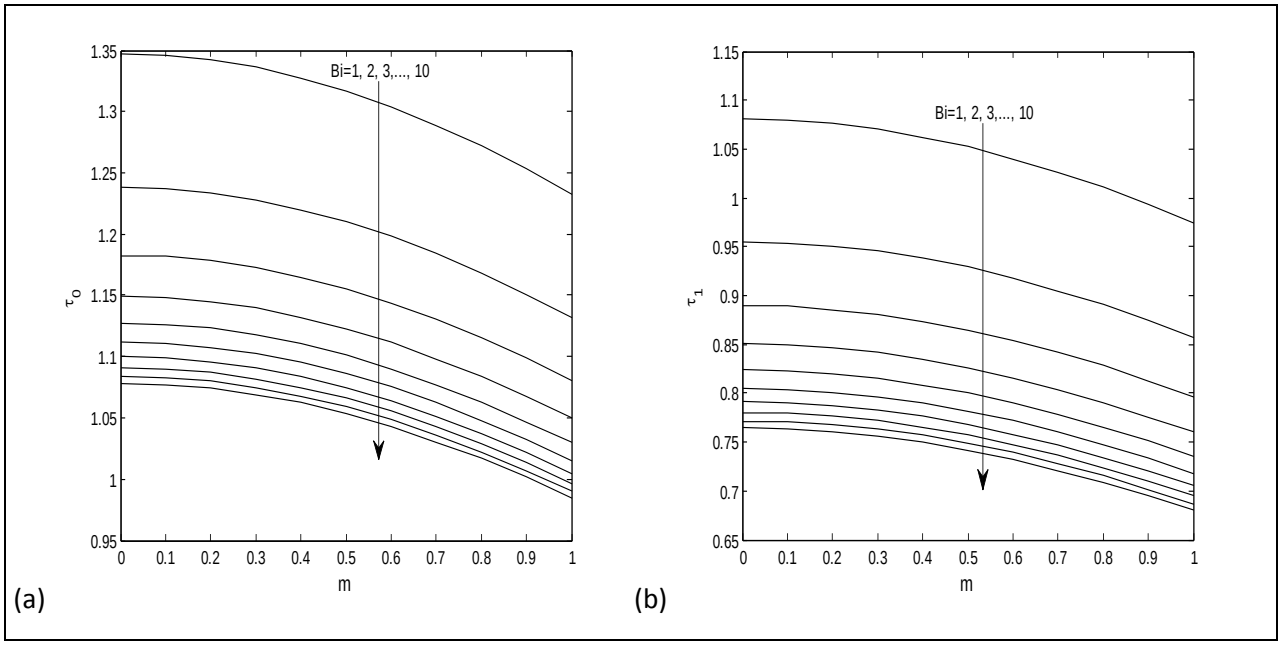


Figure 5.1.16: Skin-friction for different *Bi* (*Pr*=0.71, *N*=2, *t*=0.4, *D*=5):

(a) heated plate and (b) cold plate

One very striking phenomenon that can be noticed in figure 5.1.16 is that both *Bi* and m impact heavily on the skin-friction at both plates. It is observed that skin-friction reduces as both *Bi* and

m grow bigger in value. This can be attributed to convective heat transfer at the plate surface and also the resistive magnetic force (Lorentz force) on the fluid flow.

Using trapezoidal rule, equations (4.1.18), (4.1.20) and (4.1.22) are then evaluated numerically with $\Delta y_i = 0.001$. Numerical values from the simulation are tabulated and presented in Tables 1-3.

Table 1: Effect of different flow parameters on mass flux through the channel

t=0.2; Kn=0.01; τ_T=0.01							
		(Bi=5, D=1)		(Bi=5, D=10)		(Bi=10, D=10)	
τ_q		Pr=0.71	Pr=7	Pr=0.71	Pr=7	Pr=0.71	Pr=7
$\tau_q < \tau_T$	0.001	0.0923	0.0604	0.2412	0.0860	0.2175	0.0863
	0.004	0.0928	0.0605	0.2441	0.0862	0.2202	0.0865
	0.008	0.0935	0.0605	0.2482	0.0863	0.2241	0.0867
m=0.5							
$\tau_q > \tau_T$	0.02	0.0955	0.0605	0.2616	0.0867	0.2388	0.0871
	0.05	0.1011	0.0584	0.2780	0.0843	0.2699	0.0850
	0.07	0.0975	0.0553	0.3000	0.0801	0.8107	0.0810
$\tau_q < \tau_T$	0.001	0.0885	0.0580	0.2304	0.0826	0.2076	0.0828
	0.004	0.0890	0.0580	0.2332	0.0827	0.2102	0.0830
	0.008	0.0897	0.0581	0.2371	0.0829	0.2139	0.0832
m=1							
$\tau_q > \tau_T$	0.02	0.0917	0.0581	0.2501	0.0834	0.2282	0.0838
	0.05	0.0973	0.0563	0.2655	0.0813	0.2589	0.0820
	0.07	0.0940	0.0535	0.2882	0.0774	0.7907	0.0783

From Table 1, it is observed that increase in mass flux can be made possible by increasing the Dufour effect (*D*). However, the influence of Biot number on the mass flux is controlled by the type of fluid considered. For instance, in the presence of growing boundary convection, the mass flux decreases when the working fluid is air (*Pr*=0.71) while it increases when the working fluid is water (*Pr*=7.0).Meanwhile, the effect of an increase in the magnetic parameter (*m*) causes mass flux to drop within the channel. In addition, mass flux is seen to be on the rise with growing heat flux phase lag (τ_q) particularly when temperature gradient phase lag (τ_T) dominates heat flux phase lag (τ_q), (i.e. $\tau_q < \tau_T$). Conversely, a further delay of τ_q would lead to a decrease in mass flux (i.e. $\tau_q > \tau_T$).

Table 2: Effect of different flow parameters on mean concentration of chemical species.

t=0.2;					
		λ_C =0.01		λ_C =0.03	
	λ_q	Sc=0.78 Sc=0.97		Sc=0.78	Sc=0.97
$\lambda_q \le \lambda_C$	0.001	0.4873	0.4631	0.4785	0.4565
	0.005	0.4896	0.4650	0.4804	0.4582
	0.01	0.4926	0.4675	0.4827	0.4601
Kn=0.01					
$\lambda_q > \lambda_C$	0.04	0.5164	0.4827	0.5008	0.4740
	0.07	0.5290	0.4858	0.5175	0.4827
	0.09	0.5291	0.4826	0.5216	0.4826
$\lambda_q \le \lambda_C$	0.001	0.4368	0.4180	0.4315	0.4149
	0.005	0.4386	0.4193	0.4330	0.4162
	0.01	0.4408	0.4208	0.4349	0.4176
Kn=0.1					
$\lambda_q > \lambda_C$	0.04	0.4536	0.4291	0.4476	0.4269
	0.07	0.4592	0.4330	0.4543	0.4310
	0.09	0.4598	0.4333	0.4540	0.4301

The effects of different flow parameters on mean concentration of chemical specie is considered in Table 2. The table indicated that mean concentration reduces with growing rarefaction and boundary jump. Also, mean concentration can generally be reduced by increasing phase lag in concentration gradient (λ_C). Furthermore, the effect of an increase in mass flux-phase lag (λ_q) on mean concentration within the channel can be looked at in two ways. Firstly, as λ_q increases,

it causes an increase in mean concentration. This is the case when $\lambda_q \leq \lambda_C$. Secondly, when $\lambda_q >$ λ_C, a further increase in λ_q would result in an increase in mean concentration.

Table 3: Effect of different flow parameters on mean temperature of fluid

t=0.2; Kn=0.01; Sc=0.78; m=2							
		(τ_T=0.01, Bi=5)		(τ_T=0.02, Bi=5)		(τ_T=0.02, Bi=10)	
	τ_q	Pr=0.71	Pr=7	Pr=0.71	Pr=7	Pr=0.71	Pr=7
$\tau_q < \tau_T$	0.001	0.6136	0.1291	0.6104	0.1293	0.6157	0.1623
	0.004	0.6191	0.1292	0.6156	0.1293	0.6205	0.1628
	0.008	0.6268	0.1292	0.6229	0.1294	0.6272	0.1634
D=1							
$\tau_q > \tau_T$	0.03	0.6800	0.1297	0.6705	0.1298	0.6151	0.1674
	0.04	0.6766	0.1299	0.6838	0.1299	0.6993	0.1692
	0.05	2.8318	0.1301	0.5783	0.1299	0.7306	0.1711
$\tau_q < \tau_T$	0.001	0.8144	0.1790	0.8089	0.1779	0.7713	0.2080
	0.004	0.8222	0.1795	0.8163	0.1783	0.7776	0.2088
	0.008	0.8333	0.1801	0.8266	0.1788	0.7864	0.2100
D=2							
$\tau_q > \tau_T$	0.03	0.9172	0.1843	0.8999	0.1826	0.7773	0.2172
	0.04	0.9171	0.1863	0.9256	0.1843	0.8958	0.2206
	0.05	6.9321	0.1881	0.7894	0.1857	0.9455	0.2239

Finally, from Table 3, it is observed that mean temperature of fluid can be raised by increasing the Dufour number. On the other hand, an increase in temperature gradient phase lag (τ_T) would see a drop in the fluid's mean temperature particularly for air (i.e. Pr=0.71). Meanwhile, for

water (*Pr*=7), mean temperature shows a positive response to increase in Biot number (*Bi*). This is physically true due to the influence of convective heat mass transfer at the plate surface. More so, mean temperature is noticed to be on the rise for smaller increaments in the values of heat flux vector (τ_q) as well as when τ_q grows bigger. However, in the latter, a few pockets of irregular behaviour on mean temperature is observed and this is attributable to Dufour effect.

Table 4: Comparison of the velocity in the present work with Ajibade (2014)

(t=0.2, Kn=0.01, $\tau_q = 0.001$, $\tau_T = 0.01$, Pr=0.71, Sc=0.78, y=0.5)						
	Ajibade(2014) ($Da \to \infty$, $\gamma = 1$)	**Present Work** ($Bi \to \infty$, m=0)				
	(Da=1000000, $\gamma = 1$)	Bi=50	Bi=100	Bi=500	Bi=50000	Bi=1000000
D=1	0.136980	0.136997	0.137075	0.137131	0.137144	0.137144
D=2	0.153059	0.154246	0.153745	0.153328	0.153223	0.153221

From table 4, we can observe an excellent agreement between this present problem with that investigated by Ajibade (2014) by setting $Bi \to \infty$ and $m = 0$ with $\gamma = 1$ as well as $Da \to \infty$.

5.2 Heat Generating Fluid in Porous Microchannel

This study looks at the unsteady MHD natural convection double diffusive flow of heat generating fluid in a vertical porous microchannel. The governing equations have been solved analytically in Laplace domain while the method of Riemann-sum was used to invert the transformed expressions to time domain. The Schmidt, Knudsen, Prandtl and Dufour numbers, the phase lags (τ_f) and (τ_T) (which respectively give, the duration of free time during which the heat flux vector due to phonon collision and phase-lag in temperature gradient increase), and suction/injection parameter (S) which were simultaneously applied at the opposite walls of the micro-channel are the basic parameters that govern the transient flow of the system under

consideration. The values obtained from the numerical inversion were presented graphically in Figures 5.2.1–5.2.17 so that the influence of the different parameters on the flow characteristics can easily be discussed. These figures also reveal the observable effects of suction/injection on the fluid flow. It should be noted that for the purpose of this discussion, the values of some dimensionless parameters have been defined within the ranges of $0.001 \le Kn \le 0.01$, $1 \le D \le 10$, $0 < m \le 10$ and $1 \le \delta \le 10$. Meanwhile, ammonia (*Sc*=0.78) is the only important diffusing species (for air) used in this analysis as seen in Gebhart and Pera (1971).

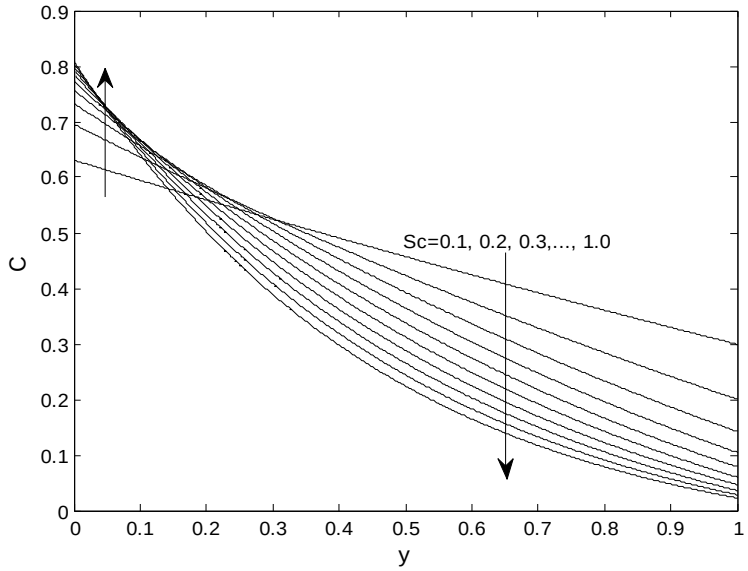


Figure 5.2.1a: Concentration profile for different *Sc*
(*Kn*=0.1, *t*=0.4, *S*=2, λ_f =0.001, λ_C =0.01)

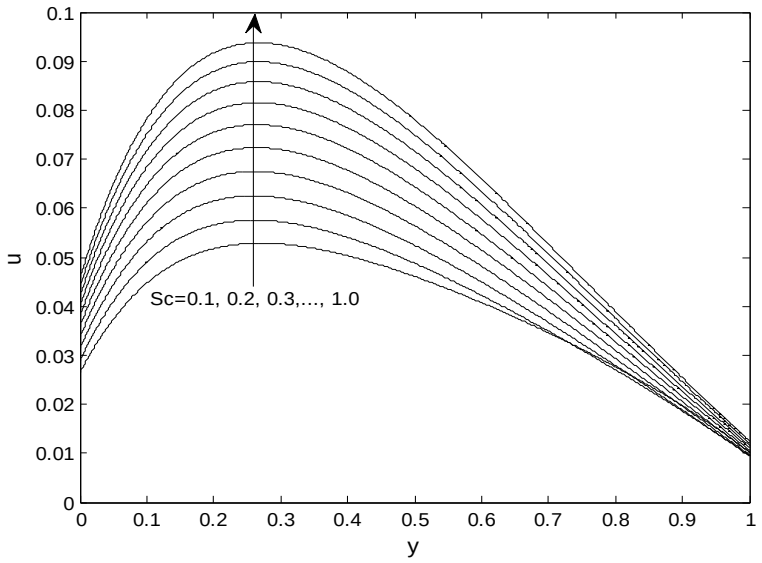


Figure 5.2.1b: Velocity profile for different *Sc*
(*Pr*=0.71, *t*=0.4, *D*=5, λ_f =0.001, *m*=5, λ_C =0.01, *S*=2)

Figure 5.2.1a illustrates the effect of Schmidt number (*Sc*) on concentration profiles. From the figure, it can be observed that fluid concentration decreases within the microchannel about the heated plate and towards the cold plate. This can be attributed to the combined effect of *Sc* and also the influence of suction/injection (*S*) on fluid concentration. Constant injection coupled with increase in Schmidt number results to decreasing concentration jump on the boundaries. The boundary jump is more pronounced near the cold porous plate in comparison with the heated porous plate. This is physically true since the diffusivity of the chemical specie decreases with growing *Sc* which contributes a decrease in the concentration jump on the boundaries. It can also be observed that the jump condition due to diffusion of chemical species imposed on the microchannel plates is not significantly felt due to the effect of suction/injection parameter. The response of this increase can be visualised on the hydrodynamic behaviour in figure 5.2.1b where it can clearly be seen that the convective bouyancy force is enhanced due to concentration decrease caused by increase in *Sc*. However, the rise is significantly felt towards the heated plate.

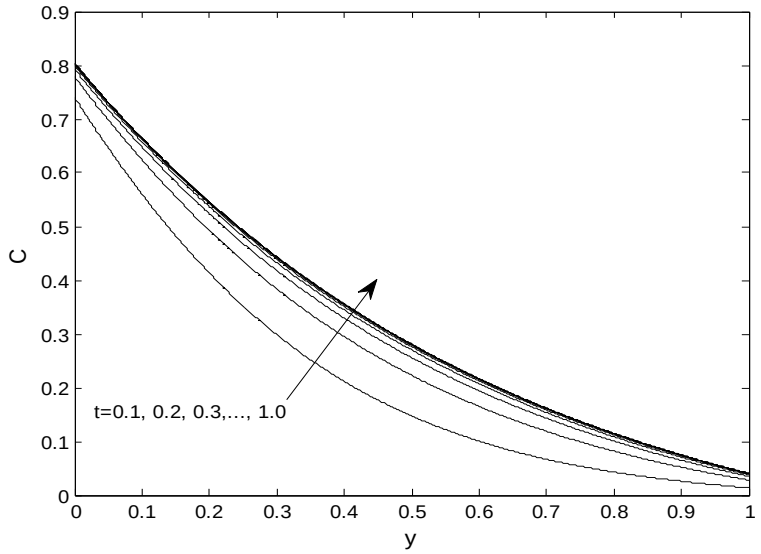


Figure 5.2.2a: Concentration profile for different *t*
(*Kn*=0.1, *Sc*=0.78, *S*=2, λ_f =0.001, λ_C =0.01)

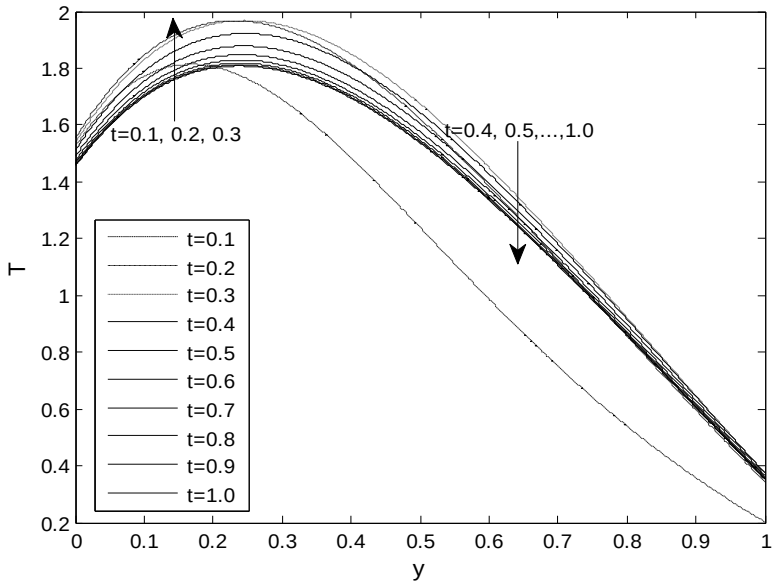


Figure 5.2.2b: Temperature profile for different *t*
(*Sc*=0.78, *Kn*=0.1, *Pr*=0.71, *D*=5, λ_f =0.001, λ_C =0.01, *S*=2)

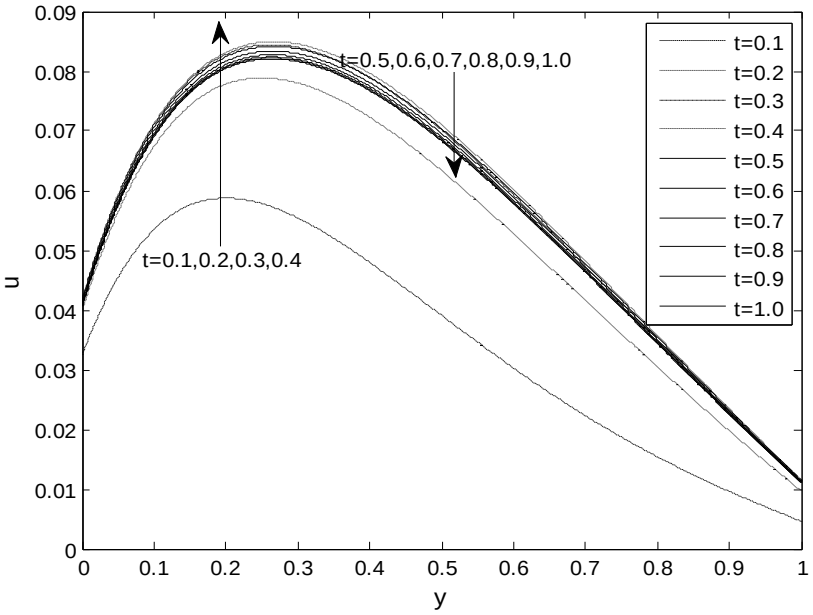


Figure 5.2.2c: Velocity profile for different *t*

(*Sc*=0.78, *Pr*=0.71, δ =1, *D*=5, λ_f =0.001, *m*=5, λ_C =0.01, *S*=2)

In figure 5.2.2a, the behaviour of fluid concentration due to transient time (*t*) is showcased. From this figure, it is obvious that fluid concentration increases with time. However, the increase becomes less significant at large time since the composition of the chemical specie is not changing (steady state). The effect of this concentration increase with time on the hydrodynamics and thermal behaviour of the fluid is presented in figure 5.2.2b and 5.2.2c. It can be seen from these figures that fluid temperature and velocity are highly dependent on *t* due to the presence of Dufour effect. Hence, for small time, when concentration is low, the thermal diffusivity of the fluid is high yielding to an increase in fluid temperature (Figure 5.2.2b). However, with further increase in time, the fluid concentration becomes higher and its effect on temperature becomes significant due to the Dufour effect. This now contributes a decrease in temperature as time increases further until a steady state is reached. The same trend of an initial increase with time and a decrease with further time increase is revealed in the velocity profile and this is attributed to the Dufour effect on the fluid temperature within the channel.

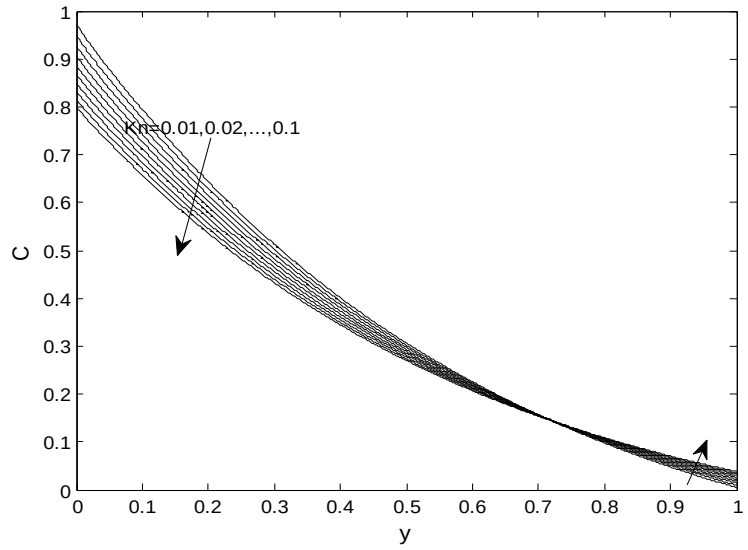


Figure 5.2.3a: Concentration profile for different *Kn*
(*Sc*=0.78, *t*=0.4, λ_f =0.001, λ_C =0.01, *S*=2)

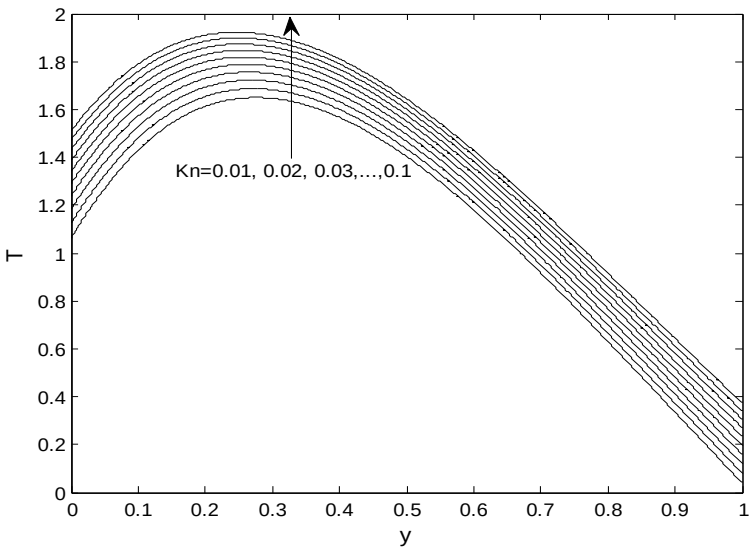


Figure 5.2.3b: Temperature profile for different *Kn*
(*S*=2, *t*=0.4, *Sc*=0.78, *Pr*=0.71, *D*=5, λ_f =0.001, λ_C =0.01)

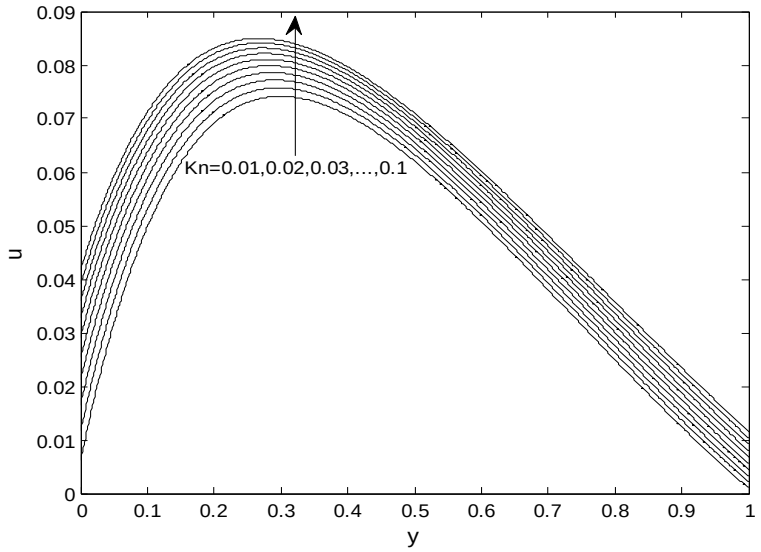


Figure 5.2.3c: Velocity profile for different *Kn*
(*Sc*=0.78, *Pr*=0.71, *t*=0.4, *D*=5, λ_f =0.001, *m*=5, λ_C =0.01, *S*=2)

The influence of Knudsen number on concentration, thermal and momentum profiles are displayed in figures 5.2.3a-5.2.3c. From figure 5.2.3a, it is observed that fluid concentration decreases about the heated plate while it increases towards the cold plate. This is owing to the effect of boundary jump on fluid concentration within the microchannel boundary plates which decreases the fluid-plate molecular interaction and hence amplifies the boundary jump. It is noticed from figure 5.2.3b that due to diffusion-thermo effects, fluid temperature increases within the microchannel. This is as a result of decrease in concentration with increase in *Kn*. This has contributed to enhancing the bouyancy force of the fluid thereby resulting to an increase in the resultant velocity of the fluid as seen in figure 5.2.3c.

From figure 5.2.4, it can be observed that chemical concentration is greatly dependent on concentration gradient (λ_C) as well as the mass flux (λ_f) phase lags. This is because increase in λ_f results to increase in concentration whereas increase in λ_C leads to either a drop or rise in chemical concentration depending on the value of λ_C . This is physically true since an increase in

λ_f retards the flux of the diffusing specie so that the concentration increases. However an increase in λ_C delays the concentration gradient so that the concentration decreases at small λ_C while it increases as λ_C becomes large.

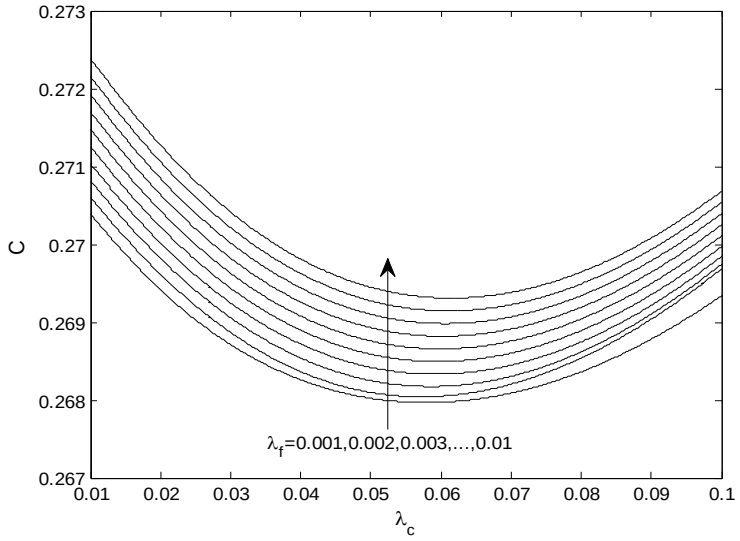


Figure 5.2.4: Cross-sectional concentration for different λ_f

(*S*=2, *t*=0.4, *Kn*=0.1, *Sc*=0.78, *Pr*=0.71, λ_C =0.01,*y*=0.5)

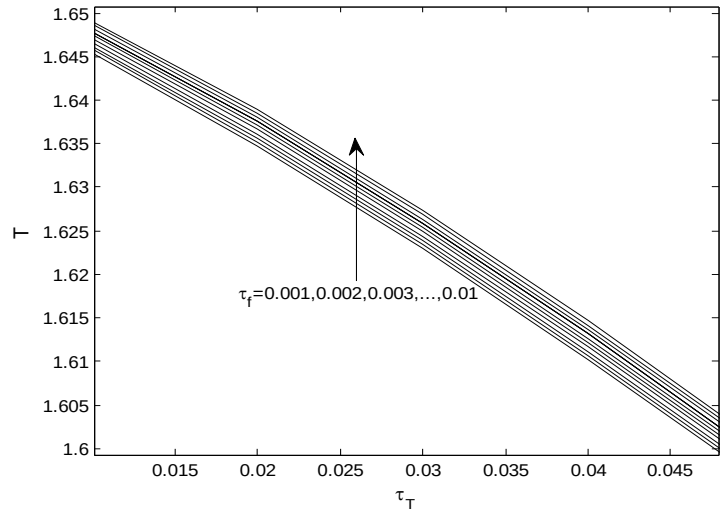


Figure 5.2.5: Cross-sectional temperature for different τ_f

(*Sc*=0.78, *Pr*=0.71, *t*=0.4, *D*=5, λ_f =0.001, *m*=5, λ_C =0.01, δ =1,*y*=0.5)

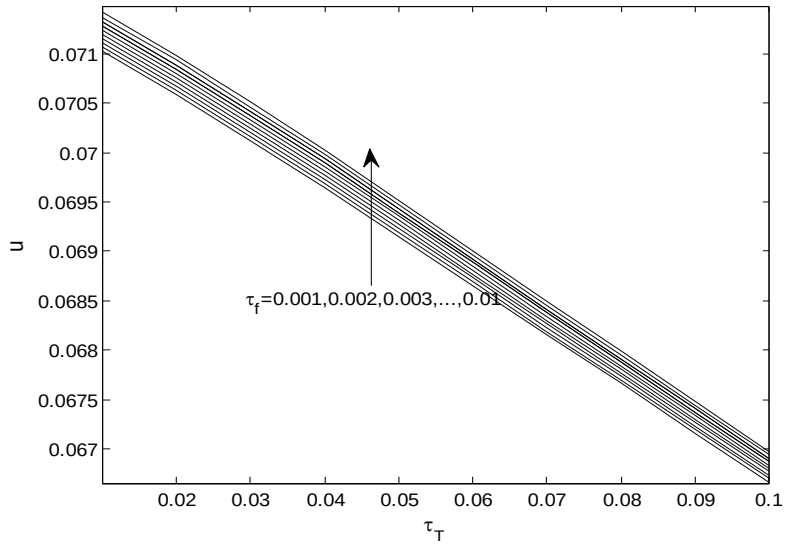


Figure 5.2.6: Cross-sectional Velocity for different τ_f

(S=2, t=0.4, Kn=0.1, Sc=0.78, δ =1, λ_f =0.001, λ_C =0.01, m=5,y=0.5)

Figures 5.2.5 and 5.2.6 show the effect of thermal relaxation time (τ_f) and thermal retardation time (τ_T) on thermal and hydrodynamical behaviour of the fluid. From these figures, it is observed that fluid temperature grows linearly with τ_f while it reduces with τ_T. A similar behaviour is also observed in figure 5.2.6 as fluid velocity is seen to be increasing with increase in τ_f. Increasing the thermal relaxation time, τ_f delays heat flux across the cross sectional areas within the microchannel. Therefore, heat accumulation occur due to delay in diffusing heat generated within the channel so that fluid temperature increases with growing τ_f. An increase in thermal retardation time τ_T on the other hand delays change in temperature gradient leading to a decrease in fluid temperature. The explanation of this phenomenon on the hydrodynamic behaviour is due to the strenghtening of the convective bouyancy force induced by the increase in thermal relaxation time and also the presence of heat generation.

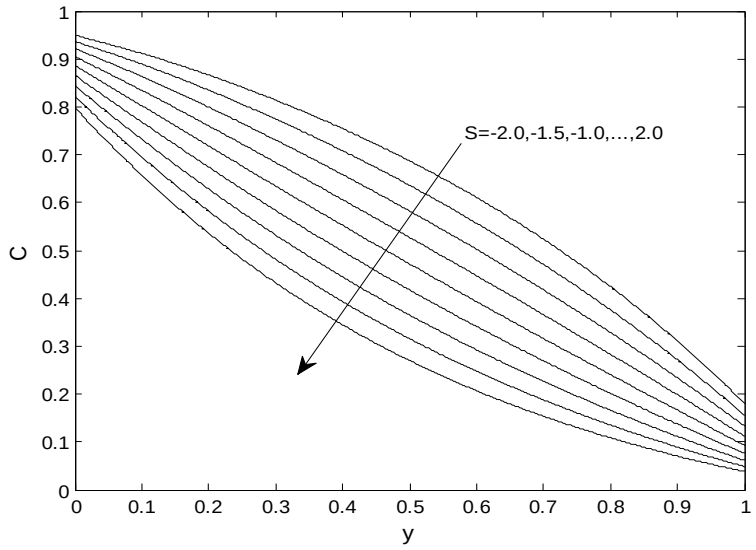


Figure 5.2.7a: Concentration profile for different *S*
(*Kn*=0.1, *Sc*=0.78, λ_f =0.001, λ_C =0.01)

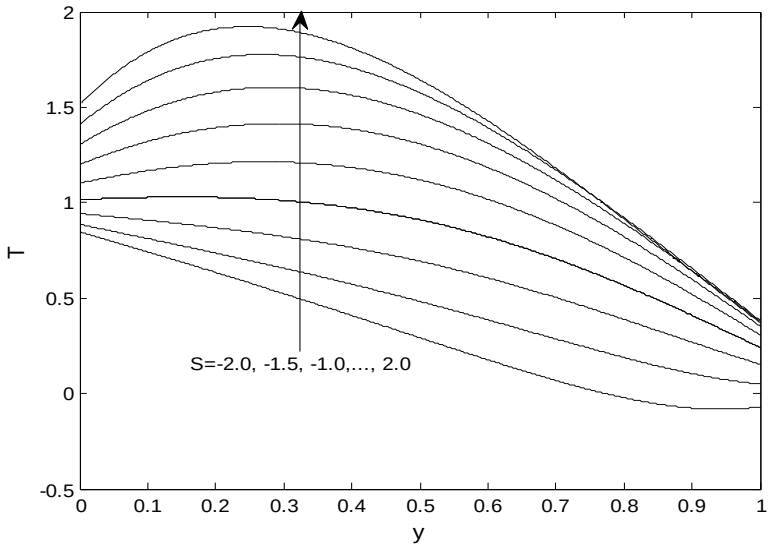


Figure 5.2.7b: Temperature profile for different *S*
(δ =1, *t*=0.4, *Kn*=0.1, *D*=5, *Sc*=0.78, *Pr*=0.71, λ_f =0.001, λ_C =0.01)

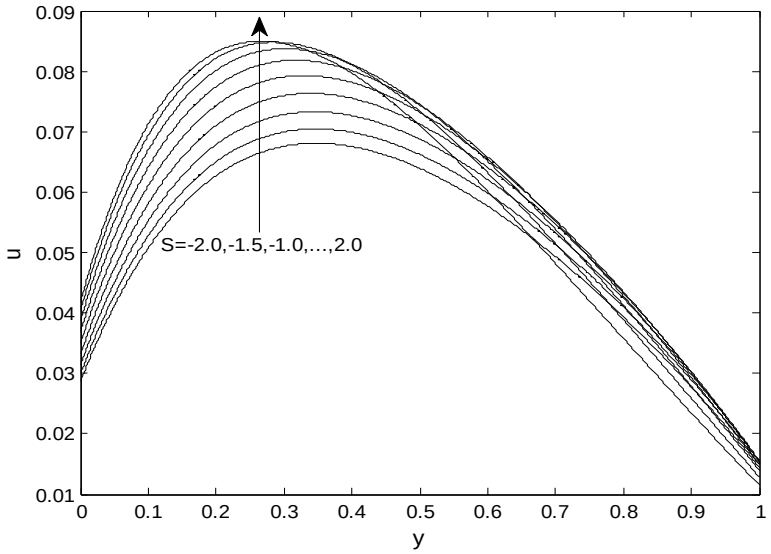


Figure 5.2.7c: Velocity profile for different *S*
(*Sc*=0.78, *Pr*=0.71, *t*=0.4, *D*=5, λ_f =0.001, *m*=5, λ_C =0.01, δ =1)

From figure 5.2.7a, it is observed that with continuous injection and suction on the boundary plates, the chemical specie is significantly affected hence leading to a decrease in fluid concentration with growing suction through the heated plate (*y*=0) thereby increasing the rate of thermal diffusion causing an increase in fluid temperature (figure 5.2.7b). The resultant effect of temperature increase due to increase in suction/injection parameter is observed to increase in fluid velocity due to the strenghtening of convection currents as shown in figure 5.2.7c.

In Figure 5.2.8a, it is clear that fluid temperature drops as Prandtl (*Pr*) number grows. Also, it is observed that the effect of temperature jump on the boundary plates becomes significant with fluids of low *Pr*. This decrease in temperature is attributed to decrease in the rate of thermal diffusivity as Pr increases thereby weakening the convective currents within the microchannel and consequently, it results to a decrease in fluid velocity as *Pr* increases (figure 5.2.8b).

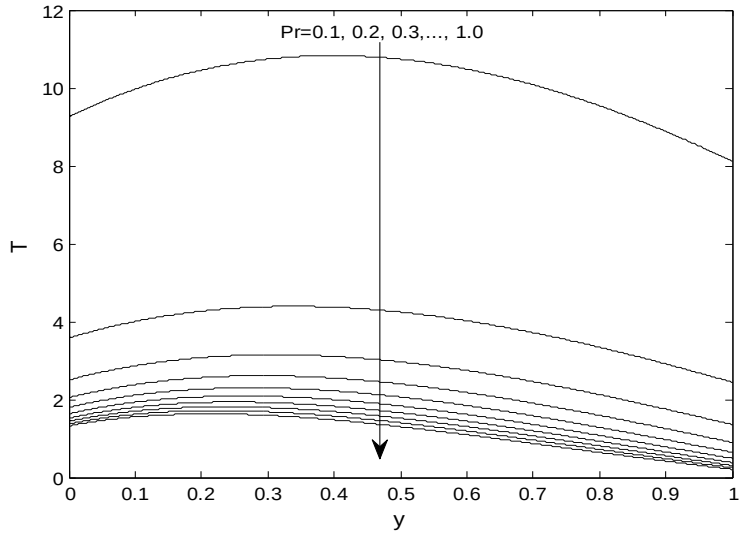


Figure 5.2.8a: Temperature profile for different *Pr*
(*Sc*=0.78, *Kn*=0.1, *t*=0.4, *D*=5, λ_f =0.001, λ_C =0.01, *S*=2)

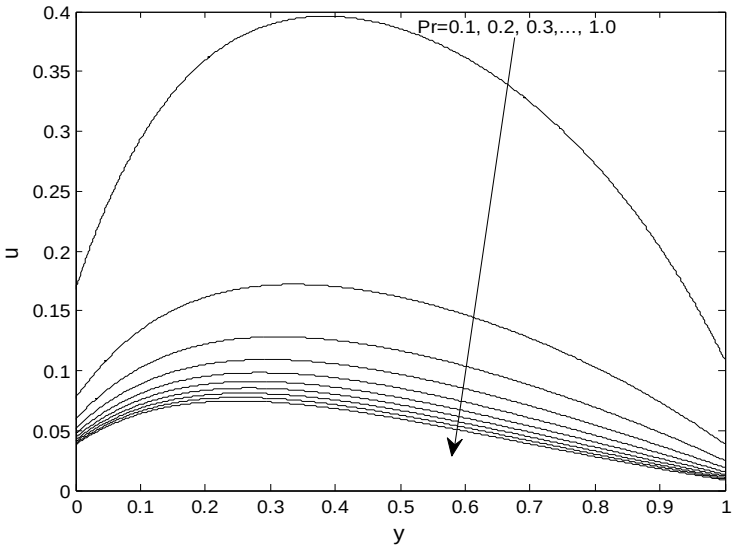


Figure 5.2.8b: Velocity profile for different *Pr*
(*S*=2, *t*=0.4, *Kn*=0.1, *Sc*=0.78, δ =1, λ_f =0.001, λ_C =0.01, *m*=5)

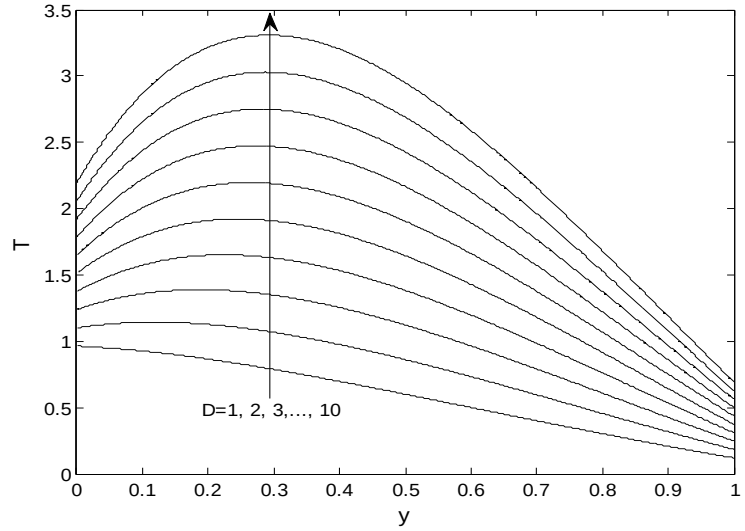


Figure 5.2.9a: Temperature profile for different *D*
(*S*=2, *t*=0.4, *Kn*=0.1, *Sc*=0.78, *Pr*=0.71, λ_f =0.001, λ_C =0.01)

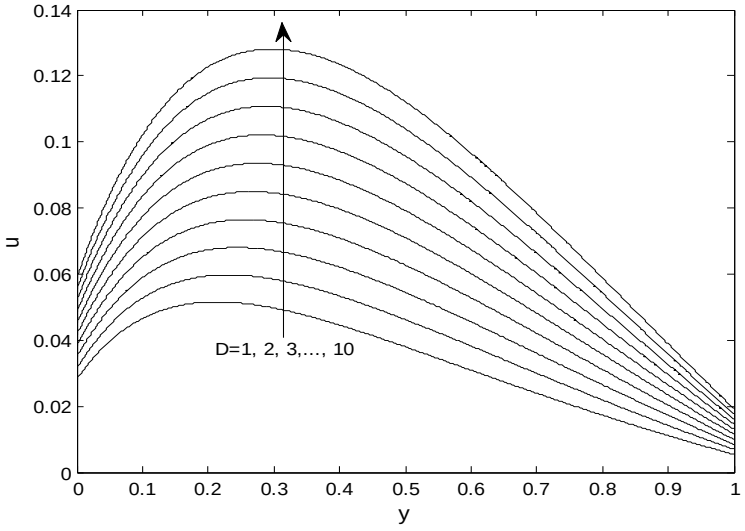


Figure 5.2.9b: Velocity profile for different *D*
(*S*=2, *t*=0.4, *Kn*=0.1, *Sc*=0.78, *Pr*=0.71, λ_f =0.001, λ_C =0.01, *m*=5)

The diffusion-thermo (Dufour) effect on the hydrodynamic and thermal behaviour of the fluid is presented in Figures 5.2.9a and 5.2.9b. It is noticed that increasing Dufour number (*D*) leads to amplifying the effect of concentration, which increases the concentration of fluid causing an accumulation of heat due to a reduction in the rate of thermal diffusivity giving rise to energy

flux. The resultant increase in fluid temperature is observed to have a strenghtening effect on the bouyancy force, hence, fluid velocity increases within the channel (figure 5.2.9b).

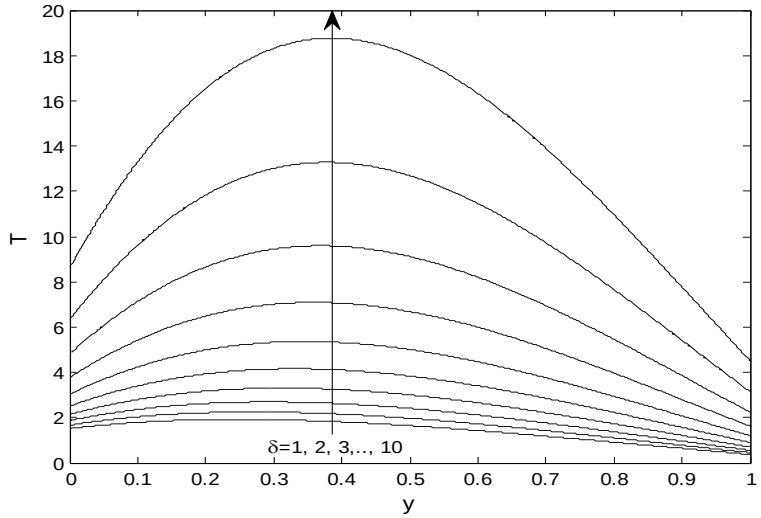


Figure 5.2.10a: Temperature profile for different δ
(*Sc*=0.78, *Kn*=0.1, *t*=0.4, *D*=5, λ_f =0.001, λ_C =0.01, *S*=2)

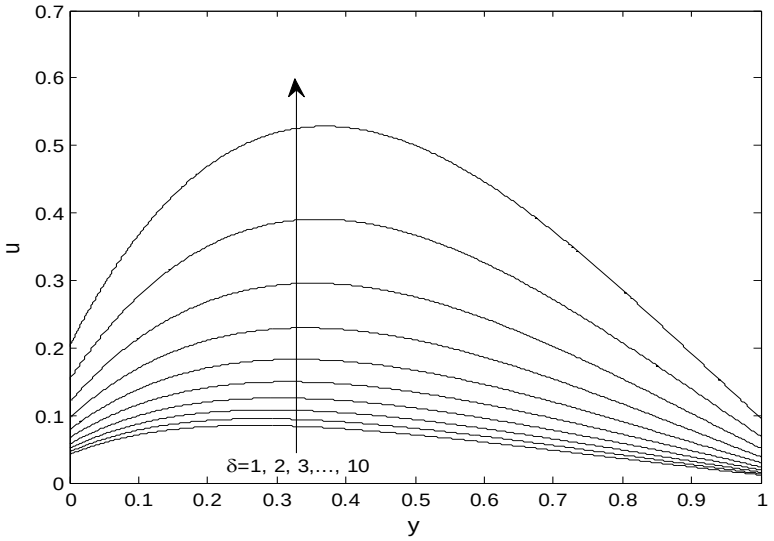


Figure 5.2.10b: Velocity profile for different δ
(*S*=2, *t*=0.4, *Kn*=0.1, *Sc*=0.78, *Pr*=0.71, λ_f =0.001, λ_C =0.01, *m*=5)

Figures 5.2.10a and 5.2.10b illustrate the effects of heat generation (δ) on temperature and velocity of the flow. From figure 5.2.10a, it is seen that the thermal boundary layer decreases

with increase in δ resulting to an increase in the energy flux within the microchannel. The rise in energy flux consequently increases the temperature of the fluid thereby boosting the convective bouyancy force as observed in figure 5.2.10b.

The response of velocity to varying Hartmann number (*m*) is shown in figure 5.2.11. Here, it is evident that the presence of the magnetic field is to decrease the velocity. This is physically true since growing *m* creates a mechanical damping force known as Lorentz force which tends to limit fluid motion. The effect of an increase in sustentation parameter (*N*) is the subject of figure 5.2.12. From this figure, it is observed that increase in *N* enhances the bouyancy due to mass transfer thereby increasing the fluid velocity. However, near the heated plate, the increase is significant due to the slip condition imposed on the microchannel boundary.

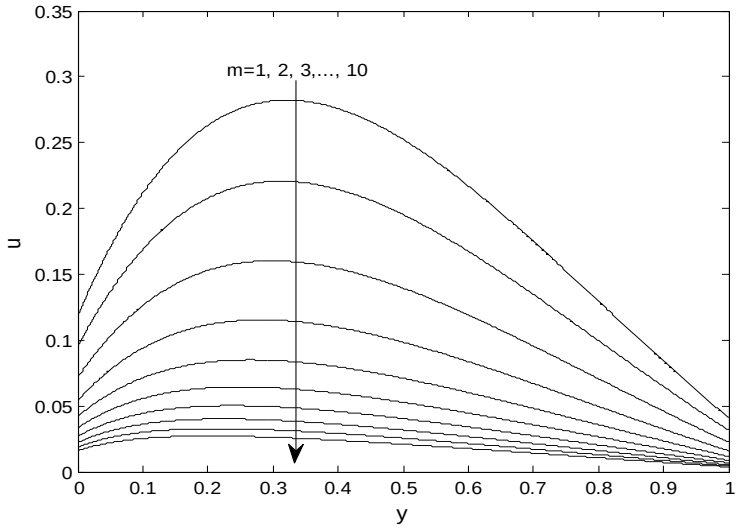


Figure 5.2.11: Velocity profile for different *m*
(*Sc*=0.78, *Pr*=0.71, *t*=0.4, *D*=5, λ_f =0.001, λ_C =0.01, *S*=2)

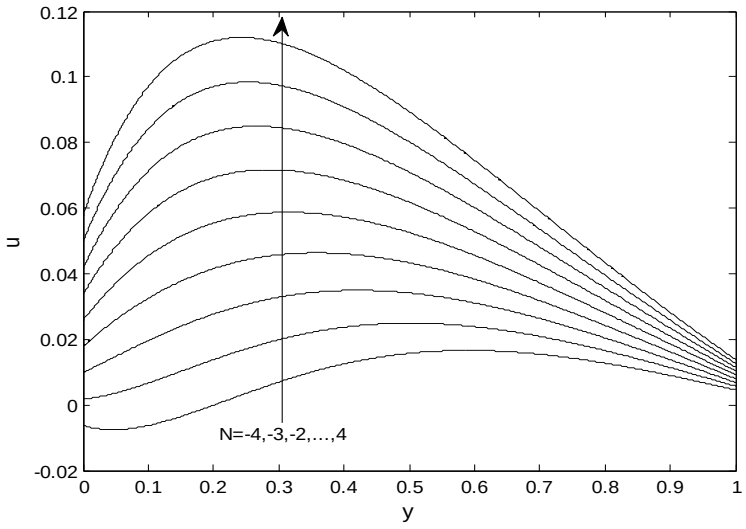


Figure 5.2.12: Velocity profile for different N
(S=2, t=0.4, Kn=0.1, Sc=0.78, Pr=0.71, λ_f =0.001, λ_C =0.01, m=5)

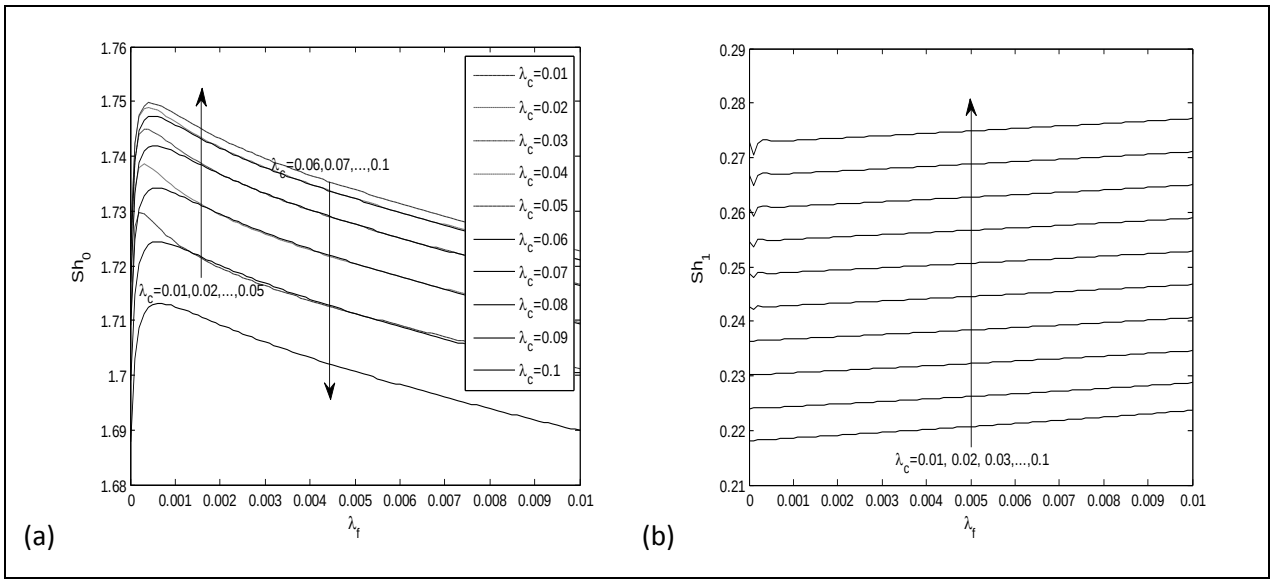


Figure 5.2.13: Sherwood number vs λ_f for different λ_C (S=2, t=0.4, Kn=0.1, Sc=0.78):

(a) heated plate and (b) cold plate

Figure 5.2.13 describes phase-lags effect on the transfer of chemical specie on the boundaries. On the heated plate ($y = 0$), it can be noticed that mass transfer increases with increase in λ_C , it

reaches a maximum point and then decreases whereas increase in λ_f results to a decrease in mass transfer. This is physically true since an increase in λ_f acts to delay the propagation speed of the diffusing specie causing a decrease in the mass transfer through the plate ($y = 0$). On the other hand, the chemical concentration is observed to increase with λ_C leading to an increase in mass transfer on the cold plate ($y = 1$).

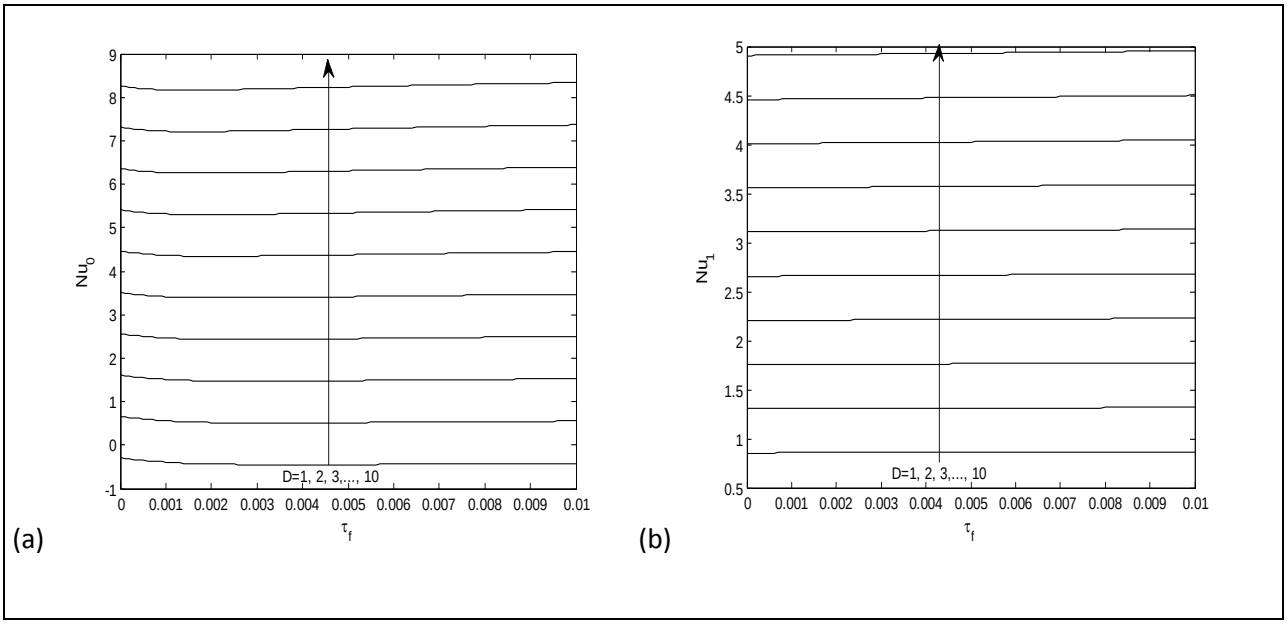


Figure 5.2.14: Nusselt number vs τ_f for different D(Pr=0.71, t=0.4, S=2, τ_T =0.01, δ =1):
(a) heated plate and (b) cold plate

The response of heat transfer to Dufour number (D) and heat flux phase lag (τ_f) is shown in Figure 5.2.14(a) and (b). It is observed that Nusselt number increases with growing D on both walls. This is physically true since an increase in diffusion-thermo effect would act to amplify the influence of chemical concentration on temperature so that thermal diffusivity is enhanced thereby resulting to a rise in fluid temperature. However, heat transfer effect becomes insignificant with increase in τ_f.

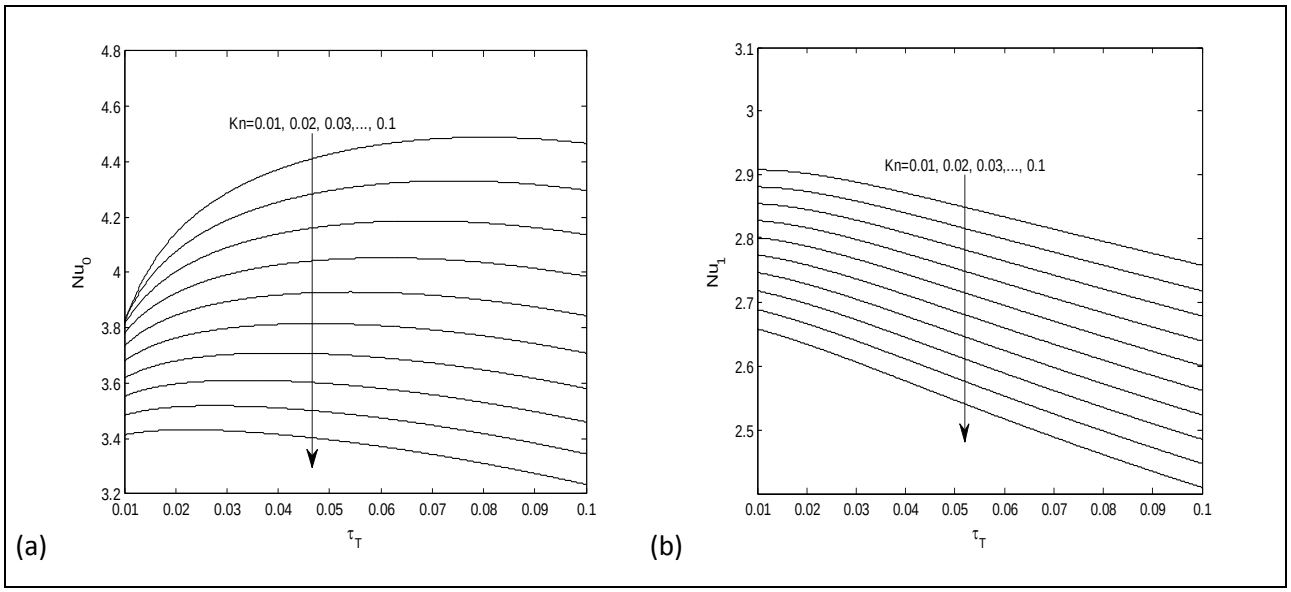


Figure 5.2.15: Nusselt number vs τ_T for different *Kn* (*Pr*=0.71, *t*=0.4, *D*=2, *S*=2, δ =1, τ_f =0.001): (a) heated plate and (b) cold plate

The combined effects of Knudsen number (Kn) and thermal retardation time (τ_T) on the rate of heat transfer on the microchannel boundary plates is shown in figure 5.2.15(a) and (b). it is noticed from these figures that heat transfer decreases on both plates as rarefaction increases. More so, the rate of heat transfer reduces with an increase in τ_T and this is more pronounced on the cold plate. This is obvious from figure 5.2.5, since an increase in τ_T delays change in temperature gradient and as such would lead to a drop in fluid temperature.

Figure 5.2.16(a) amd (b) presents the effects of Dufour and Knudsen numbers on skin friction at the boundary plates. From these figures, it is clearly seen that the presence of diffusion-thermo effect would lead to an increase in skin friction on both plates. Again, increase in rarefaction decreases the skin friction at the plate ($y = 0$) when *D* is small whereas this effect becomes negligible as *D* grows large. Moreso, a similar behaviour is observed at the plate ($y = 1$).

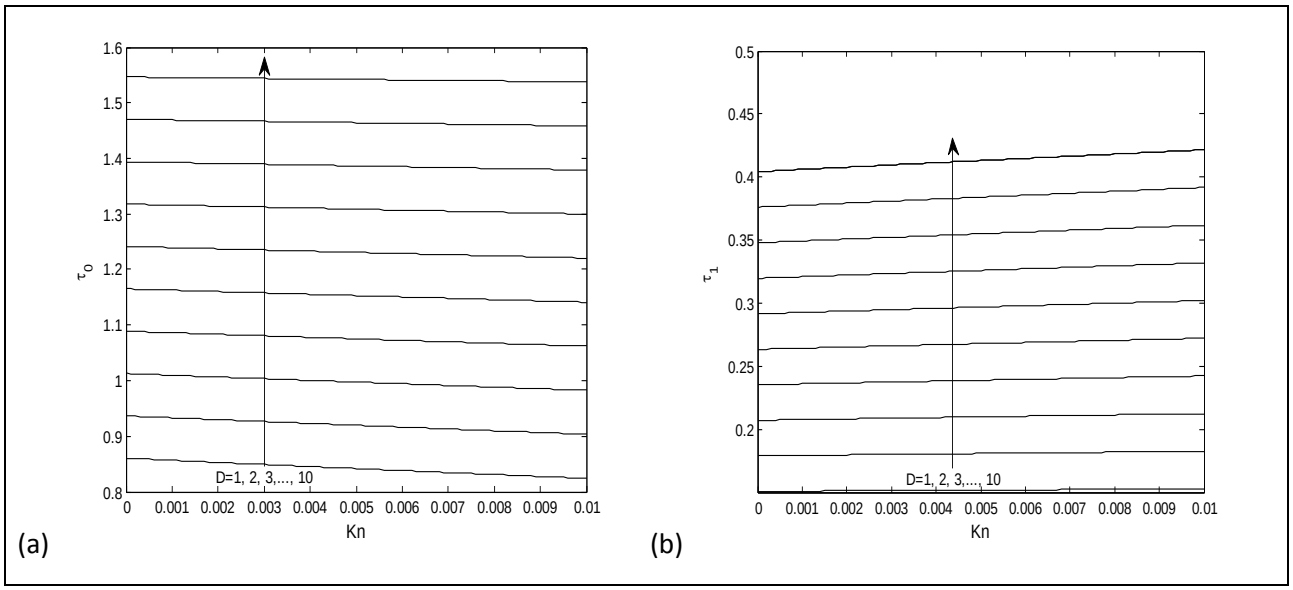


Figure 5.2.16: Skin-friction vs*Kn* for different *D* (*Pr*=0.71, *t*=0.4, *m*=2, *S*=2, *N*=2, δ =1):
(a) heated plate and (b) cold plate

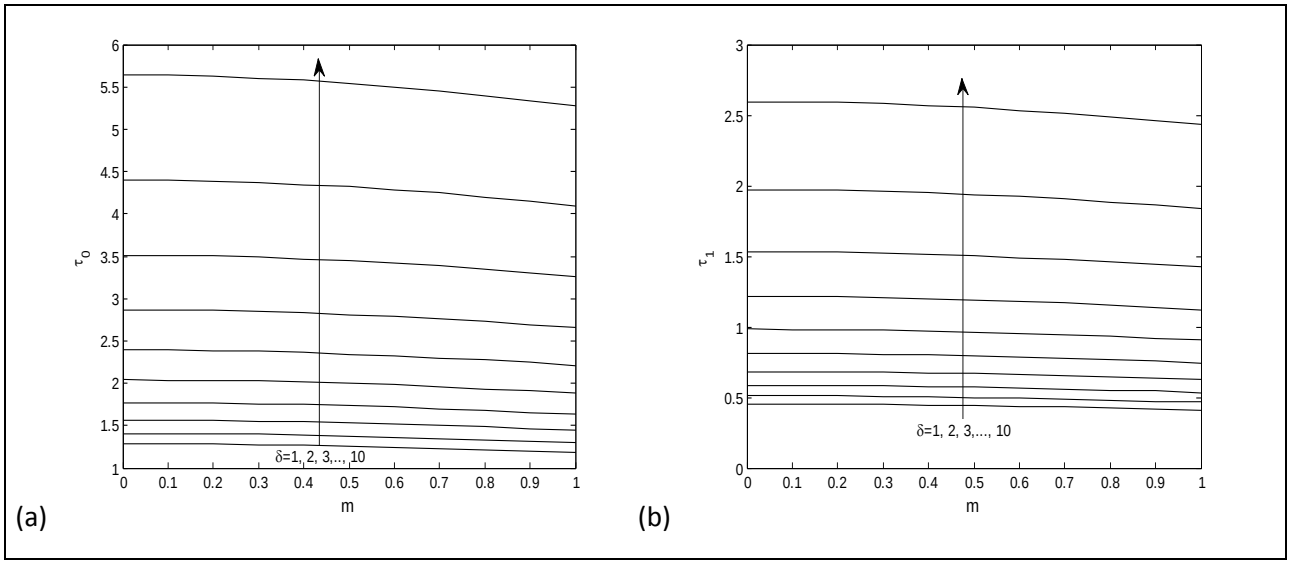


Figure 5.2.17: Skin-friction vs*m* for different δ (*Pr*=0.71, *t*=0.4, *S*=2, *N*=2, τ_f =0.001, τ_T =0.01):
(a) heated plate and (b) cold plate

The response of skin friction to Heat generation (δ) as well as magnetic parameter (*m*) is displayed in 5.2.17(a) and (b) where it is observed that an increase in Hartmann number causes skin friction to drop at both plates. This could be attributed to the Lorentz force factor as shown

in Figure 5.2.11. Also, skin friction is noticed to be on the rise on both plates following an increase in δ. This is physically correct because a rise in energy flux would result to an increase in fluid temperature and as such enhancing the convective bouyancy force as observed in figure 5.2.10b.

Table 5: Effect of different flow parameters on mass flux through the channel

(τ_T = 0.01; *Kn* = 0.01; *t* = 0.2; *Pr* = 0.71; *D* = 5; *m* = 5)						
τ_f		*S* = -2	*S* = -1	*S* = 0	*S* = 1	*S* = 2
$\tau_f < \tau_T$	0.001	0.0498	0.0506	0.0506	0.0494	0.0470
	0.004	0.0503	0.0511	0.0510	0.0498	0.0474
	0.008	0.0510	0.0518	0.0517	0.0503	0.0478
δ = 1						
$\tau_f > \tau_T$	0.02	0.0542	0.0550	0.0544	0.0526	0.0496
	0.05	0.0682	0.0667	0.0640	0.0602	0.0555
	0.1	0.0758	0.0716	0.0667	0.0615	0.0560
$\tau_f < \tau_T$	0.001	0.0524	0.0534	0.0535	0.0524	0.0499
	0.004	0.0529	0.0540	0.0540	0.0528	0.0502
	0.008	0.0538	0.0548	0.0548	0.0534	0.0507
δ = 2						
$\tau_f > \tau_T$	0.02	0.0573	0.0582	0.0577	0.0558	0.0526
	0.05	0.0714	0.0698	0.0669	0.0629	0.0581
	0.1	0.0779	0.0735	0.0685	0.0632	0.0576

From Table 5, it is observed that increase in heat generation parameter results to an increase in mass flux within the channel. This is true because a rise in energy flux would by implication increase the temperature of the fluid thereby boosting the convective bouyancy force as seen in figure 5.2.10b. Also, regardless of a small or large increase in thermal relaxation time τ_f it is

noticed that mass flux grows within the channel. More so, the effect of growing injection ($S < 0$) through the heated plate causes mass flux to rise to a maximum value and then decreases when $\tau_f < \tau_T$ whereas mass flux reduces within the channel with increasing *S*when $\tau_f > \tau_T$.

Table 6: Effect of different flow parameters on mean concentration of chemical species.

($\lambda_C = 0.01$; *Sc* = 0.78; *t* = 0.2)							($\lambda_C = 0.03$; *Sc* = 0.78; *t* = 0.2)				
	λ_f	*S* = -2	*S* = -1	*S* = 0	*S* = 1	*S* = 2	*S* = -2	*S* = -1	*S* = 0	*S* = 1	*S* = 2
$\lambda_f \le \lambda_C$	0.001	0.6130	0.5544	0.4979	0.4452	0.3977	0.5878	0.5350	0.4839	0.4355	0.3908
	0.005	0.6196	0.5607	0.5040	0.4514	0.4039	0.5971	0.5442	0.4930	0.4446	0.3998
	0.01	0.6244	0.5647	0.5076	0.4546	0.4070	0.6018	0.5487	0.4975	0.4492	0.4046
Kn= 0.01											
$\lambda_f > \lambda_C$	0.04	0.6484	0.5822	0.5216	0.4669	0.4181	0.6194	0.5642	0.5122	0.4636	0.4187
	0.07	0.6361	0.5732	0.5165	0.4657	0.4200	0.6251	0.5705	0.5198	0.4727	0.4293
	0.1	0.6098	0.5585	0.5112	0.4675	0.4271	0.6126	0.5634	0.5176	0.4747	0.4347
$\lambda_f \le \lambda_C$	0.001	0.5645	0.5001	0.4393	0.3837	0.3342	0.5465	0.4877	0.4316	0.3791	0.3313
	0.005	0.5686	0.5040	0.4433	0.3879	0.3386	0.5536	0.4949	0.4390	0.3869	0.3393
	0.01	0.5710	0.5058	0.4450	0.3897	0.3406	0.5565	0.4977	0.4420	0.3901	0.3428
Kn = 0.1											
$\lambda_f > \lambda_C$	0.04	0.5708	0.5047	0.4454	0.3924	0.3454	0.5624	0.5037	0.4492	0.3989	0.3529
	0.07	0.5489	0.4938	0.4433	0.3971	0.3547	0.5521	0.4988	0.4493	0.4033	0.3607
	0.1	0.5333	0.4887	0.4464	0.4061	0.3680	0.5337	0.4884	0.4457	0.4054	0.3672

The impact of different flow parameters on mean concentration of the chemical specie is shown in Table 6. It is noticed from this table that mean concentration declines with increased rarefaction. Mean concentration is also observed to have initially risen to a maximum value with a small increase in mass flux phase lag, λ_f and then decreases as λ_f further grows bigger in

value. Again, an increase in concentration gradient phase lag, λ_C as well as suction/injection (S) would see a considerable drop in mean concentration of fluid.

Table 7: Effect of different flow parameters on mean temperature of fluid

$Kn = 0.01;\ Sc = 0.78;\ m = 5;\ t = 0.2$											
$(\tau_T = 0.01;\ Pr = 0.71;\ \delta = 1)$							$(\tau_T = 0.03;\ Pr = 0.71;\ \delta = 2)$				
	τ_f	$S = -2$	$S = -1$	$S = 0$	$S = 1$	$S = 2$	$S = -2$	$S = -1$	$S = 0$	$S = 1$	$S = 2$
$\tau_f \le \tau_T$	0.001	0.6858	0.6880	0.6881	0.6848	0.6773	0.7360	0.7294	0.7211	0.7107	0.6978
	0.004	0.6930	0.6956	0.6958	0.6923	0.6847	0.7464	0.7395	0.7307	0.7196	0.7061
	0.008	0.6988	0.7018	0.7019	0.6980	0.6898	0.7545	0.7474	0.7382	0.7267	0.7129
$D = 1$											
$\tau_f > \tau_T$	0.04	0.7943	0.7882	0.7758	0.7587	0.7384	0.8233	0.8066	0.7879	0.7676	0.7463
	0.07	0.9210	0.8817	0.8439	0.8079	0.7738	0.9016	0.8697	0.8383	0.8077	0.7782
	0.1	0.9708	0.9209	0.8756	0.8344	0.7966	0.9400	0.9003	0.8628	0.8275	0.7944
$\tau_f \le \tau_T$	0.001	0.7984	1.2995	1.7746	2.1893	2.5233	1.1109	1.5300	1.9226	2.2722	2.5671
	0.004	0.8111	1.3187	1.7957	2.2094	2.5414	1.1385	1.5575	1.9474	2.2932	2.5845
	0.008	0.8239	1.3411	1.8201	2.2313	2.5594	1.1699	1.5882	1.9740	2.3143	2.6006
$D = 10$											
$\tau_f > \tau_T$	0.04	1.4538	1.9680	2.3714	2.6791	2.9058	1.6667	2.0159	2.3162	2.5704	2.7813
	0.07	3.0590	3.1121	3.1602	3.2028	3.2386	2.4744	2.6464	2.7941	2.9209	3.0291
	0.1	3.8879	3.6968	3.5639	3.4744	3.4159	3.0535	3.0806	3.1101	3.1416	3.1742

From Table 7, the effect of a simultaneous increase of heat generation (δ), suction/injection (S) and thermal retardation time (τ_T) implies that mean temperature is seen to be rising to a maximum level and then drops subsequently when $\tau_f < \tau_T$. However, when $\tau_f > \tau_T$, mean temperature is observed to be reducing following an increase of δ, S and τ_T. In addition, it is noticed that mean temperature of fluid can be raised by increasing the Dufour number (D), this is

physically true since diffusion-thermo effect exerts a very significant influence on fluid temperature distribution.

Table 8: Comparison of the present work with Ajibade (2014)

Ajibade (2014) ($Da = 1000000, \gamma = 1$)		**Present Work** ($m = 0; \delta = 0; S = 0$)
	Velocity	Velocity
D=1	0.136980	0.136980
D=2	0.153059	0.153059

As $Da \to \infty$ in Ajibade (2014), the effect of porous medium is minimized on the flow and as such the effective viscosity of the porous medium becomes same as viscosity of the fluid so that $\gamma = 1$. This is compared with the present problem by setting S=0, δ =0 and $m = 0$ as shown in Table 8.

CHAPTER SIX

SUMMARY, CONCLUSION AND RECOMMENDATION

6.1 Summary

This dissertation presented a computational study on thermo-solutal convection MHD flow with Dufour effect. The model examined the effect of dual-phase-lag on transient MHD natural convection heat and mass transfer flow in a vertical microchannel with convective boundary conditions.The problem extended further to investigate the flow characteristics in a vertical porous microchannel. Fluid motion was subjected to asymmetric heating of the channel plates with slip and jump conditions on the boundary. The solutions of the governing equations such as velocity, temperature and concentration are obtained in closed form using Laplace transform technique. Riemann-sum approximation method was then applied to invert the Laplace domain analytical solutions into time domain in order to obtain velocity, temperature, skin-friction and the rate of heat transfer. The response of mean chemical concentration, bulk fluid temperature and mass flux within the channel to different flow parameters are examined and discussed.

6.2 Conclusion

Using MATLAB software package, the hydrodynamic behaviour of the fluid flow to different flow parameters such as; Biot number (*Bi*), Dufour number (*D*), Hartmann number (*m*), suction/injection (*S*), Heat generation parameter (δ) amongst others are presented graphically in order to have a physical understanding of the problem. It is also worth mentioning that the problem was validated numerically and an excellent agreement was established with Ajibade (2014) in the absence of Biot number, magnetic field and heat generation parameter with $\gamma = 1$.

It is found that the resultant mass flux increases by growing Dufour number. Also, when the working fluid is air (*Pr*=0.71), massflux decreases in the presence of growing boundary

convection while it increases when the working fluid is water (*Pr*=7.0).Mass flux is again seen to grow within the channel regardless of a small or large increase in thermal relaxation time τ_f .Mean concentration drops within the channel as rarefaction and concentration gradient phase lag (λ_C) increase. In particular, it is observed that mean concentration of the chemical specie, ammonia (*Sc*=0.78) reduces due to an increase in suction/injection as well as rarefaction.Also, it is shown that mean temperature rises following an increase in Dufour (*D*) number but decreases with growing thermal retardation time (τ_T). In addition, diffusion-thermo (Dufour) effect wields a very significant influence on fluid temperature and velocity distribution. Furthermore, the presence of heat generation parameter (*H*), increases temperature, velocity profile and also skin friction of the fluid. Finally, the magnetic field effect is to decrease the fluid velocity within the microchannel.

6.3 Recommendations

This present research work which centres on the computational study of thermo-solutal convection MHD flow with Dufour effect has its many applications in the advancement of the frontiers of science and technological innovations particularly in meteorology, astrophysics, geophysics, design of nuclear reactors, petroleum reservoirs etc. This present study however could be extended to capture what impact magnetic field, heat source as well as convective heat exchange parameter could have on the fluid flow when the microchannel is oriented horizontally. This dissertation considered MHD flow of electrically conducting fluid with applied magnetic field. It can however be reconsidered in the presence of induced magnetic field.

REFERENCES

Ahmed, S., and Khatun, H., (2013), Magnetohydrodynamics oscillatory flow in a planar porous channel with suction and injection, *Int. J. EngTechnol*, 11:1024-1029

Ajibade, A. O., (2014), Dual-phase-lag and Dufour effects on unsteady double-diffusive convection flow in a vertical microchannel filled with porous material, *J Process MechEng*; 228(4): 272–285.

Attia, A. H., (2010), The effect of suction and injection on unsteady Couette flow with variable properties, *KragujevacJ Sci*, 32: 17–24.

Aziz, A., (2009), A similarity solution for laminar thermal boundary layer over a flat plate with a convective surface boundary condition, *Comm. Non. Sci. Num. Sim.*14(14): 1064–1068.

Aziz, A., (2010), Hydrodynamic and thermal slip flow boundary layers over a flat plate with constant heat flux boundary condition, *Comm. Non. Sci. Num. Sim*., 15(3): 573–580.

Bég, O. A., Uddin, M. J., Rashidi, M. M., and Kavyani, N., (2014), Double-diffusive radiative magnetic mixed convective slip flow with Biot number and Richardson number effects, *J. Eng. Thermophys.*23(2): 79–97.

Cattaneo, C., (1958), Sur uneforme de l'e´quation de la chaleure´liminant le paradoxed'une propagation instantane´ e. *C R AcadSci*, 247: 431–433.

Chawla, S.S., (1967), Magnetohydrodynamics unsteady free convection, ZAMM; 47:499–508.

Cramer, K. R., and Pai, S., (1973), *Magneto fluid dynamics for engineers and applied physicists*, New York: McGraw-Hill.

Crepeau, J. C., and Clerksean, R., (1997), Similarity Solutions of Natural Convection with Internal Heat Generation, *J. Heat Transfer*, 119(1):183-185.

Foraboschi, F. P., and Federico, I. D., (1964), Heat Transfer in Laminar Flow of Non-Newtonian Heat Generating Fluids, *Int. J. Heat Mass Transfer*, 7(3):315-318.

Gebhart, B., and Pera, L., (1971), The Nature of Vertical Natural Convection Flows Resulting From the Combined Buoyancy Effects of Thermal and Mass Diffusion, *Int. J. Heat Mass Trans*, 14:2025–2050.

Gupta, A. S., (1961), Steady and transient free convection of an electrically conducting fluid from a vertical plate in the presence of magnetic field, *Appl. Sci. Res*., 9A:319-333.

Ishak, A., (2010), Similarity solutions for flowand heat transfer over a permeable surface with convective boundary condition, *Appl. Math. Comput.*,217(2):837–842.

Jha, B. K., and Ajibade, A. O., (2010), Free convection heat and mass transfer flow in a vertical channel with Dufour effect. *J Process MechEng*; 224(2): 91–101.

Jha, B. K., and Ajibade, A. O., (2011), Diffusion-thermo effects on free convective heat and mass transfer flow in a vertical channel with symmetric boundary conditions, *Trans ASME: J Heat Trans*; 133(5): 052502(1–8).

Jha, B. K., Samaila, A. K., and Ajibade, A. O., (2012),Natural Convection Flow of Heat Generating/Absorbing Fluid near a Vertical Plate with Ramped Temperature,*Journal of Encapsulation and Adsorption Sciences*, 2:61-68.

Jha, B. K., Aina, B., and Ajiya, A. T., (2014), MHD natural convection flow in a vertical parallel plate microchannel, *Ain Shams Eng J*, 6(1):289-295

Jha, B. K., Isah, B.Y., Uwanta, I. J., (2016), Combined effect of suction/injection on MHD free-convection flow in a vertical channel with thermal radiation, *Ain Shams Eng J*., http://dx.doi.org/10.1016/j.asej.2016.06.001

Joseph, D. D., and Preziosi, L., (1989), Heat waves. *Rev Modern Phys*; 61: 41–73

Kafoussias, N.G., and Williams, (1995), EW., Thermal-diffusion and diffusion-thermo effects on mixed free-convective and mass transfer boundary layer flow with temperature dependent viscosity, *Int. J Eng Sci.*; 33: 1369-84.

Khadrawi, A. F., Othman, A., and Al-Nimr, M. A., (2005), Transient free convection fluid flow in a vertical microchannelas described by the hyperbolic heat conduction model, *Int J Thermophys*; 26: 905–918.

Khadrawi, A. F., and Al-Nimr, M. A., (2007), Unsteady natural convection fluid flow in a vertical microchannel under the effect of the dual-phase-lag heat-conduction model, *Int J Thermophys*; 28: 1387–1400.

Labroopulu, F., Dorrepael, J. M., and Chandna, O.P., (1996), Oblique flow impinging on a wall with suction or blowing. *Acta Mech*;115:15–25.

Lienhard IV, J.H., andLienhard V, J.H., (2006), A heat transfer textbook, 3rd ed. Cambidge, MA: Phlogiston Press, 1.24: 707-718.

Makinde, O. D., (2009), On MHD boundary-layer flow and mass transfer past a vertical plate in a porous medium with constant heat flux, *Int. J. Num. Methods Heat Fluid Flow*, 19(3/4): 546-554.

Makinde, O. D., and Aziz, A., (2010), MHD mixed convection from a vertical plate embedded in a porous medium with a convective boundary condition, *Int. J. Therm. Sci*,49(9): 1813–1820.

Makinde, O. D., and Olanrewaju, P. O., (2010), Buoyancy effects on thermal boundary layer over a vertical plate with a convective surface boundary condition, *ASME Int. J. Fluids Eng*,132(4): 044502.

Makinde, O. D., Chinyoka, T., and Rundora, L., (2011), Unsteady flow of a reactive variable viscosity non-Newtonian fluid through a porous saturated medium with asymmetric convective boundary conditions, *Comput. Math. Appl.*, 62:3343–52.

Mohammed, I. S., (2014), Unsteady MHD Free Convective Flow Along A Vertical Porous Plate Embedded In A Porous Medium With Heat Generation, Variable Suction And Chemical Reaction Effects. *Chemical and Process Engineering Research*, 21:86-97.

Mutuku-Njane, W., and Makinde, O. D., (2013), Combined effect of buoyancy forced and Navier slip on MHD flow of a nanofluid over a convectively heated vertical porous plate, *Sci World J.*, 2013(2013):725643.

Postelnicu, A., (2004), Influence of a magnetic field on heat and mass transfer by natural convection from vertical surfaces in porous media considering Soret and Dufour effects, *International Journal of Heat and Mass Transfer*, vol. 47(6-7):1467–1472.

Qiu, T. Q., and Tien, C. L., (1992), Short-pulse laser heating on metals. *Int. J. Heat Mass Trans*, 35: 719–726.

Qiu, T. Q., and Tien, C.L., (1993), Heat transfer mechanisms during short-pulse laser heating of metals. *Journal of Heat Transfer*, 115: 835–841.

Raptis, A. and Singh A. K., (1983), MHD free convection flow past an accelerated vertical plate, *Int. Comm. Heat Mass Transf*, 10:313e321.

Sharma, P. R., and Singh, G., (2008), Unsteady MHD Free Convective flow and heat transfer along a vertical porous plate with variable suction and internal heat generation, *International Journal of Appl. Math. And Mech.*,4(5): 1-8.

Singh A. K., (1984), Stokes Problem for a Porous Vertical Plate with Heat Sinks by Finite Difference Method, *Astrphysics and Space Science*, 103(2):241- 248.

Soundalgekar, V. M., and Takhar H. S., (1977), On MHD flow and heat transfer over a semi-infinite plate under transverse magnetic field, *NuclEng Des*; 42:233–6.

Soundalgekar, V. M., and Wavre P. D., (1977), Unsteady free convection flow past an infinite vertical plate with constant suction and mass transfer, *Int. J. of Heat Mass Trans*,20: 1363-1373.

Soundalgekar, V. M., (1979), Effects of mass transfer and free convection currents on the flow past an impulsively started vertical plate, *J ApplMech*, 46: 757–760.

Tzou, D. Y., (1995a), The generalized lagging response in small-scale and high-rate heating, *Int J Heat Mass Trans*, 38: 3231–3240.

Tzou, D. Y., (1995b), Experimental support for the lagging behavior in heat propagation. *J. Thermophys Heat Trans*, 9: 686–693.

Tzou, D. Y., (1997), *Macro to microscale heat transfer: the lagging behavior*. Washington, DC: Taylor & Francis, 1–64.

Wang, L., and Wei, X., (2009), Heat conduction in nanofluids. *Chaos Solitons Fractals* 39: 2211–2215.

Wubshet, I., and Makinde, O. D., (2013), The effect of double stratification on boundary-layer flow and heat transfer of nanofluid over a vertical plate. *Computers & Fluids*, 86, 433–441.

Xu, F., Seffen, K. A., and Liu, T. J., (2008), Non-Fourier analysis of skin biothermomechanics. *Int J Heat Mass Trans*, 51: 2237–2259.

Zhou, J., Chen, J.K., and Zhang, Y., (2009), Dual-phase-lag effects on thermal damage to biological tissues caused by laser irradiations, *ComputBiol Med*, 39: 286–293.

APPENDIX A

List of constants used to define the solutions of the problem in the dissertation

DUAL-PHASE-LAG HEAT CONDUCTION WITH CONVECTIVE BOUNDARY

$$A_1 = \frac{1}{s(1-\tau_q s)}\ A_2 = \left(\frac{1}{1-\tau_q s}\right)\left(\frac{1}{Bi} + \frac{Kn}{\Pr} + \frac{s\tau_T}{Bi}\right)\ A_3 = -\frac{1}{(1+\tau_q s)}\left(\frac{1}{Bi} + \frac{Kn}{\Pr} + \frac{s\tau_T}{Bi}\right)$$

$$B_2 = Sc(\lambda_q s^2 + s)\ B_3 = \frac{B_2}{B_1}\ B_4 = \left(1 - \frac{Kn}{Sc}\sqrt{B_3}\right)\ B_5 = \left(1 + \frac{Kn}{Sc}\sqrt{B_3}\right)\ B_6 = \left(1 + \frac{Kn}{Sc}\sqrt{B_3}\right)e^{\sqrt{B_3}}$$

$$B_7 = \left(1 - \frac{Kn}{Sc}\sqrt{B_3}\right)e^{-\sqrt{B_3}}\ B_8 = (1 + s\tau_T)\ B_9 = \Pr(\tau_q s^2 + s)\ B_{10} = \frac{B_9}{B_8}\ B_{11} = -\frac{DB_3C_1}{B_8}$$

$$B_{12} = -\frac{DB_3C_2}{B_8}\ B_{13} = \frac{B_{11}}{B_3 - B_{10}}\ B_{14} = \frac{B_{12}}{B_3 - B_{10}}\ B_{15} = (1 - A_2\sqrt{B_{10}})\ B_{16} = (1 + A_2\sqrt{B_{10}})$$

$$B_{17} = A_1 + B_{13}(A_2\sqrt{B_3} - 1) - B_{14}(A_2\sqrt{B_3} + 1)\ B_{18} = (1 - A_3\sqrt{B_{10}})e^{\sqrt{B_{10}}}$$

$$B_{19} = (1 + A_3\sqrt{B_{10}})e^{-\sqrt{B_{10}}}\ B_{20} = B_{13}(A_3\sqrt{B_3} - 1)e^{\sqrt{B_3}} - B_{14}(A_3\sqrt{B_3} + 1)e^{-\sqrt{B_3}}$$

$$C_1 = \frac{B_7}{s(B_4B_7 - B_5B_6)}\ C_2 = \frac{B_6}{s(B_5B_6 - B_4B_7)}\ C_3 = \frac{B_{17}B_{19} - B_{16}B_{20}}{B_{15}B_{19} - B_{16}B_{18}}$$

$$C_4 = \frac{B_{17}B_{18} - B_{15}B_{20}}{B_{16}B_{18} - B_{15}B_{19}}\ C_5 = \frac{E_{16}E_{24} - E_{15}E_{25}}{E_{14}E_{24} - E_{15}E_{23}}\ C_6 = \frac{E_{16}E_{23} - E_{14}E_{25}}{E_{15}E_{23} - E_{14}E_{24}}$$

$$E_1 = (s + m^2)\ E_2 = -\frac{NC_1}{B_3 - E_1}\ E_3 = -\frac{NC_2}{B_3 - E_1}$$

$$E_4 = -\frac{C_3}{B_{10} - E_1}\ E_5 = -\frac{C_4}{B_{10} - E_1}\ E_6 = -\frac{B_{13}}{B_3 - E_1}$$

$$E_7 = -\frac{B_{14}}{B_3 - E_1}\ E_8 = E_2(Kn\sqrt{B_3} - 1)\ E_9 = E_3(Kn\sqrt{B_3} + 1)$$

$$E_{10} = E_4(Kn\sqrt{B_{10}} - 1)\ E_{11} = E_5(Kn\sqrt{B_{10}} + 1)\ E_{12} = E_6(Kn\sqrt{B_3} - 1)$$

$$E_{13} = E_7(Kn\sqrt{B_3}+1)\ E_{14} = (1-Kn\sqrt{E_1})\ E_{15} = (1+Kn\sqrt{E_1})$$

$$E_{16} = E_8 - E_9 + E_{10} - E_{11} + E_{12} - E_{13}\ E_{17} = (Kn\sqrt{B_3}+1)E_2 e^{\sqrt{B_3}}$$

$$E_{18} = (Kn\sqrt{B_3}-1)E_3 e^{-\sqrt{B_3}}\ E_{19} = (Kn\sqrt{B_{10}}+1)E_4 e^{\sqrt{B_{10}}}\ E_{20} = (Kn\sqrt{B_{10}}-1)E_5 e^{-\sqrt{B_{10}}}$$

$$E_{21} = (Kn\sqrt{B_3}+1)E_6 e^{\sqrt{B_3}}\ E_{22} = (Kn\sqrt{B_3}-1)E_7 e^{-\sqrt{B_3}}\ E_{23} = (1+Kn\sqrt{E_1})e^{\sqrt{E_1}}$$

$$E_{24} = (1-Kn\sqrt{E_1})e^{-\sqrt{E_1}}\ E_{25} = -E_{17} + E_{18} - E_{19} + E_{20} - E_{21} + E_{22}$$

DUAL-PHASE-LAG HEAT CONDUCTION IN VERTICAL POROUS CHANNEL

$$A_1 = (\lambda_f L^2 + L)\ A_2 = \frac{(1+L\lambda_C)}{Sc}\ A_3 = \frac{S}{A_2}$$

$$A_4 = \frac{A_1}{A_2}\ A_5 = -\frac{A_3}{2}\ A_6 = \sqrt{\frac{A_3^2}{4} + A_4}$$

$$A_7 = A_5 + A_6\ A_8 = A_5 - A_6\ A_9 = \left(1 - \frac{KnA_7}{Sc}\right)$$

$$A_{10} = \left(1 - \frac{KnA_8}{Sc}\right)\ A_{11} = \left(-\frac{KnA_7 e^{A_7}}{Sc} - e^{A_7}\right)\ A_{12} = \left(e^{A_8} + \frac{KnA_8 e^{A_8}}{Sc}\right)$$

$$A_{13} = \left(\frac{A_9 A_{12}}{A_{11}} + A_{10}\right)\ A_{14} = (\tau_f L^2\,\mathrm{Pr} + L\,\mathrm{Pr} - H)\ A_{15} = (1+\tau_T L)$$

$$A_{16} = \frac{S\,\mathrm{Pr}}{A_{15}}\ A_{17} = \frac{A_{14}}{A_{15}}\ A_{18} = -\frac{DC_1 A_7^2}{A_{15}}$$

$$A_{19} = -\frac{DC_2 A_8^2}{A_{15}}\ A_{20} = -\frac{A_{16}}{2}\ A_{21} = \sqrt{\frac{A_{16}^2}{4} + A_{17}}$$

$$A_{22} = \frac{A_{18}}{A_{23}}\ A_{23} = (A_7^2 + A_7 A_{16} - A_{17})\ A_{24} = \frac{A_{19}}{A_{25}}$$

$$A_{25} = (A_8^2 + A_8 A_{16} - A_{17})\ A_{26} = (A_{20} + A_{21})\ A_{27} = (A_{20} - A_{21})$$

$$A_{28} = \frac{1}{L}\ A_{29} = A_{22}\left(\frac{KnA_7}{\mathrm{Pr}} - 1\right)\ A_{30} = A_{24}\left(\frac{KnA_8}{\mathrm{Pr}} - 1\right)$$

$$A_{31}=\left(1-\frac{KnA_{26}}{\Pr}\right)\ A_{32}=\left(1-\frac{KnA_{27}}{\Pr}\right)\ A_{33}=A_{28}+A_{29}+A_{30}$$

$$A_{34}=A_{22}e^{A_7}\left(\frac{KnA_7}{\Pr}+1\right)\ A_{35}=A_{24}e^{A_8}\left(\frac{KnA_8}{\Pr}+1\right)\ A_{36}=e^{A_{26}}\left(1+\frac{KnA_{26}}{\Pr}\right)$$

$$A_{37}=e^{A_{27}}\left(1+\frac{KnA_{27}}{\Pr}\right)\ A_{38}=-A_{34}-A_{35}$$

$$C_1=\frac{A_{12}}{A_{11}A_{13}L}\ C_2=\frac{1}{A_{13}L}\ C_3=\frac{A_{33}A_{37}-A_{32}A_{38}}{A_{31}A_{37}-A_{32}A_{36}}$$

$$C_4=\frac{A_{33}A_{36}-A_{31}A_{38}}{A_{32}A_{36}-A_{31}A_{37}}\ C_5=\frac{K_{14}K_{21}-K_{16}K_{19}}{K_{15}K_{21}-K_{16}K_{20}}\ C_6=\frac{K_{14}K_{20}-K_{15}K_{19}}{K_{16}K_{20}-K_{15}K_{21}}$$

$$K_1=m^2+L\ K_2=-\frac{S}{2}\ K_3=\sqrt{\frac{S^2}{4}+K_1}$$

$$K_4=K_2+K_3\ K_5=K_2-K_3\ K_6=-\frac{C_3}{A_{26}^2+SA_{26}-K_1}$$

$$K_7=-\frac{C_4}{A_{27}^2+SA_{27}-K_1}\ K_8=-\frac{A_{22}}{A_7^2+SA_7-K_1}\ K_9=-\frac{A_{24}}{A_8^2+SA_8-K_1}$$

$$K_{10}=-\frac{NC_1}{A_7^2+SA_7-K_1}\ K_{11}=-\frac{NC_2}{A_8^2+SA_8-K_1}$$

$$K_{12}=Kn(K_6A_{26}+K_7A_{27}+K_8A_7+K_9A_8+K_{10}A_7+K_{11}A_8)\ K_{13}=K_6+K_7+K_8+K_9+K_{10}+K_{11}$$

$$K_{14}=K_{12}-K_{13}\ K_{15}=(1-KnK_4)$$

$$K_{16}=(1-KnK_5)$$

$$K_{17}=-Kn(K_6A_{26}e^{A_{26}}+K_7A_{27}e^{A_{27}}+K_8A_7e^{A_7}+K_9A_8e^{A_8}+K_{10}A_7e^{A_7}+K_{11}A_8e^{A_8})$$

$$K_{18}=K_6e^{A_{26}}+K_7e^{A_{27}}+K_8e^{A_7}+K_9e^{A_8}+K_{10}e^{A_7}+K_{11}e^{A_8}$$

$$K_{19}=K_{17}-K_{18}\ K_{20}=(1+KnK_4)e^{K_4}\ K_{21}=(1+KnK_5)e^{K_5}$$

MATLAB PROGRAMS

MATLAB PROGRAM (CASE 1)

```
%EFFECT OF DUAL-PHASE-LAG ON TRANSIENT MHD NATURAL CONVECTION
 HEAT ANDMASSTRANSFERFLOWINAVERTICALMICROCHANNEL
 WITH CONVECTIVEBOUNDARYCONDITIONS
```

```
clc;
t=0.2;
h=0.001;
[y]=0:h:1;
%[Lc]=0.01:0.01:0.1;
%[Tt]=0.01:0.01:0.1;
%[Tq]=0.00:0.0001:0.01;
%[Lq]=0.00:0.0001:0.01;
%[D]=1:1:10;
%[Bi]=1:0.2:10;
%[m]=0.0:0.1:1.0;
%y=0.001;
Sc=0.78;
Bi=5;
D=5;
Tq=0.001;
Tt=0.01;
Lq=Tq;
Lc=Tt;
Pr=0.71;
N=2;
m=5;
Kn=0.01;
st=4.7;
s=st./t;


Bc1=1+s.*Lc;
Bc2=Sc.*(Lq.*s.^2+s);
B3=Bc2./Bc1;
B4=1-(Kn.*sqrt(B3))./Sc;
B5=1+(Kn.*sqrt(B3))./Sc;
B6=(1+(Kn.*sqrt(B3))./Sc).*exp(sqrt(B3));
B7=(1-(Kn.*sqrt(B3))./Sc).*exp(-sqrt(B3));
C1=B7./(s.*(B4.*B7-B5.*B6));
C2=B6./(s.*(B5.*B6-B4.*B7));

%Concentration
Ph=C1.*exp(y.*sqrt(B3))+C2.*exp(-y.*sqrt(B3));

A1=1./(s.*(1-(Tq.*s)));
A2=(1./(1-(Tq.*s))).*((1./Bi)+(Kn./Pr)+((s.*Tt)./Bi));
A3=(-1./(1+(Tq.*s))).*((1./Bi)+(Kn./Pr)+((s.*Tt)./Bi));
B8=1+s.*Tt;
B9=Pr.*(Tq.*s.^2+s);
B10=B9./B8;
B11=-(D.*B3.*C1)./B8;
B12=-(D.*B3.*C2)./B8;
B13=B11./(B3-B10);
B14=B12./(B3-B10);
B15=1-(A2.*sqrt(B10));
B16=1+(A2.*sqrt(B10));
B17=A1+(B13.*((A2.*sqrt(B3)-1)))-(B14.*((A2.*sqrt(B3)+1)));
B18=(1-(A3.*sqrt(B10))).*exp(sqrt(B10));
B19=(1+(A3.*sqrt(B10))).*exp(-sqrt(B10));
```

```
B20=(B13.*exp(sqrt(B3)).*(A3.*sqrt(B3)-1))-(B14.*exp(-
sqrt(B3)).*(A3.*sqrt(B3)+1));
C3=(B17.*B19-B16.*B20)./(B15.*B19-B16.*B18);
C4=(B17.*B18-B15.*B20)./(B16.*B18-B15.*B19);

%Temperature
TH=C3.*exp(y.*sqrt(B10))+C4.*exp(-y.*sqrt(B10));
Tp1=B13.*exp(y.*sqrt(B3));
Tp2=B14.*exp(-y.*sqrt(B3));
Tp=Tp1+Tp2;

T=TH+Tp;

Ea1=s+m.^2;
Ea2=-(N.*C1)./(B3-Ea1);
E3=-(N.*C2)./(B3-Ea1);
E4=-C3./(B10-Ea1);
E5=-C4./(B10-Ea1);
E6=-B13./(B3-Ea1);
E7=-B14./(B3-Ea1);
E8=Ea2.*(Kn.*sqrt(B3)-1);
E9=E3.*(Kn.*sqrt(B3)+1);
E10=E4.*(Kn.*sqrt(B10)-1);
E11=E5.*(Kn.*sqrt(B10)+1);
E12=E6.*(Kn.*sqrt(B3)-1);
E13=E7.*(Kn.*sqrt(B3)+1);
E14=1-Kn.*sqrt(Ea1);
E15=1+Kn.*sqrt(Ea1);
E16=E8-E9+E10-E11+E12-E13;
E17=(Kn.*sqrt(B3)+1).*Ea2.*exp(sqrt(B3));
E18=(Kn.*sqrt(B3)-1).*E3.*exp(-sqrt(B3));
E19=(Kn.*sqrt(B10)+1).*E4.*exp(sqrt(B10));
E20=(Kn.*sqrt(B10)-1).*E5.*exp(-sqrt(B10));
E21=(Kn.*sqrt(B3)+1).*E6.*exp(sqrt(B3));
E22=(Kn.*sqrt(B3)-1).*E7.*exp(-sqrt(B3));
E23=(1+Kn.*sqrt(Ea1)).*exp(sqrt(Ea1));
E24=(1-Kn.*sqrt(Ea1)).*exp(-sqrt(Ea1));
E25=-E17+E18-E19+E20-E21+E22;
C5=(E16.*E24-E15.*E25)./(E14.*E24-E15.*E23);
C6=(E16.*E23-E14.*E25)./(E15.*E23-E14.*E24);

%Velocity
VH=C5.*exp(y.*sqrt(Ea1))+C6.*exp(-y.*sqrt(Ea1));
Vp1=Ea2.*exp(y.*sqrt(B3));
Vp2=E3.*exp(-y.*sqrt(B3));
Vp3=E4.*exp(y.*sqrt(B10));
Vp4=E5.*exp(-y.*sqrt(B10));
Vp5=E6.*exp(y.*sqrt(B3));
Vp6=E7.*exp(-y.*sqrt(B3));

V=VH+Vp1+Vp2+Vp3+Vp4+Vp5+Vp6;


%Sherwood Number

Sh0=sqrt(B3).*(C1-C2);
```

```
Sh1=sqrt(B3).*(C1.*exp(sqrt(B3))-C2.*exp(-sqrt(B3)));


%Nusselt Number

Nu0=sqrt(B10).*(C3-C4)+sqrt(B3).*(B13-B14);

Nu1=sqrt(B10).*(C3.*exp(sqrt(B10))-C4.*exp(-
sqrt(B10)))+sqrt(B3).*(B13.*exp(sqrt(B3))-B14.*exp(-sqrt(B3)));

%Skin Friction

Sk0=sqrt(Ea1).*(C5-C6)+sqrt(B3).*(Ea2+E6-E3-E7)+sqrt(B10).*(E4-E5);

Sk1=sqrt(Ea1).*(C5.*exp(sqrt(Ea1))-C6.*exp(-
sqrt(Ea1)))+sqrt(B3).*((Ea2+E6).*exp(sqrt(B3))-(E3+E7).*exp(-
sqrt(B3)))+sqrt(B10).*(E4.*exp(sqrt(B10))-E5.*exp(-sqrt(B10)));


sumc=0;
sumv=0;
sumt=0;
suml=0;
sumd=0;
suma=0;
sumb=0;
sume=0;
sumf=0;


for n=1:1:1000

    s1=(s.*t+n.*pi.*1i)./t;
    Bc11=1+s1.*Lc;
    Bc21=Sc.*(Lq.*s1.^2+s1);
    B31=Bc21./Bc11;
    B41=1-(Kn.*sqrt(B31))./Sc;
    B51=1+(Kn.*sqrt(B31))./Sc;
    B61=(1+(Kn.*sqrt(B31))./Sc).*exp(sqrt(B31));
    B71=(1-(Kn.*sqrt(B31))./Sc).*exp(-sqrt(B31));
    C11=B71./(s1.*(B41.*B71-B51.*B61));
    C21=B61./(s1.*(B51.*B61-B41.*B71));


%Concentration
    Ph1=C11.*exp(y.*sqrt(B31))+C21.*exp(-y.*sqrt(B31));

    A11=1./(s1.*(1-(Tq.*s1)));
    A21=(1./(1-(Tq.*s1))).*((1./Bi)+(Kn./Pr)+((s1.*Tt)./Bi));
    A31=(-1./(1+(Tq.*s1))).*((1./Bi)+(Kn./Pr)+((s1.*Tt)./Bi));
    B81=1+s1.*Tt;
    B91=Pr.*(Tq.*s1.^2+s1);
    B101=B91./B81;
    B111=-(D.*B31.*C11)./B81;
```

```
    B121=-(D.*B31.*C21)./B81;
    B131=B111./(B31-B101);
    B141=B121./(B31-B101);
    B151=1-(A21.*sqrt(B101));
    B161=1+(A21.*sqrt(B101));
    B171=A11+(B131.*((A21.*sqrt(B31)-1)))-(B141.*((A21.*sqrt(B31)+1)));
    B181=(1-(A31.*sqrt(B101))).*exp(sqrt(B101));
    B191=(1+(A31.*sqrt(B101))).*exp(-sqrt(B101));
    B201=(B131.*exp(sqrt(B31)).*(A31.*sqrt(B31)-1))-(B141.*exp(-
sqrt(B31)).*(A31.*sqrt(B31)+1));


    C31=(B171.*B191-B161.*B201)./(B151.*B191-B161.*B181);
    C41=(B171.*B181-B151.*B201)./(B161.*B181-B151.*B191);

%Temperature
    TH1=C31.*exp(y.*sqrt(B101))+C41.*exp(-y.*sqrt(B101));
    Tp11=B131.*exp(y.*sqrt(B31));
    Tp21=B141.*exp(-y.*sqrt(B31));
    Tp1=Tp11+Tp21;

    T1=TH1+Tp1;

    Ea11=s1+m.^2;
    Ea21=-(N.*C11)./(B31-Ea11);
    E31=-(N.*C21)./(B31-Ea11);
    E41=-C31./(B101-Ea11);
    E51=-C41./(B101-Ea11);
    E61=-B131./(B31-Ea11);
    E71=-B141./(B31-Ea11);
    E81=Ea21.*(Kn.*sqrt(B31)-1);
    E91=E31.*(Kn.*sqrt(B31)+1);
    E101=E41.*(Kn.*sqrt(B101)-1);
    E111=E51.*(Kn.*sqrt(B101)+1);
    E121=E61.*(Kn.*sqrt(B31)-1);
    E131=E71.*(Kn.*sqrt(B31)+1);
    E141=1-Kn.*sqrt(Ea11);
    E151=1+Kn.*sqrt(Ea11);
    E161=E81-E91+E101-E111+E121-E131;
    E171=(Kn.*sqrt(B31)+1).*Ea21.*exp(sqrt(B31));
    E181=(Kn.*sqrt(B31)-1).*E31.*exp(-sqrt(B31));
    E191=(Kn.*sqrt(B101)+1).*E41.*exp(sqrt(B101));
    E201=(Kn.*sqrt(B101)-1).*E51.*exp(-sqrt(B101));
    E211=(Kn.*sqrt(B31)+1).*E61.*exp(sqrt(B31));
    E221=(Kn.*sqrt(B31)-1).*E71.*exp(-sqrt(B31));
    E231=(1+Kn.*sqrt(Ea11)).*exp(sqrt(Ea11));
    E241=(1-Kn.*sqrt(Ea11)).*exp(-sqrt(Ea11));
    E251=-E171+E181-E191+E201-E211+E221;
    C51=(E161.*E241-E151.*E251)./(E141.*E241-E151.*E231);
    C61=(E161.*E231-E141.*E251)./(E151.*E231-E141.*E241);

%Velocity
    VH1=C51.*exp(y.*sqrt(Ea11))+C61.*exp(-y.*sqrt(Ea11));
    Vp11=Ea21.*exp(y.*sqrt(B31));
    Vp21=E31.*exp(-y.*sqrt(B31));
    Vp31=E41.*exp(y.*sqrt(B101));
```

```
    Vp41=E51.*exp(-y.*sqrt(B101));
    Vp51=E61.*exp(y.*sqrt(B31));
    Vp61=E71.*exp(-y.*sqrt(B31));

    V1=VH1+Vp11+Vp21+Vp31+Vp41+Vp51+Vp61;

%Sherwood Number

    Sh01=sqrt(B31).*(C11-C21);
Sw=((-1)^n).*Sh01;
suml=suml+Sw;

    Sh11=sqrt(B31).*(C11.*exp(sqrt(B31))-C21.*exp(-sqrt(B31)));
Sm=((-1)^n).*Sh11;
sumd=sumd+Sm;

%Nusselt Number

    Nu01=sqrt(B101).*(C31-C41)+sqrt(B31).*(B131-B141);

    Na=((-1)^n).*Nu01;
suma=suma+Na;

    Nu11=sqrt(B101).*(C31.*exp(sqrt(B101))-C41.*exp(-
sqrt(B101)))+sqrt(B31).*(B131.*exp(sqrt(B31))-B141.*exp(-sqrt(B31)));

Nb=((-1)^n).*Nu11;
sumb=sumb+Nb;

%Skin Friction

    Sk01=sqrt(Ea11).*(C51-C61)+sqrt(B31).*(Ea21+E61-E31-
E71)+sqrt(B101).*(E41-E51);

Ske=((-1)^n).*Sk01;
sume=sume+Ske;

    Sk11=sqrt(Ea11).*(C51.*exp(sqrt(Ea11))-C61.*exp(-
sqrt(Ea11)))+sqrt(B31).*((Ea21+E61).*exp(sqrt(B31))-(E31+E71).*exp(-
sqrt(B31)))+sqrt(B101).*(E41.*exp(sqrt(B101))-E51.*exp(-sqrt(B101)));

Skf=((-1)^n).*Sk11;
sumf=sumf+Skf;


%velocity
cu=((-1)^n).*V1;
sumv=sumv+cu;

%Concentration

cN=((-1).^n).*Ph1;
sumc=sumc+cN;
```

```
%Temperature

th=((-1).^n).*T1;
sumt=sumt+th;

end


    Con2=real(sumc);
    Con1=0.5.*Ph;
phi=((exp(st)./t).*(Con1+Con2));

    Tmp2=real(sumt);
    Tmp1=0.5.*T;
theta=((exp(st)./t).*(Tmp1+Tmp2));


    u2=real(sumv);
    u1=0.5.*V;
Vel=((exp(st)./t).*(u1+u2));
    VV=Vel';
    MF=h.*trapz(VV);


    MT1=(theta.*Vel)';
    MT=(h.*trapz(MT1))./MF;


    p2=real(suml);
    p1=0.5.*Sh0;
    Shr0 =-((exp(st)./t).*(p1+p2));

    e2=real(sumd);
    e1=0.5.*Sh1;
    Shr1 =-((exp(st)./t).*(e1+e2));

    f2=real(suma);
    f1=0.5.*Nu0;
    Nusselt0 =-((exp(st)./t).*(f1+f2));

    g2=real(sumb);
    g1=0.5.*Nu1;
    Nusselt1 =-((exp(st)./t).*(g1+g2));

    h2=real(sume);
    h1=0.5.*Sk0;
    Skinf0 =((exp(st)./t).*(h1+h2));

    i2=real(sumf);
    i1=0.5.*Sk1;
    Skinf1 =-((exp(st)./t).*(i1+i2));
```

```
    MC1=(Vel.*phi)';
MeanC=(h.*trapz(MC1))./MF



%xlabel('y','fontsize',11);
%ylabel('u','fontsize',11);
%hold on
%plot(y,theta,'k','linestyle','-')
%plot(Tt,Nusselt1,'k','linestyle','-')
%hold off
```

MATLAB PROGRAM (CASE 2)

```
%UNSTEADY MHD NATURAL CONVECTION DOUBLE DIFFUSIVE FLOW OF
 HEAT GENERATINGFLUIDINAVERTICALPOROUSMICROCHANNEL

clc;

t=0.4;
h=0.0001;
%[y]=0:h:1;
%[Lc]=0.01:0.0001:0.1;
%[Tt]=0.01:0.0001:0.1;
[Kn]=0.00:0.0001:0.01;
%[Tf]=0.00:0.0001:0.01;
%[Lf]=0.00:0.0001:0.01;
%[D]=0:1:10;
%[m]=0.0:0.1:1.0;
y=0;
m=5;
Sc=0.78;
S=2;
Lf=0.001;
Lc=0.01;
Tf=Lf;
Tt=Lc;
%Kn=0.1;
H=1;
Pr=0.71;
D=5;
N=2;
st=4.7;
L=st./t;


Aa1=Lf.*L.^2+L;
Aa2=(1+L.*Lc)./Sc;
```

```
Aa3=S./Aa2;
A4=Aa1./Aa2;
A5=-Aa3./2;
A6=sqrt((Aa3.^2./4)+A4);
A7=A5+A6;
A8=A5-A6;
A9=1-(Kn.*A7)./Sc;
A10=1-(Kn.*A8)./Sc;
A11=(-1-(Kn.*A7)./Sc).*exp(A7);
A12=(1+(Kn.*A8)./Sc).*exp(A8);
A13=(A10+(A9.*A12)./A11);

C1=A12./(A11.*A13.*L);
C2=1./(A13.*L);

%Concentration
PH=C1.*exp(A7.*y)+C2.*exp(A8.*y);



A14=(Tf.*L.^2.*Pr+L.*Pr-H);
A15=(1+Tt.*L);
A16=(S.*Pr)./A15;
A17=A14./A15;
A18=-(D.*C1.*A7.^2)./A15;
A19=-(D.*C2.*A8.^2)./A15;
A20=-A16./2;
A21=sqrt((A16.^2./4)+A17);
A23=(A7.^2+A7.*A16-A17);
A22=A18./A23;
A25=(A8.^2+A8.*A16-A17);
A24=A19./A25;
A26=A20+A21;
A27=A20-A21;
A28=1./L;
A29=A22.*(((Kn.*A7)./Pr)-1);
A30=A24.*(((Kn.*A8)./Pr)-1);
A31=(1-(Kn.*A26)./Pr);
A32=(1-(Kn.*A27)./Pr);
A33=A28+A29+A30;
A34=A22.*exp(A7).*(1+(Kn.*A7)./Pr);
A35=A24.*exp(A8).*(1+(Kn.*A8)./Pr);
A36=exp(A26).*(1+(Kn.*A26)./Pr);
A37=exp(A27).*(1+(Kn.*A27)./Pr);
A38=-A34-A35;

C3=(A33.*A37-A32.*A38)./(A31.*A37-A32.*A36);
C4=(A33.*A36-A31.*A38)./(A32.*A36-A31.*A37);

%Temperature
TH=C3.*exp(y.*A26)+C4.*exp(y.*A27);
Tp1=A22.*exp(y.*A7);
Tp2=A24.*exp(y.*A8);
Tp=Tp1+Tp2;

T=TH+Tp;
Ka1=L+m.^2;
```

```
Ka2=-S./2;
K3=sqrt((S.^2./4)+Ka1);
K4=Ka2+K3;
K5=Ka2-K3;
K6=-C3./(A26.^2+S.*A26-Ka1);
K7=-C4./(A27.^2+S.*A27-Ka1);
K8=-A22./(A7.^2+S.*A7-Ka1);
K9=-A24./(A8.^2+S.*A8-Ka1);
K10=-(N.*C1)./(A7.^2+S.*A7-Ka1);
K11=-(N.*C2)./(A8.^2+S.*A8-Ka1);
K12=Kn.*(K6.*A26+K7.*A27+K8.*A7+K9.*A8+K10.*A7+K11.*A8);
K13=K6+K7+K8+K9+K10+K11;
K14=K12-K13;
K15=1-Kn.*K4;
K16=1-Kn.*K5;
K17=-
Kn.*(K6.*A26.*exp(A26)+K7.*A27.*exp(A27)+K8.*A7.*exp(A7)+K9.*A8.*exp(A8)+K10.
*A7.*exp(A7)+K11.*A8.*exp(A8));
K18=K6.*exp(A26)+K7.*exp(A27)+K8.*exp(A7)+K9.*exp(A8)+K10.*exp(A7)+K11.*exp(A
8);
K19=K17-K18;
K20=(1+Kn.*K4).*exp(K4);
K21=(1+Kn.*K5).*exp(K5);

C5=(K14.*K21-K16.*K19)./(K15.*K21-K16.*K20);
C6=(K14.*K20-K15.*K19)./(K16.*K20-K15.*K21);

%Velocity
VH=C5.*exp(y.*K4)+C6.*exp(y.*K5);
Vp1=K6.*exp(y.*A26);
Vp2=K7.*exp(y.*A27);
Vp3=K8.*exp(y.*A7);
Vp4=K9.*exp(y.*A8);
Vp5=K10.*exp(y.*A7);
Vp6=K11.*exp(y.*A8);
Vp=Vp1+Vp2+Vp3+Vp4+Vp5+Vp6;

V=VH+Vp;

%Sherwood Number
Sh=A7.*C1.*exp(A7.*y)+A8.*C2.*exp(A8.*y);

%Nusselt Number
Nu=C3.*A26.*exp(y.*A26)+C4.*A27.*exp(y.*A27)+A7.*A22.*exp(y.*A7)+A8.*A24.*exp
(y.*A8);

%Skin Friction
Sk=C5.*K4.*exp(y.*K4)+C6.*K5.*exp(y.*K5)+K6.*A26.*exp(y.*A26)+K7.*A27.*exp(y.
*A27)+K8.*A7.*exp(y.*A7)+K9.*A8.*exp(y.*A8)+K10.*A7.*exp(y.*A7)+K11.*A8.*exp(
y.*A8);

sumc=0;
sumv=0;
sumt=0;
suma=0;
sumb=0;
```

```
sumd=0;

for n=1:1:100
    L1=(L.*t+n.*pi.*1i)./t;
    Aa11=Lf.*L1.^2+L1;
    Aa21=(1+L1.*Lc)./Sc;
    Aa31=S./Aa21;
    A41=Aa11./Aa21;
    A51=-Aa31./2;
    A61=sqrt((Aa31.^2./4)+A41);
    A71=A51+A61;
    A81=A51-A61;
    A91=1-(Kn.*A71)./Sc;
    A101=1-(Kn.*A81)./Sc;
    A111=(-1-(Kn.*A71)./Sc).*exp(A71);
    A121=(1+(Kn.*A81)./Sc).*exp(A81);
    A131=(A101+(A91.*A121)./A111);

    C11=A121./(A111.*A131.*L1);
    C21=1./(A131.*L1);

%Concentration
    PH1=C11.*exp(A71.*y)+C21.*exp(A81.*y);

A141=(Tf.*L1.^2.*Pr+L1.*Pr-H);
    A151=(1+Tt.*L1);
    A161=(S.*Pr)./A151;
    A171=A141./A151;
    A181=-(D.*C11.*A71.^2)./A151;
    A191=-(D.*C21.*A81.^2)./A151;
    A201=-A161./2;
    A211=sqrt((A161.^2./4)+A171);
    A231=(A71.^2+A71.*A161-A171);
    A221=A181./A231;
    A251=(A81.^2+A81.*A161-A171);
    A241=A191./A251;
    A261=A201+A211;
    A271=A201-A211;
    A281=1./L1;
    A291=A221.*(((Kn.*A71)./Pr)-1);
    A301=A241.*(((Kn.*A81)./Pr)-1);
    A311=(1-(Kn.*A261)./Pr);
    A321=(1-(Kn.*A271)./Pr);
    A331=A281+A291+A301;
    A341=A221.*exp(A71).*(1+(Kn.*A71)./Pr);
    A351=A241.*exp(A81).*(1+(Kn.*A81)./Pr);
    A361=exp(A261).*(1+(Kn.*A261)./Pr);
    A371=exp(A271).*(1+(Kn.*A271)./Pr);
    A381=-A341-A351;

    C31=(A331.*A371-A321.*A381)./(A311.*A371-A321.*A361);
    C41=(A331.*A361-A311.*A381)./(A321.*A361-A311.*A371);

%Temperature
    TH1=C31.*exp(y.*A261)+C41.*exp(y.*A271);
    Tp11=A221.*exp(y.*A71);
```

```
    Tp21=A241.*exp(y.*A81);
    Tp1=Tp11+Tp21;

    T1=TH1+Tp1;

Ka11=L1+m.^2;
    Ka21=-S./2;
    K31=sqrt((S.^2./4)+Ka11);
    K41=Ka21+K31;
    K51=Ka21-K31;
    K61=-C31./(A261.^2+S.*A261-Ka11);
    K71=-C41./(A271.^2+S.*A271-Ka11);
    K81=-A221./(A71.^2+S.*A71-Ka11);
    K91=-A241./(A81.^2+S.*A81-Ka11);
    K101=-(N.*C11)./(A71.^2+S.*A71-Ka11);
    K111=-(N.*C21)./(A81.^2+S.*A81-Ka11);
    K121=Kn.*(K61.*A261+K71.*A271+K81.*A71+K91.*A81+K101.*A71+K111.*A81);
    K131=K61+K71+K81+K91+K101+K111;
    K141=K121-K131;
    K151=1-Kn.*K41;
    K161=1-Kn.*K51;
    K171=-
Kn.*(K61.*A261.*exp(A261)+K71.*A271.*exp(A271)+K81.*A71.*exp(A71)+K91.*A81.*e
xp(A81)+K101.*A71.*exp(A71)+K111.*A81.*exp(A81));

K181=K61.*exp(A261)+K71.*exp(A271)+K81.*exp(A71)+K91.*exp(A81)+K101.*exp(A71)
+K111.*exp(A81);
    K191=K171-K181;
    K201=(1+Kn.*K41).*exp(K41);
    K211=(1+Kn.*K51).*exp(K51);

    C51=(K141.*K211-K161.*K191)./(K151.*K211-K161.*K201);
    C61=(K141.*K201-K151.*K191)./(K161.*K201-K151.*K211);

%Velocity
    VH1=C51.*exp(y.*K41)+C61.*exp(y.*K51);
    Vp11=K61.*exp(y.*A261);
    Vp21=K71.*exp(y.*A271);
    Vp31=K81.*exp(y.*A71);
    Vp41=K91.*exp(y.*A81);
    Vp51=K101.*exp(y.*A71);
    Vp61=K111.*exp(y.*A81);
    Vp1=Vp11+Vp21+Vp31+Vp41+Vp51+Vp61;

    V1=VH1+Vp1;


%Sherwood Number
    Sh1=A71.*C11.*exp(A71.*y)+A81.*C21.*exp(A81.*y);

Sw=((-1)^n).*Sh1;
suma=suma+Sw;


%Nusselt Number
```

```
Nu1=C31.*A261.*exp(y.*A261)+C41.*A271.*exp(y.*A271)+A71.*A221.*exp(y.*A71)+A8
1.*A241.*exp(y.*A81);

    Na=((-1)^n).*Nu1;
sumb=sumb+Na;


%Skin Friction

Sk1=C51.*K41.*exp(y.*K41)+C61.*K51.*exp(y.*K51)+K61.*A261.*exp(y.*A261)+K71.*
A271.*exp(y.*A271)+K81.*A71.*exp(y.*A71)+K91.*A81.*exp(y.*A81)+K101.*A71.*exp
(y.*A71)+K111.*A81.*exp(y.*A81);

Skd=((-1)^n).*Sk1;
sumd=sumd+Skd;

%Concentration
    CN=((-1).^n).*PH1;
sumc=sumc+CN;

%Temperature
Th=((-1).^n).*T1;
sumt=sumt+Th;

%velocity
cu=((-1)^n).*V1;
sumv=sumv+cu;


end

    e2=real(suma);
    e1=0.5.*Sh;
Shr =-((exp(st)./t).*(e1+e2));

    f2=real(sumb);
    f1=0.5.*Nu;
Nusselt =-((exp(st)./t).*(f1+f2));

    h2=real(sumd);
    h1=0.5.*Sk;
Skinf=((exp(st)./t).*(h1+h2));

    Con2=real(sumc);
    Con1=0.5.*PH;
phi=((exp(st)./t).*(Con1+Con2));
    Tmp2=real(sumt);
    Tmp1=0.5.*T;
theta=((exp(st)./t).*(Tmp1+Tmp2));

    u2=real(sumv);
    u1=0.5.*V;
Vel=((exp(st)./t).*(u1+u2));
```

```
    VV=Vel';
    MF=h.*trapz(VV);

    MT1=(theta.*Vel)';
    MT=(h.*trapz(MT1))./MF;

    MC1=(Vel.*phi)';
MeanC=(h.*trapz(MC1))./MF;

xlabel('y','fontsize',11);
ylabel('u','fontsize',11);
holdon
    %plot(y,theta,'k','linestyle','-')
plot(Kn,Skinf,'k','linestyle','-')
   holdoff
```